



REACTOR-BASED MOLYBDENUM-99 SUPPLY SYSTEM PROJECT

CRITICAL HEAT FLUX TESTING AT THE UNIVERSITY OF WISCONSIN FINAL REPORT

Prepared by General Atomics
for the U.S. Department of Energy/National Nuclear Security
Administration and Nordion Canada Inc.

Cooperative Agreement DE-NA0002773



GA Project 30441
WBS 1250



Attachment 10

REVISION HISTORY

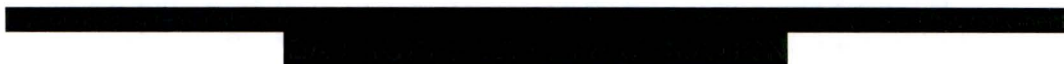
Revision	Date	Description of Changes
A	14APR17	Initial Release

POINT OF CONTACT INFORMATION

PREPARED BY:			
Name	Position	Email	Phone
J. Stone	Engineer	josh.stone@ga.com	858-455-3617
APPROVED BY:			
Name	Position	Email	Phone
B. Schleicher	Chief Engineer	Bob.Schleicher@ga.com	858-455-4733
K. Murray	Project Manager	Katherine.Murray@ga.com	858-455-3272
K. Partain	Quality Engineer	Katherine.Partain@ga.com	858-455-3225

DESIGN CONTROL SYSTEM DESCRIPTION

<input type="checkbox"/>	R & D	DISC	QA LEVEL	SYS
<input checked="" type="checkbox"/>	DV&S			
<input type="checkbox"/>	DESIGN			
<input type="checkbox"/>	T&E			
<input type="checkbox"/>	NA	N	I	N/A



Preface

This report was written by the University of Wisconsin for GA under GA Purchase Order (PO) 4500063597 and is being released in its entirety through the GA Configuration Management System.

Executive Summary

The results compiled by the University of Wisconsin (UW) on the convective behavior of a rod cooled by water at high mass flux and high heat flux are the best possible representation of the cooling performance of the SGE target rods, and provide an anchor for the safety case with regard to the critical heat flux (CHF) margin. In total, the results of the test demonstrated (i) a more than adequate critical heat flux ratio (CHFR) exists for the expected operating conditions, (ii) the resiliency of the CHFR under extreme operating conditions beyond those that could be expected in MURR, and (iii) minimal vapor generation takes place under expected operating conditions. This is important to MURR's licensing effort, as outside of the data acquired from this experiment there is very little information in the literature to help predict the boiling behavior in the design flow regime for the SGE targets.

The test apparatus devised by UW team was an excellent representation for the SGE target cartridge. Its hydraulic diameter matches that of a center-channel SGE rod to within one percent, and instrumentation allows for the control of the critical flow parameters of mass flux, heat flux, temperature and pressure. Notwithstanding these features, the UW test apparatus is not a perfect replica. The heater tube used to simulate the fission in the SGE pin is heated via electrical resistance, which creates a uniform axial heat flux profile, not a cosine-shaped profile expected in the MURR core. The differences were accounted for by monitoring the flow conditions at the heated section outlet, which is very close to where the critical heat flux occurs (for a uniform heat flux profile). The outlet pressure was easily controlled to desired values. However, the outlet temperature was could not be kept stable for long periods of time at high heat inputs, as the cooling of the primary coolant reservoir was limited by the secondary cooling system's chiller outlet temperature. Therefore, the heater was intermittently turned off to allow the reservoir to cool and keep the outlet temperature close to the desired values.

Using the outlet conditions to correlate the observed CHF's to those predicted by Groeneveld's table produced excellent agreement. All observed CHF values were within 10% of Groeneveld's predicted values. This was expected, as Groeneveld's publication notes that these regions in his table should accurately predict CHF conditions.

The UW test also provided important data regarding the amount of vapor generation expected at nominal operating conditions. Overall, that data confirms GA's previous assessment that the vapor generation amount will be small, with vapor volume fractions of approximately [REDACTED] at the maximum heat flux location. This value is slightly higher than the vapor fraction calculated [REDACTED]

5a, d, e, f

from Del Valle and Kenning's data¹, which was also on the order of [REDACTED] and significantly higher than the amount predicted by ANSYS FLUENT's RPI boiling model (about [REDACTED]) as documented in GA Report 30441R00033/B².

5a, d, e, f

There are two plausible explanations why the FLUENT model underestimates the vapor generation. First, the uniform heat flux profile should increase the vapor generated, as the entire rod is operating at the maximum heat flux. This effect is more pronounced the further downstream the flow travels, as bubbles generated over the length of the tube accumulate. Second, the FLUENT boiling model is typically applied to lower heat and mass fluxes, and is not likely to be calibrated to the conditions of the SGE target rods. The FLUENT verification case examined in GA Report 30441R00028/A³ used a mass flux of 900 kg/(s*m²) and a heat flux of 0.57 MW/m², compared to the target design's nominal values of [REDACTED] and [REDACTED] respectively. In a study by Colombo and Fairweather⁴ comparing the results of 20 experiments to a similar computational fluid dynamics (CFD) boiling model, none of the reference experiments exceeded mass flux of 3000 kg/(s*m²) and heat flux of 1.2 MW/m². This demonstrates the general dearth of existing data for subcooled nucleate boiling around the SGE rods' operating parameters, which is why the UW CHF experiment was needed to verify GA's design performance.

5a, d, e, f

As stated in GA Report 30441R00033/B², the data of Del Valle and Kenning provided the closest match to GA's SGE rod operating conditions. The UW experiment confirmed two of their previous observations: that flow remains bubbly up to burnout under high subcooling, and that the bubbles are small. However, unlike in some of the other literature references, which reported bubbles growing and collapsing in place, the bubbles in the UW experiment clearly traveled with the flow. This difference is likely due to the fact that GA's test conditions utilized higher coolant velocities than the experiments reported in the literature. The bubbles traveled relatively slowly compared to the bulk coolant, which indicates the bubbles remain close to the cladding, per the velocity profile in Appendix A of 30441R00038/A⁵.

Regardless of the differences between the test results, the literature, and predictions from FLUENT, the data gathered by UW ultimately confirms that the conditions for the SGE target rod cooling provide a more than adequate margin of safety. Videographic study confirms that the vapor volume fraction in the coolant [REDACTED], the observed CHF values provide CHF values of greater than 2 for conditions much more extreme than will be allowed in

5a, d, e, f

¹ International Journal of Heat and Mass Transfer 28 (1985) 1907-1920

² GA Report, "Analysis of Forced Convection Cooling of Target Rods with 2 Phase Considerations," 30441R00033/B, 25 January, 2017

³ GA Report, "FLUENT (Version 16.0) Software Verification Test Report," 30441R00028/A, 10 August 2016

⁴ International Journal of Heat and Mass Transfer 103 (2016) 28-44

⁵ GA Report, "Computational Fluid Dynamics of Target Housing Design Calculation Report," 30441R00038/A, 25 January, 2017

Attachment 10

Critical Heat Flux Testing at the University of Wisconsin Final Report

30441R00041/A

the SGE target. In short, the UW CHF testing has provided GA with full confidence that SGE target cooling design provides more than adequate safety margins, even with the high power rating of the target rods inducing a small amount of subcooled nucleate boiling.





WISCONSIN
UNIVERSITY OF WISCONSIN-MADISON

Critical Heat Flux Testing
Direct (Resistance) Heated Rod
0.635cm O.D. Rod in 1.67cm I.D. Glass Tube
Maximum Heat Flux of 9.6 Mw/m²
January 4 – February 27, 2017

University of Wisconsin, Thermal Hydraulics Laboratory

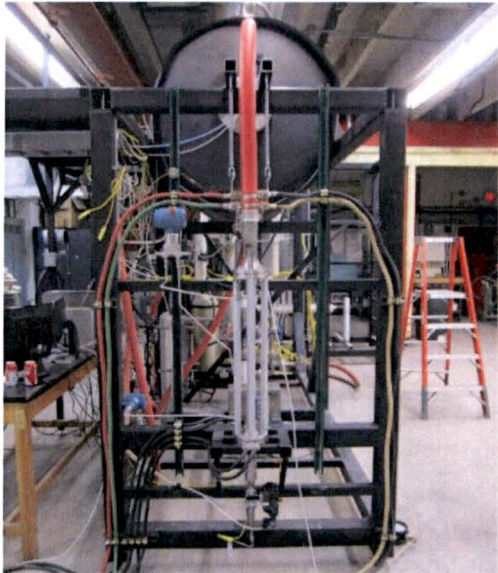


Figure 2: End View of Experiment

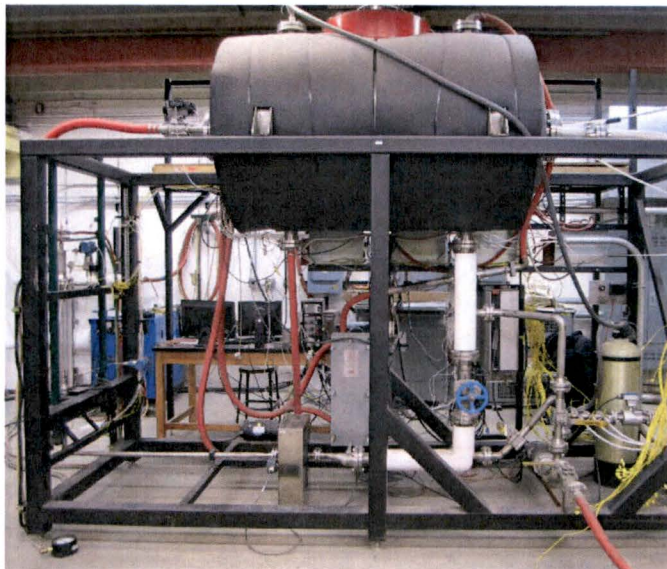


Figure 1: Side View of Experiment

Paul Brooks, Bryan Coddington, Julianna Duarte, Phillip Buelow
Mike Corradini and Mark Anderson

Contact information:

Mark Anderson

Director University of Wisconsin – Thermal Hydraulics Laboratory

737 Engineering Research Bldg

1500 Engineering Dr, Madison WI 53706

Phone: 608-263-2802

e-mail: manderson@engr.wisc.edu

Table of Content:

<u>Introduction:</u>	<u>Page3</u>
<u>System Description:</u>	<u>Page3</u>
<u>Flow Path Description:</u>	<u>Page4</u>
<u>Heated Rod Assembly:</u>	<u>Page5</u>
<u>Test Section:</u>	<u>Page6</u>
<u>Optical Imaging</u>	<u>Page9</u>
<u>Power Supply</u>	<u>Page9</u>
<u>Pressure Measurements:</u>	<u>Page10</u>
<u>Void Fraction Measurements:</u>	<u>Page10</u>
<u>Operation:</u>	<u>Page13</u>
<u>Individual Experiment Descriptions:</u>	<u>Page14</u>
<u>Results:</u>	<u>Page35</u>
<u>Discussion:</u>	<u>Page38</u>

Appendices

<u>#1, TRACE Code Calculations</u>	<u>Page39</u>
<u>#2, Operational Procedure</u>	<u>Page52</u>
<u>#3, Sample Error Calculations</u>	<u>Page55</u>
<u>#4, Instrument Calibrations</u>	<u>Page58</u>
<u>#5, Void Generation Reference</u>	<u>Page69</u>
<u>#6, Rod Surface Roughness</u>	<u>Page71</u>
<u>#7, List of Experimental Runs</u>	<u>Page75</u>
<u>#8, Mechanical Drawings</u>	<u>Page79</u>
<u>#9, Computer Platform and Software</u>	<u>Page89</u>

Introduction:

This report describes experimental studies of critical heat flux values conducted for conditions encountered in open pool test reactors with forced water flow. Testing was conducted at the University of Wisconsin thermal hydraulic lab during January and February of 2017. The objective of this work was to produce CHF at various pressures and temperatures typical of research reactors, and to then compare these results with Groeneveld et al. (2007) look up table⁶.

System Description:

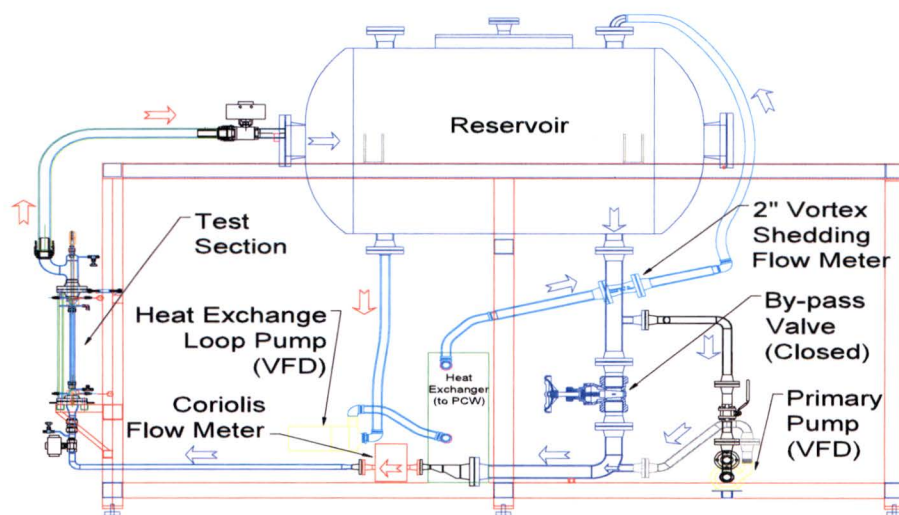


Figure 3: Labeled Drawing, Overall Side View

These test were conducted on the University of Wisconsin, Thermal Hydraulics Lab critical heat flux testing rig. The rig consists of an insulated, stainless steel upper reservoir 1.23m in diameter by 1.7m length. During testing this upper reservoir was filled with deionized water to a level slightly above the return port from the test section, containing approximately 1.5m^3 (400 gallons) of water. This water was maintained at 3-7mohm of purity via a mixed bed deionizing filtration system. The thermal energy from the testing was rejected through a water to glycol heat exchanger attached to the system. The flow through the (experimental) water side of this heat exchanger was forced with a 2.2kw (3hp) stainless steel centrifugal pump, which was controlled via a variable frequency drive. This flow was maintained at approximately $0.21\text{m}^3/\text{m}$ [55 gpm] through all testing. This flow also contributed to the mixing of the upper reservoir to maintain steady test section inlet temperatures. The flow through the glycol side (facility side) of the heat exchanger was controlled via flow and bypass valves. The heated glycol was directed to a roof mounted chiller where the experimental heat was ultimately rejected.

^{6 6} D.C., Groeneveld, J.Q., Shan, A.Z., Vasic, L.K.H., Leung, A. Durmayza, J. Yang, S.C., Cheng, A. Tanase, "The 2006 CHF look-up table", Nuclear Engineering and Design 237 (2007) 1909-1922

Flow Path Description:

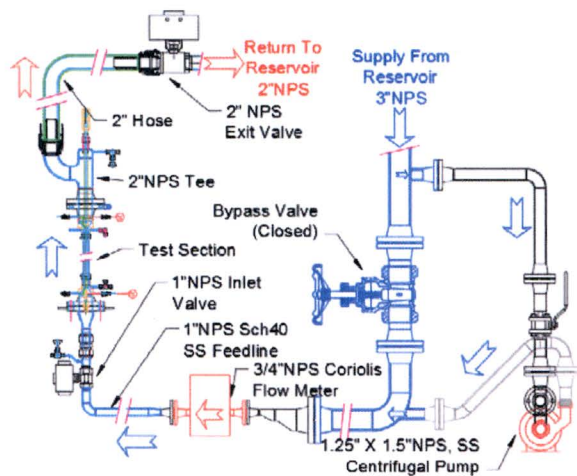


Figure 4: Drawing, Labeled Flow Path



Figure 5: Picture, Flow Path

Water is supplied to the test section circuit via a 3" NPS bottom tap from the upper reservoir. The supply water from the tank flows downward 0.6m through the 3" NPS supply piping, and then proceeds into a 1.5" NPS branch pipe. This pipe proceeds horizontally then downward into the 1.5" NPS intake of a centrifugal, 3 hp, stainless steel pump. The water is then propelled upward from the pump through a 1.5" pipe, through a 135-degree bend and into the main 3" NPS supply line. The flow proceeds through 0.5m length of the 3" NPS, through a 3" NPS flange set, and into an eccentric reducer set ending in a 0.75" NPS, 150lb, RF flange. This flange is mated to the Foxboro Coriolis flow meter, model CFT10/15, last calibration date of 7/11/16. The water flows through the Coriolis, through another 0.75" NPS flange set, and into a 0.75" NPS to 1" NPS concentric reducer (used as diffuser). The flow then proceeds through 1.3m of 1" NPS schedule 40 horizontal pipe to a matching long radius 1" NPS upward turning 90° elbow. The flow then proceeds upward through a 1" NPS full port, pneumatically driven ball valve, through a 1.25" Swagelok straight union and into the test section.

The flow exits the top of the test section through the horizontal branch of a 2" NPS, schedule 40, butt weld tee. A 2" NPS schedule 40, 90° upward turning elbow is directly welded to this tee. The flow then proceeds through a 2" hose size cam lock fitting, through 1.5 meters of 2" ID hose and into an additional 2" hose size cam lock fitting. This fitting is directly coupled to a 2" NPS, pneumatically driven ball valve which is attached to the end of the main tank via a 2" NPS schedule 40, 0.15m length pipe section. The water is returned to the upper reservoir through this 2" NPS pipe, into an end flange of the tank, just below the water surface in the tank.

All piping, fittings, pumps, tanks, flowmeters, and heat exchangers are constructed of 300 series stainless steel. All water hoses used in the system were either EPDM or NBR. The two pneumatically operated ball valves were installed to both isolate the test section in the event of a failure of the glass tube, and to allow work on the test section without draining the upper reservoir. A failure of the glass tube did not occur.

Heated Rod Assembly:

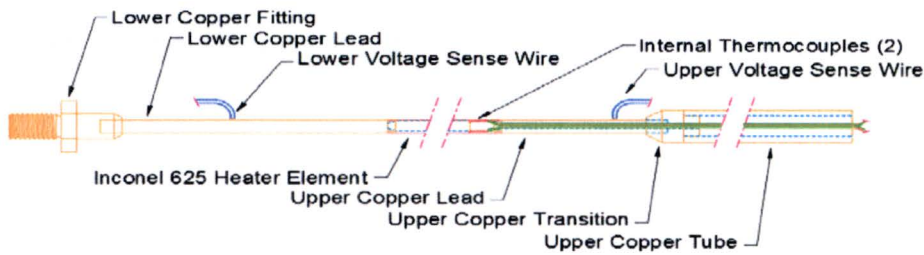


Figure 6: Diagram of Heater Assembly

A custom heater was designed and six were fabricated to complete the requested testing. The

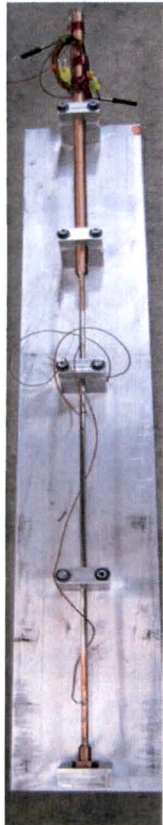


Figure 7:
Picture of
Heater on Jig

heater was designed to convey a maximum of 1200 amps, a maximum of 80volts, and create greater than 9Mw/m^2 heat flux. The method used to create the heat flux was direct ohmic heating of the tubular Inconel 625 element. The element was 0.25" (6.35 mm) outside diameter, with a nominal wall thickness of .02" (0.51mm), and an overall length of 17.97" (456mm). The uniformity of the electrical resistance of the original stock was checked resulting in a standard deviation over 100mm lengths of less than 1.85%. Heaters #1 and #2 were also checked for uniformity of electrical resistance along the length of the heater rod, at intervals of 1" (25.4mm), resulting in standard deviations of 1.6% and 1.2% respectively. The surface of the inconel tube was polished with Scotch-Brite, #7447, very fine, maroon hand pad. Heaters #1 and #2 surface roughnesses were measured after testing, heaters #3, #4, and #5 were measured before and after testing, and heater #6 was only measured before testing. The results are presented in appendix 6.

5a, d, e, f

The lower end of the heater assembly consisted of a "lower copper fitting" with a $\frac{1}{2}$ -13 thread on the lowest end, a 0.25" socket on the upper end, and a flange with wrench flats in the center. The 0.25" diameter round "lower copper lead" was soldered into the socket of the "lower copper fitting". The upper 0.125" (3.2mm) of the "lower copper lead" had a reduced diameter for a slight interference fit into the bottom of the heater element. The heater element was soldered onto this boss. The rod was then filled with approximately 10 grams of tightly packed vermiculite. Two 0.02" (0.51mm) diameter holes were then drilled into the vermiculite, from the top of the heater rod, at the outside edge of the vermiculite, 0.5" (12.7mm) deep as measured from the end of the rod, at azimuthal angle of 180 degrees relative to each other.

The top of the heater assembly consisted of a 0.625" (15.9mm) outside diameter "upper copper tube" with a 0.121" (3.1mm) wall and a length of approximately 19" (483mm). Beneath this, the "upper copper transition" fit into the "upper copper tube" on the top end, had a socket on the lower end to receive the upper copper lead, and a bore through of 0.094" (2.39mm) diameter. The upper copper lead was tubular, with a 0.25" (6.35mm) outside diameter, and 0.094" (2.39mm) inside diameter. The lower 0.125" (3.2mm) of the "upper copper lead" had a reduced diameter for a slight interference fit into the top of the heater element. These three components were soldered together and two Omega TJC 36-CAIN-020U-36 thermocouples of 0.02" (0.51mm) diameter with fiberglass sleeves were fed through the upper assembly from the top.

The tips of the thermocouples were forced into the drilled holes in the vermiculite packing, the lower end of the "upper copper lead" was pressed into the upper end of the heater element, and this final joint was soldered. With the heater assembly complete, 2 Belden (part number 83026 001) 16 gauge wires 0.0625" (1.6mm) outside diameter wires were soldered onto the copper leads for voltage sensing to calculate actual power. All copper power conducting joints were soldered with Harris STAY-SILV white flux and Harris Saftey-Silv 56 solder, utilizing a

precision oxy-acetylene torch as the heat source. The two voltage sensing wires were soldered to the copper leads with Oatey No. 95 lead free tinning flux and Sn63/Pb37 solder utilizing the same heat source as above.

Test Section:

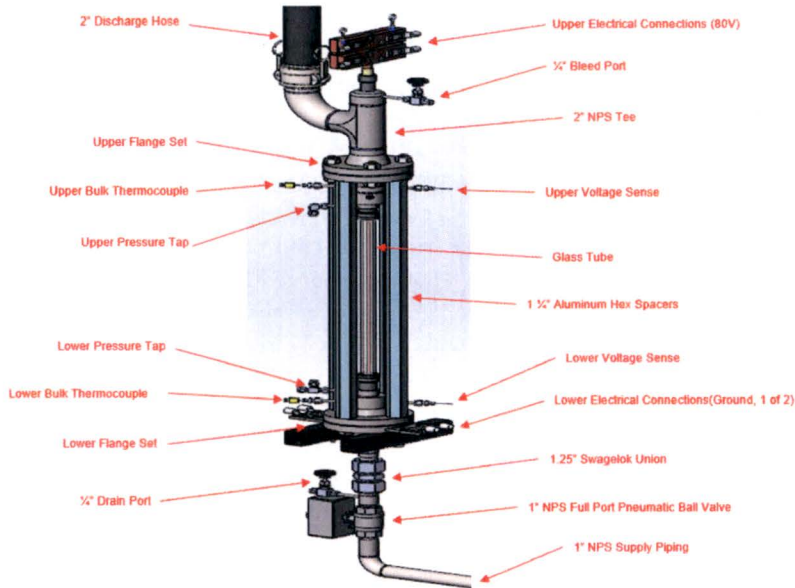


Figure 8: Labeled Solid Rendering of Test Section



Figure 9: Picture Test Section

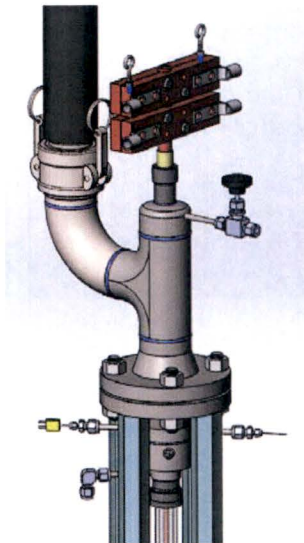


Figure 12: Rendering of Top of Test Section

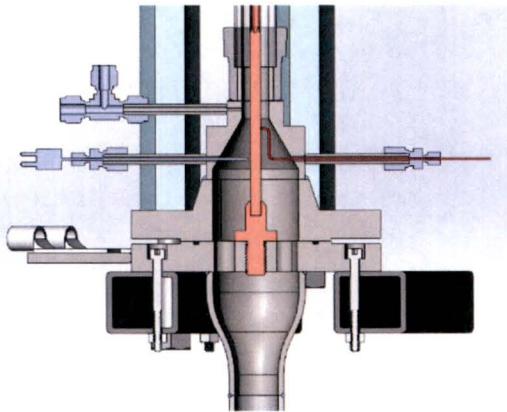


Figure 11: Cut-away of Lower Test Section

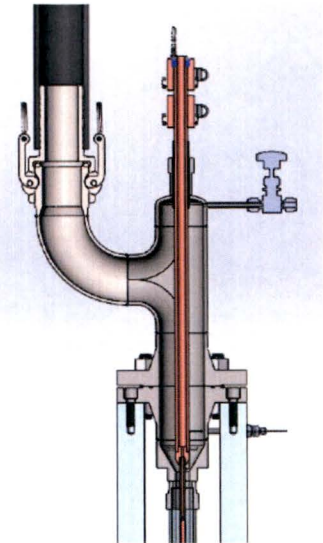


Figure 10: Cut-away of Upper Test Section

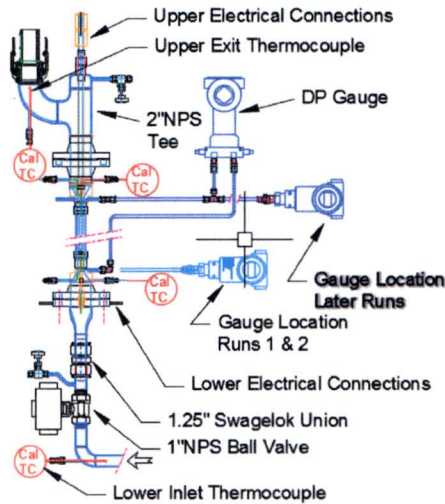


Figure 13: Labeled Diagram of Test Section

Water is supplied to the test section from the bottom via a horizontal 1" NPS schedule 40 pipe. As the flow approaches and flows through the upward turning long radius 1" NPS elbow, it passes around the lower inlet thermocouple. This was a calibrated thermocouple, manufactured by Omega, model number KMQ316SS-125U-12-CAL-3, ID# OM-121123315-2, 0.125" (3.2mm) diameter, k-type, sheathed, and ungrounded, inserted to a minimum in-pipe depth of 2" (51mm).

Once through the elbow, the flow passed through a 1" NPS full port ball valve and then through a 1.25" tube size union. From the union, the flow proceeded upwards through a 1" NPS – 2" NPS schedule 40 reducer (used as diffuser). The large end of this reducer was directly welded to the custom 2" NPS, 150# blind flange. This custom blind flange contained a 1/2-13 tapped hole in the center to receive the lower end of the test section and 4 ports machined through to allow water flow. Additionally an O-ring groove was machined into the blind flange to allow sealing to the mating flange, and two stainless lugs were welded to the outer rim to allow electrical connections.

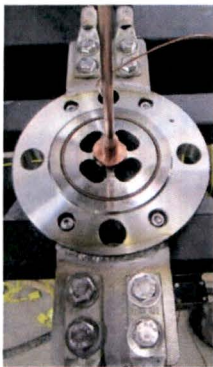


Figure 15: Picture of Lower Flange



Figure 14: Picture of Lower Flange

A weld neck 2" NPS 150# flange was fixed above with 4 bolts. A custom reducer was directly welded to this flange. This custom reducer was machined with a large diameter of 2.067" (52.5mm) to match the lower flange, a small diameter of 0.656" (16.66mm) to match test section, and an included angle of 60 degrees on the taper. In the tapered section, this reducer had four equally spaced radial ports tapped 6-32 for rod locating pins. At this same elevation, two additional ports 0.125" (3.2mm) diameter were equally spaced between the locating pin ports. These two ports were utilized for the voltage sensing wire and the near rod inlet thermocouple. The near rod inlet thermocouple was inserted so the tip was approximately 0.125" (3.2mm) from the "lower copper lead" leaving approximately 0.56" (14.2mm) wetted length. This

calibrated thermocouple was manufactured by Omega, model number KMQ316SS-062U-18-CAL-4-3P, ID#OM-121123377-1, 0.0625" (1.59mm) diameter, k-type, sheathed, and ungrounded.

This reducer also contained a 0.656" (16.66mm) diameter throat section. A 0.0625" (1.59mm) diameter hole was drilled in this throat section to allow for the pressure tap at the inlet conditions. To allow for acceptable sealing to the glass tube a custom Ultra-Torr O-ring type fitting was welded directly to the small end of the tapered section. This fitting was modified so the through bore matched the glass tube inside diameter.

The outside of the test section was made from a glass tube to allow flow visualization. Six of these precision bore borosilicate glass tubes were purchased from Wilmad-Labglass/SP Scienceware, part number P-656-985-0-28. The bore on this glass was

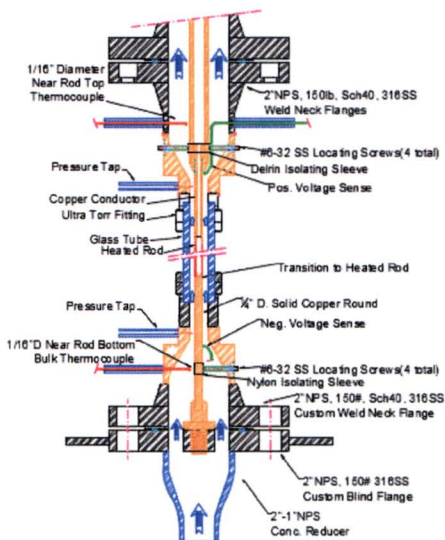


Figure 16: Labeled Diagram of Test Section

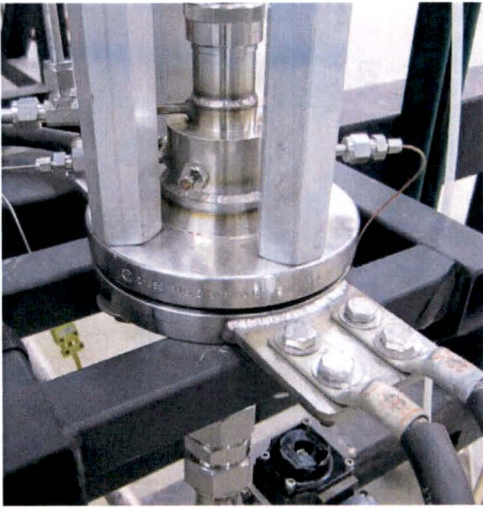


Figure 17: Picture of Lower Test Section

specified at 0.656 [REDACTED] (16.66 [REDACTED] mm) and the outside diameter was specified at 0.985" (25.02mm). The inside diameter was measured with a telescoping gauge and micrometer and found to be within the factory specification. The glass tube was cut on a diamond saw to the desired length and the ends were flame polished before assembly into the test section.

At the top end of the glass an identical Ultra-Torr fitting was used to seal. This fitting was directly welded to a custom taper section similar to the one located at the entrance to the rod. The upper taper section again had the pressure tap machined in the throat, the four radial holes in the taper to accommodate locating screws (to keep the rod centered), identical diameters, and identical taper angle. A 2" NPS, 150#, schedule 40 bore weld neck flange (with O-ring groove) was directly welded to the large, upper end of the custom taper section.

Two 0.125" (3.2mm) diameter radial ports were machined into the neck of this flange. One port was utilized for the voltage sensing wire,

while the near rod exit thermocouple was inserted into the other port. This thermocouple was inserted so the tip was approximately 0.125" (3.2mm) from the "upper copper lead" leaving approximately 0.79" (20.1mm) wetted length. This calibrated thermocouple was manufactured by Omega, model number KMQ316SS-062U-18-CAL-4-3P, ID#OM-121123377-2, 0.0625" (1.59mm) diameter, k-type, sheathed, and ungrounded.

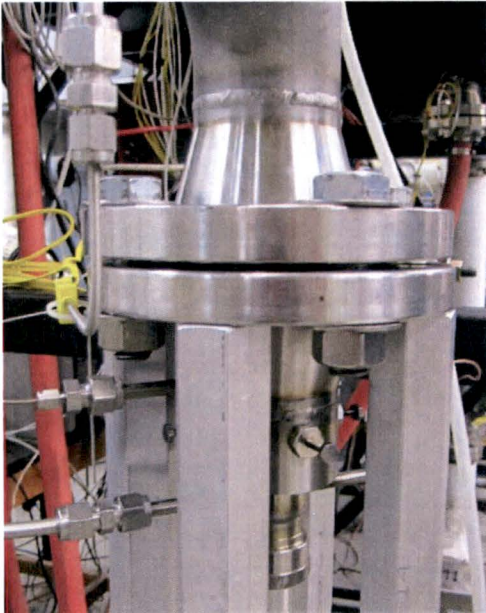


Figure 18: Picture of Upper Test Section

An additional mating 2" NPS weld neck flange was fixed to the above assembly with four bolts. A 2" NPS schedule 40 butt weld tee, through end, was welded to the pipe end of this flange. A cap was welded to the upper end of this tee. The cap had a hole bored through the end and a custom fitting welded on top to both seal and electrically isolate the upper copper tube of the heater rod assembly. The branch of this tee had an upward turning 90-degree long radius butt weld elbow, directly welded on. As the water flowed through this tee it flowed around the upper exit thermocouple. This was a calibrated thermocouple, manufactured by Omega, model number KMQ316SS-125U-12-CAL-3, ID# OM-121123315-1, 0.125" (3.2mm) diameter, k-type, sheathed, and ungrounded, inserted to a minimum in-pipe depth of 2" (51mm). A 2" hose camlok fitting was directly welded to the top of this elbow to return flow to the tank.

The thermocouple readings of the DAQs were verified via a calibrated Omega HH506A thermocouple reader, with a maximum error of 0.3 C.

Optical Imaging:

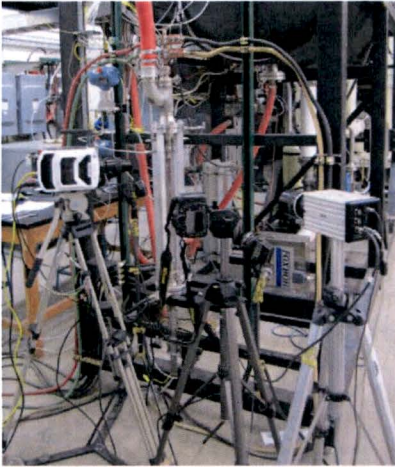


Figure 19: Picture of Experimental Set-up

The heater rod was enclosed in a borosilicate glass tube to allow optical imaging of void generation and critical heat flux events. The glass tube length and location allowed imaging on the entire length of the heated surface. Imaging was conducted with three cameras. The first was a Nikon D7000 SLR with a 105mm Nikkor micro lens. This was located approximately 4' (1.2m) from the test section and recorded standard video imaging of testing at 24 frames per second as well as still images. The second camera was an Integrated Design Tools Incorporated (IDTI), model HS3-M-4, serial number 23-0405-0007, high speed video camera, with a Nikkor 105mm lens. This camera was also located approximately 5' (1.5m) from the test section, and recorded a large portion of the heater rod at 500 frames per second. The third camera was an Ametek Phantom model v1211, serial number 18092, high speed camera with a similar 105mm micro lens used for near imaging a small portion of the rod for detail. The lens of this camera was located approximately 8.75" (0.22m) from the test section and recorded at 12,696 frames per second. A pair of Lowel P2-10 Pro-Lights were used for illumination.

Power Supply:



Figure 22: Power Supply

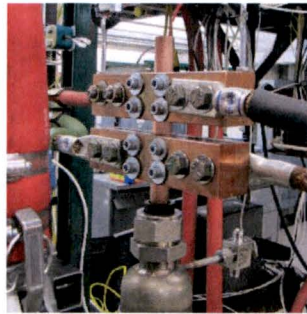


Figure 20: Upper Power Connection



Figure 21: Lower Power Connection

Power was provided to the heater element via a Miller PS-100, serial number JH249574 plasma spray power supply. The power supply is rated at 100% duty cycle for a maximum of 1200 amps direct current at 80 volts. The power supply was operated in controlled current mode. The current demand signal was manually entered into the National Instruments DAQ program by the operator (excepting first two experiments where an auto stepped ramp was used). Current was carried from the negative lead of the power supply, through a calibrated shunt, and to the bottom of the heater via four 3/0 welding cable wired in parallel. Current was carried from the positive lead of the power supply directly to the top of the heater rod via four 4/0 copper welding cables wired in parallel. Current was measured with a calibrated shunt provided by Ram Meter, model 22M, serial#SR0005420, 1200amp, 50mv. The voltage signal output of the shunt was measured with a calibrated Agilent 34401A multimeter and confirmed with the signal generated by the National Instruments DAQ to better than 1% accuracy. Heater voltage for rod power calculations was measured at the upper and lower copper leads. This voltage was divided across two identical 4.62 k ohm resistors, with the resulting (half of full scale) voltage sent to the National Instruments DAQ. The actual voltage signal was measured with the same multimeter and confirmed with the signal generated by the National Instruments DAQ to better than 1% accuracy.

Pressure Measurements:



Figure 23: Pressure Transducers

Two pressure sensors were used in this experiment. A calibrated Rosemount delta pressure transmitter, part number 3051S1CD4A2E12A1AM5Q4, serial number 0887364 was utilized to measure the pressure drop across the test section. Both pressure taps were placed in the throats of the reducing sections both prior to and after the test section. The lines to both sides of this gauge were bled of air before experiments to result in a reading of zero when flow was stopped. A calibrated Rosemount pressure transmitter, part number 3051TG3A2B21AQ4M5, serial number 16114932 was utilized to measure the gauge pressure. This transmitter was tied to the entrance pressure tap for the first two experiments, and tied to the exit pressure tap for the subsequent experiments. In both locations it was mounted in the same horizontal plane as the pressure tap it was connected to. The zero on this transmitter was verified when it was vented to ambient conditions. The range on the delta pressure transmitter was set to 10 psi [68.9kPa], resulting in a calculated accuracy of +/- 0.11 psi [0.765kPa]. The range on the gauge pressure transmitter was set to 50psig [345kPa], resulting in a calculated accuracy of +/-0.06psi [0.414kPa].

Void Fraction Measurements:



Figure 24: Initial Image

Void fraction measurements were conducted at 11 distinct experimental conditions. To complete these measurements, 10 frames were chosen from available data to analyze. These frames were not consecutive, but were chosen on basis of maximum image contrast between the background (rod) and the bubbles. The first step in the analysis was to determine the actual distance represented per image pixel, which was based on the 0.25" diameter heated rod and scaled images. Once this relationship was determined, the image was cropped to a large fraction of the rod diameter in width and approximately 4mm in height. This image file was then converted to an RGB type for recognition in ImageJ software. The recognition software was run on the image to recognize the edges of bubbles. Any not noted by the software were manually drawn in to the image. This edge data was then imported into an excel file and converted to volume based on the assumption of a circular/spherical bubble volume. This calculated volume of gas was then referenced to the volume of liquid in the analysis area.

5a, d, e, f



Figure 25: Cropped Image

In addition to this analysis a bubble velocity was also calculated. This velocity calculation was accomplished by determining the number of consecutive images required for a bubble to traverse the imaged frame. This time was recorded for ten bubble traverses and averaged for the final result. Void and velocity were only conducted on images with small bubbly flow at low heat flux.

5a, d, e, f



Figure 26: Image with Edges

Results of void fraction estimates along with images are presented on the following pages. For all examined conditions, the void fraction did not exceed [redacted], and in general were much lower. The void fraction measurements followed logical trends except for the bottom to mid change on the nominal [redacted] run on 02/21/17. It is assumed the error in our measurements were greater than the change in void fraction between those two conditions.

5a, d, e, f

5a, d, e, f



Figure 27:1/5/17
10:56



Figure 28:1/5/17
11:16

5a, d, e, f

Table A: Void Fraction Measurements, Early Experiments

Date/Time	Heat Flux Mw/m ²	Location on rod	Pressure psig	DP psi	Inlet Press [kPa abs]	Out Press [kPa abs]	m_dot [kg/sec]	Mass Flux [kg/(s*m ²)]	Av. Bubble Diameter[mm]	Bubble Diam Std. Dev[mm]	Volume Void Fraction	Avg Vel. [m/s]	Inlet Temp [C]	Exit Temp [C]
1/5/17-10:56														
1/5/17-11:16														
1/26/17-16:59														
1/30/17-10:56														
2/9/17-11:32														

5a, d, e, f

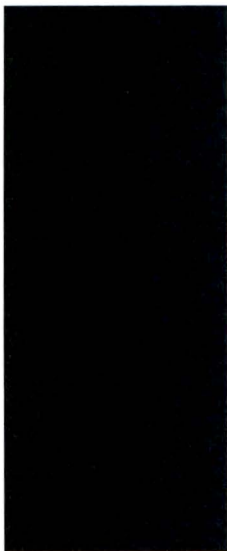


Figure 31:1/5/17
16:59



Figure 29:1/30/17
10:56



Figure 30:2/9/17
11:32

5a, d, e, f



Attachment 10



Figure 32:2/21/17
10:23



Figure33:2/21/17
10:45



Figure 34:2/21/17
11:08

5a, d, e, f

Table B: Void Fraction Measurements, Later Experiments

Date/Time	Heat Flux Mw/m ²	Location on rod	Pressure psig	DP psi	Inlet Press [kPa abs]	Out Press [kPa abs]	m_dot [kg/sec]	Mass Flux [kg/(s*m ²)]	Av. Bubble Diameter[mm]	Bubble Diam Std. Dev[mm]	Volume Void Fraction	Avg Vel. [m/s]	Inlet Temp [C]	Exit Temp [C]
02/21/17-10:23														
02/21/17-10:45														
02/21/17-11:08														
02/21/17-11:46														
02/21/17-11:35														
02/21/17-11:27														

5a, d, e, f

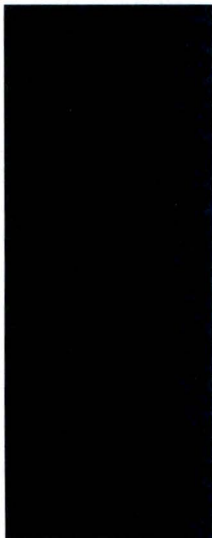


Figure 35:2/21/17
11:46

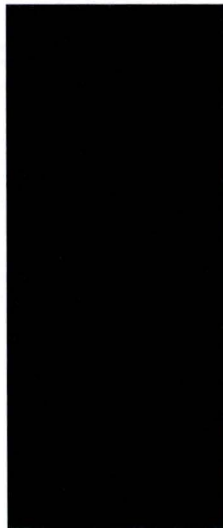


Figure36:2/21/17
11:35



Figure 37:2/21/17
11:27

5a, d, e, f

Experimental Operation:

Operation of the University of Wisconsin, Thermal Hydraulics Lab critical heat flux test rig involves a number of procedures that are outlined in more detail in Appendix 2. For the purpose of describing the operation for each individual test, an abbreviated operational procedure will be outline here:

1. Fill reservoir with deionized water to level slightly above test section return port
2. Energize glycol chiller for heat exchanger cooling
3. Turn on heat exchange pump to flow reservoir water through heat exchanger
4. Open pneumatic ball valves at the entrance and exit of the test section
5. Energize and adjust primary pump to flow water through test section at desired mass flow rate
6. Use regulator to pressurize system to desired pressure level
7. Turn on heater rod power supply
8. Adjust power supply output to achieve desired heat flux
9. Adjust glycol flow through heat exchanger to maintain desired inlet water temperature
10. Follow test matrix until CHF or maximum power output ($9.6\text{MW}/\text{m}^2$) is reached

Test 1 – Heater Rod 1 - 01/05/17

Target Conditions: $T_{in} =$ [REDACTED], $P_{in} =$ [REDACTED], $G =$ [REDACTED]

5a, d, e, f

After initially pressurizing the system to ~ [REDACTED] at the inlet to test section, the bulk water in the reservoir needed to be changed from room temperature (~20°C) to the target inlet temperature of 31.1°C. This was accomplished by flowing water through the test section at a mass flow rate of [REDACTED] and increasing the power to the heater rod to ~ [REDACTED]. Once the target inlet temperature was reached, the glycol flow valve was partially opened to allow cold glycol from the roof mounted chiller to flow through the glycol-water heat exchanger. The glycol flow was adjusted until the heat removal matched the heat input from the heater rod indicated by a stable inlet temperature. At this point the power was increased to the heater rod until a heat flux of [REDACTED] was reached. Concurrent to this power adjustment, the cooling was increased to maintain the desired inlet temperature. Data was taken at these baseline conditions as well as various videos at select points in time. Once the baseline data and video was recorded, a critical heat flux run was completed.

5a, d, e, f

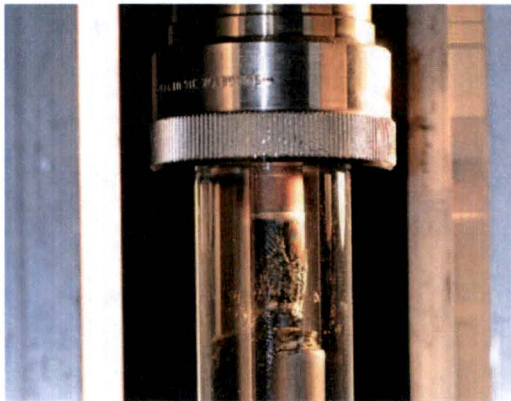


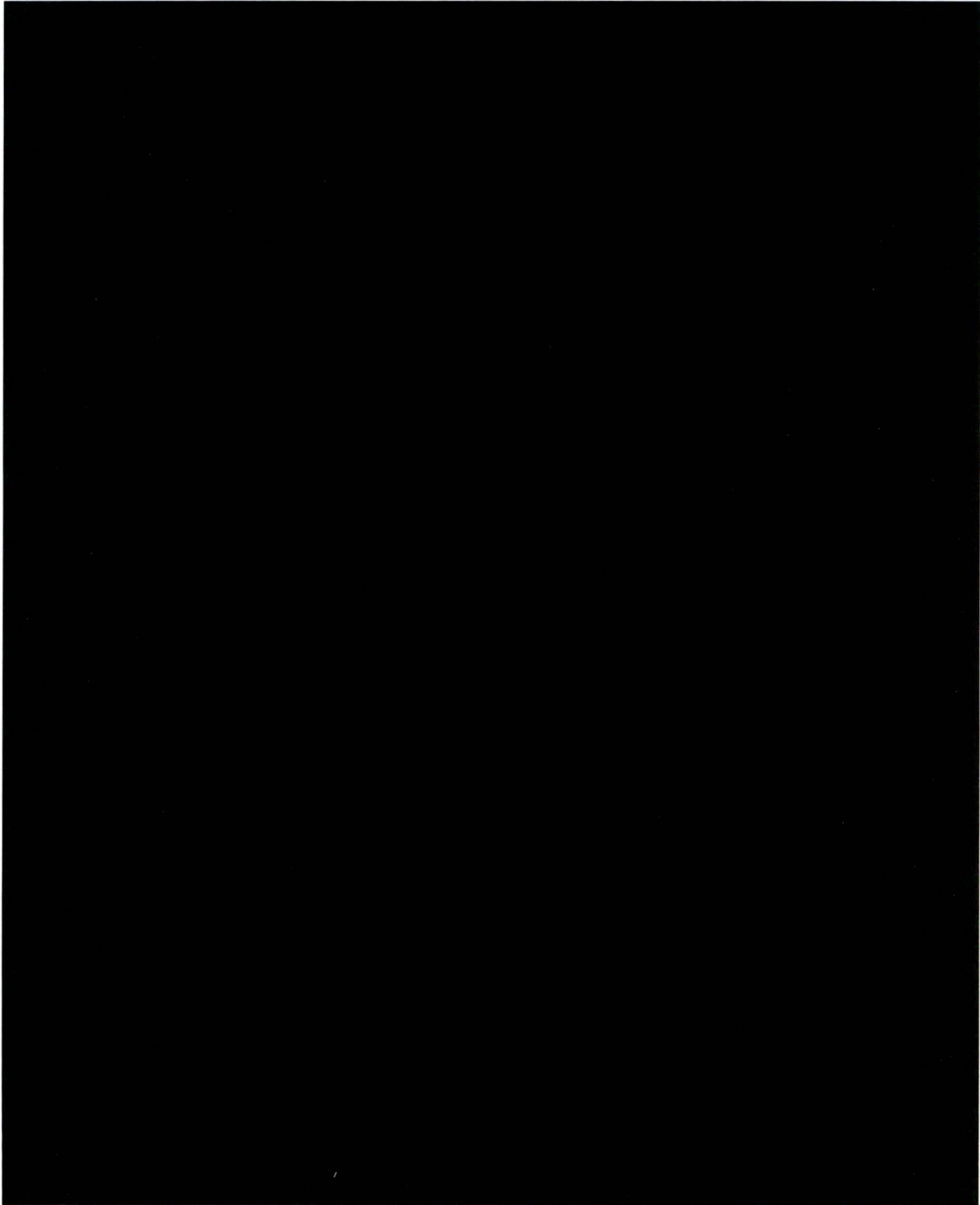
Figure 38: Failed Heater #1

The critical heat flux run was initiated at the baseline conditions of [REDACTED]. The rod power level was increased every 30 seconds by increments of ~1.25kW until CHF was observed or the maximum power level was reached. As the power level was increased, the glycol flow was also increased to maintain the desired inlet temperature. The pressure and mass flow rate were monitored and adjusted as necessary. Automatic triggers were used to initiate the high speed cameras in order to capture the CHF event. The IDTI HS#-M-4 camera utilized a thermal trigger that was based off two thermocouples placed inside the heater rod at the expected location that CHF would occur, ~1.3cm from the top of the heater rod. This thermal trigger was also used to shut down the heater rod power supply in an effort to save the heater rod from failure due to the CHF event. The Ametek Phantom camera was set to trigger off of either a flash of light which occurred at rod failure, or the same thermal trigger as the IDTI camera.

5a, d, e, f

Test 1 achieved critical heat flux at [REDACTED], 3.34% higher than the estimated CHF of [REDACTED] derived from the Groenveld LUT. Due to the unpredictable azimuthal location where CHF initiated, and the rapid nature of the CHF event, the power supply was not able to be shut down prior to the rod failing. Conditions at the highest heat flux prior to CHF as well as the conditions when CHF occur can be found in Table 1.

5a, d, e, f



5a, d, e, f

Figure 39: High Speed Video Images, Test#1



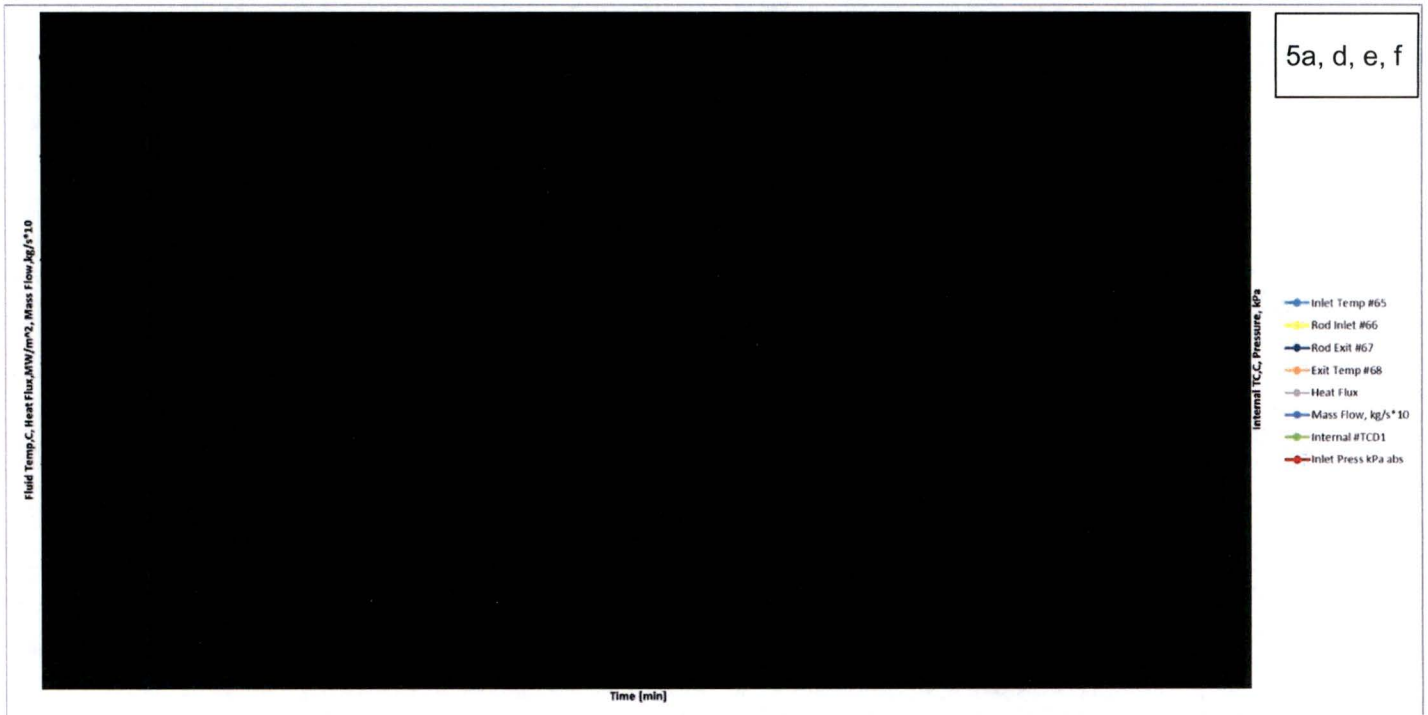


Figure 40: Data from Test#1, Stepped Power, Constant Inlet Temperature

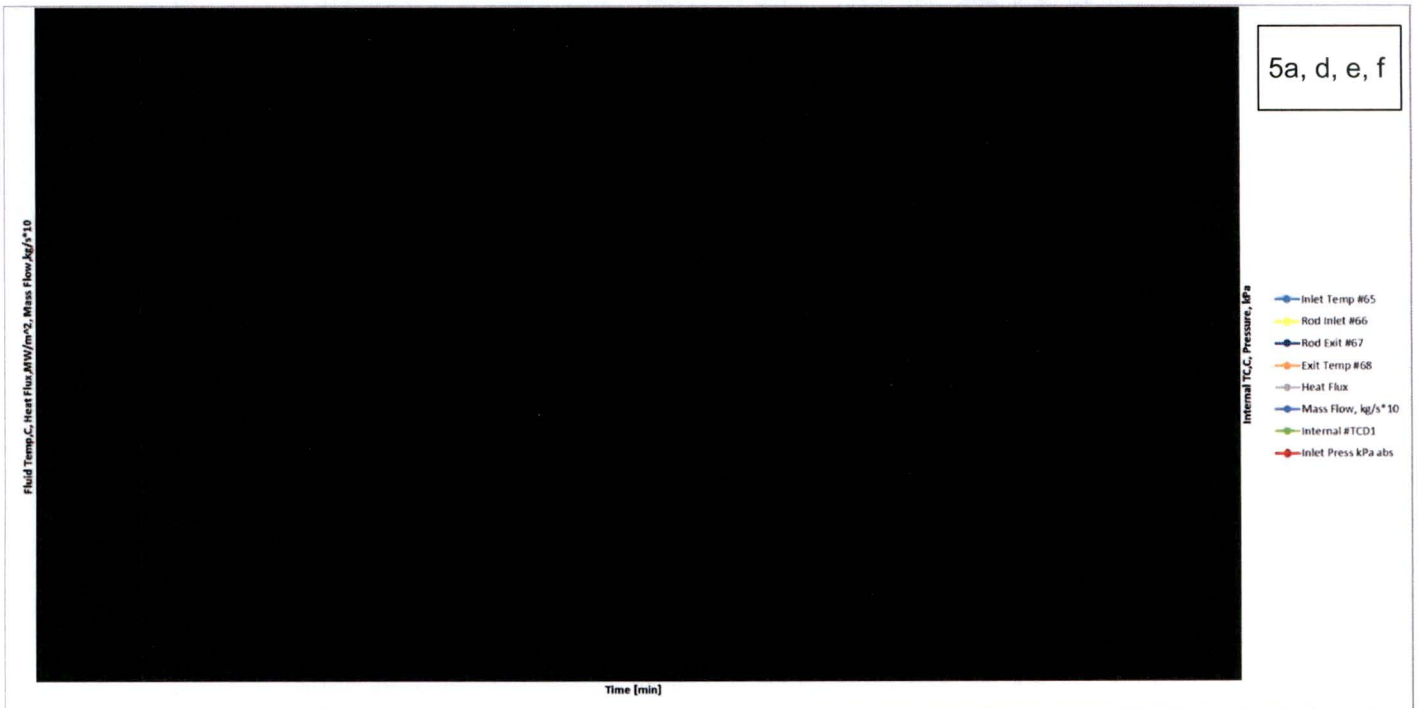


Figure 41: Data from CHF Event, Test #1



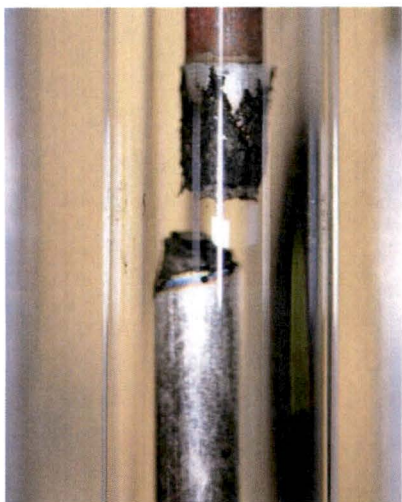
Test 2 – Heater Rod 2 – 01/11/17

Target Conditions: $T_{in} =$ [REDACTED], $P_{in} =$ [REDACTED], $G =$ [REDACTED]

5a, d, e, f

Test 2 was run in an identical fashion as test 1, except that the mass flux was reduced to from $5000\text{kg/m}^2\cdot\text{s}$ to $4250\text{kg/m}^2\cdot\text{s}$. This equated to a mass flow rate of 0.792kg/s . The test section was brought to the target conditions with a baseline heat flux of 3.4MW/m^2 and data was taken as well as low and high speed video.

Once the baseline data and video was recorded, a critical heat flux run was completed.



The critical heat flux run was initiated at the baseline conditions of [REDACTED]. The rod power level was increased every 30 seconds by increments of $\sim 1.25\text{kW}$, as before, until CHF was observed or the maximum power level was reached. As the power level was increased the glycol flow was also increased to maintain the desired inlet temperature. The pressure and mass flow rate were monitored and adjusted as necessary. Test 2 achieved critical heat flux at [REDACTED], 0.62% higher than the estimated CHF of [REDACTED] derived from the Groenveld LUT. As in test 1, the heater element failed before the power supply could be shut down. Conditions at the highest heat flux prior to CHF as well as the conditions when CHF occur can be found in Table 1.

5a, d, e, f

5a, d, e, f

Figure 42: Failed Rod #2

5a, d,
e, f

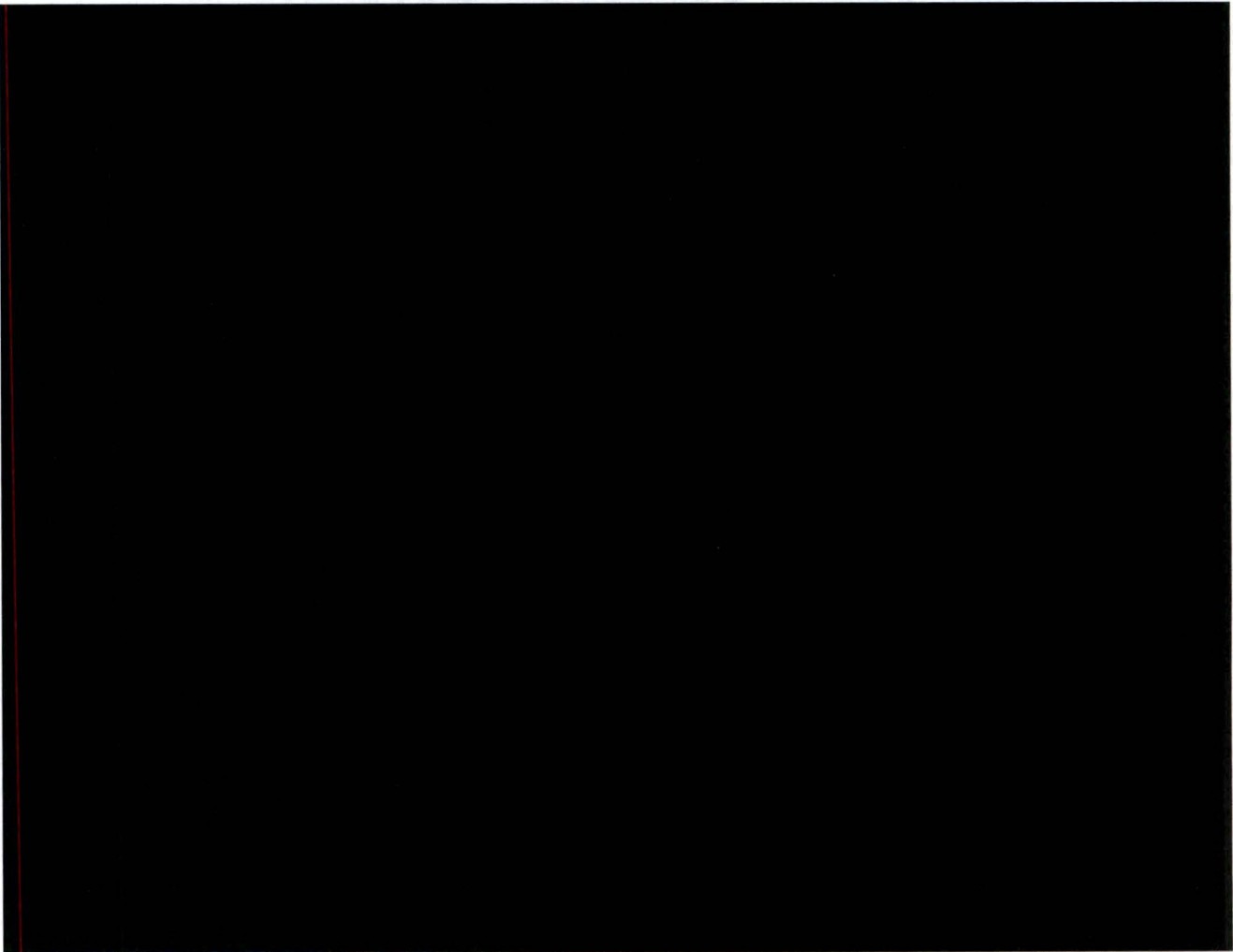


Figure 43: High Speed Video, Test #2



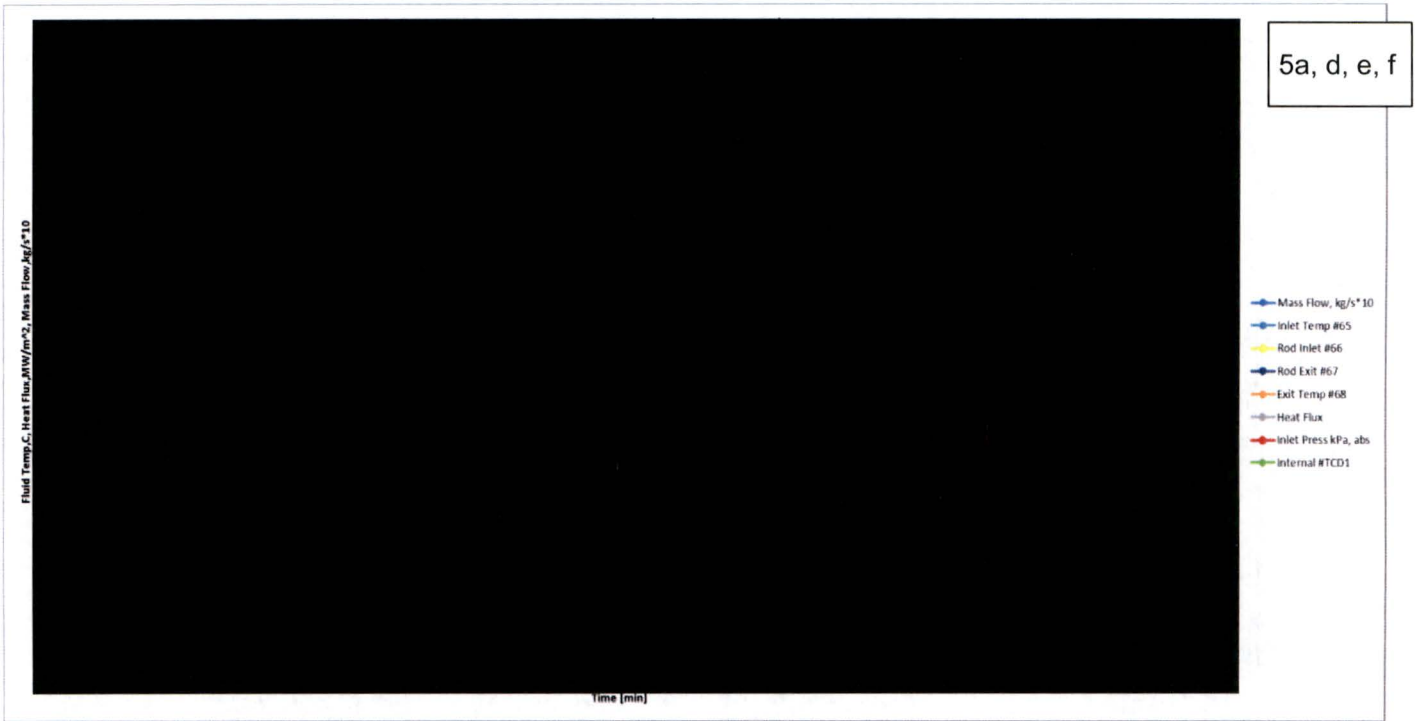


Figure 44: Data from Test #2, Constant Inlet Temperature, Stepped Power

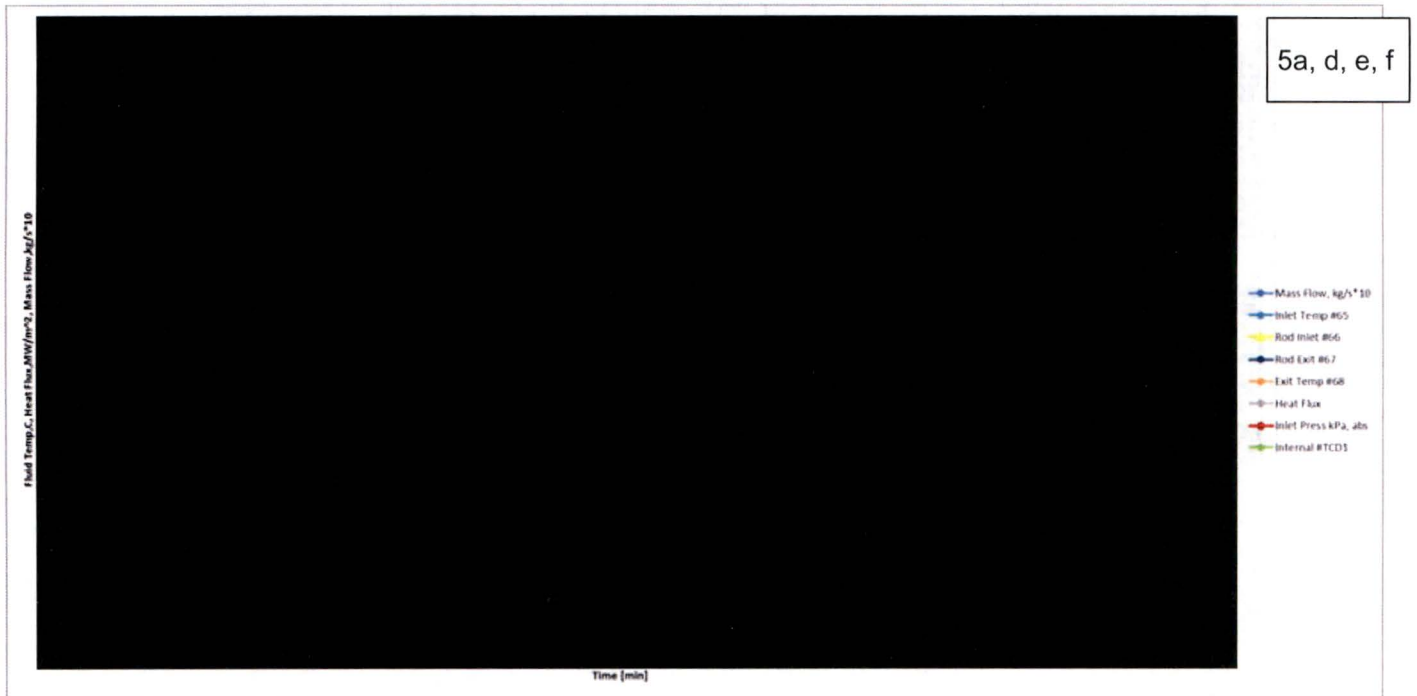


Figure 45: Data from CHF Event, Test #2



Test 3 – Heater Rod 3 – 01/28/17

Target Conditions: $T_{out} =$ [redacted], $P_{out} =$ [redacted], $G =$ [redacted]

5a, d, e, f

Upon completion of test 2, it was determined that adjusting the local conditions for the CHF event to match the local conditions of General Atomics system’s maximum heat flux was preferred. This translated to controlling the outlet conditions as opposed to inlet conditions. All subsequent testing was completed while controlling the outlet conditions. Significant sub cooling was required to maintain the desired outlet temperatures, as well as a change in how the test was performed. Instead of increasing the heater rod power output every 30 seconds while matching the cooling level to maintain the inlet temperature, the inlet temperatures would need to be pre-calculated for each desired heat flux and the reservoir temperature set accordingly. As the heat flux increased, the inlet sub cooling also needed to be increased. Due to this change, all future tests would need to be operated as individual constant heat flux runs, with heat flux increasing between runs, and inlet temperature lowered between runs. The test 3 matrix is shown in Figure 47. All future runs utilize the same progression in heat flux over 16 runs. Prior to test 3, but after test 2, the gauge pressure transducer was moved from the inlet of the test section to the exit of the test section.

After setting the system to a test section exit pressure of [redacted] for test 3, the bulk water in the reservoir needed to be changed from room temperature (~20°C) to the target inlet temperature of [redacted]. This was accomplished by flowing water through the test section at a mass flow rate of [redacted] and increasing the power to the heater rod to [redacted]. Once the target inlet temperature was reached, the glycol flow valve was partially opened to allow cold glycol from the roof mounted chiller to flow through the glycol-water heat exchanger. The glycol flow was then adjusted until the heat removal matched the heat input from the heater rod indicated by a stable inlet temperature. At this point the power to the heater rod was dropped to 0 to allow the inlet temperature to drop ~0.5°C below the desired inlet temperature. At this point the heater rod power was increased to a heat flux of [redacted]. The inlet temperature was then allowed to increase until it reached a value ~0.5°C above the desired inlet temperature. At this point the heater power was shut down and the inlet temperature was allowed to cool until ~0.5°C below the desired inlet temperature for run number 2 in the test matrix. The outlet temperature was also monitored to make sure that the desired outlet temperature was crossed during the run. Each subsequent run was completed in the same manner. Cooling was increased as the heat flux increased to limit the ramp rate of inlet and outlet temperatures. In a typical run the inlet and outlet temperatures would increase ~1°C over ~5 minutes.

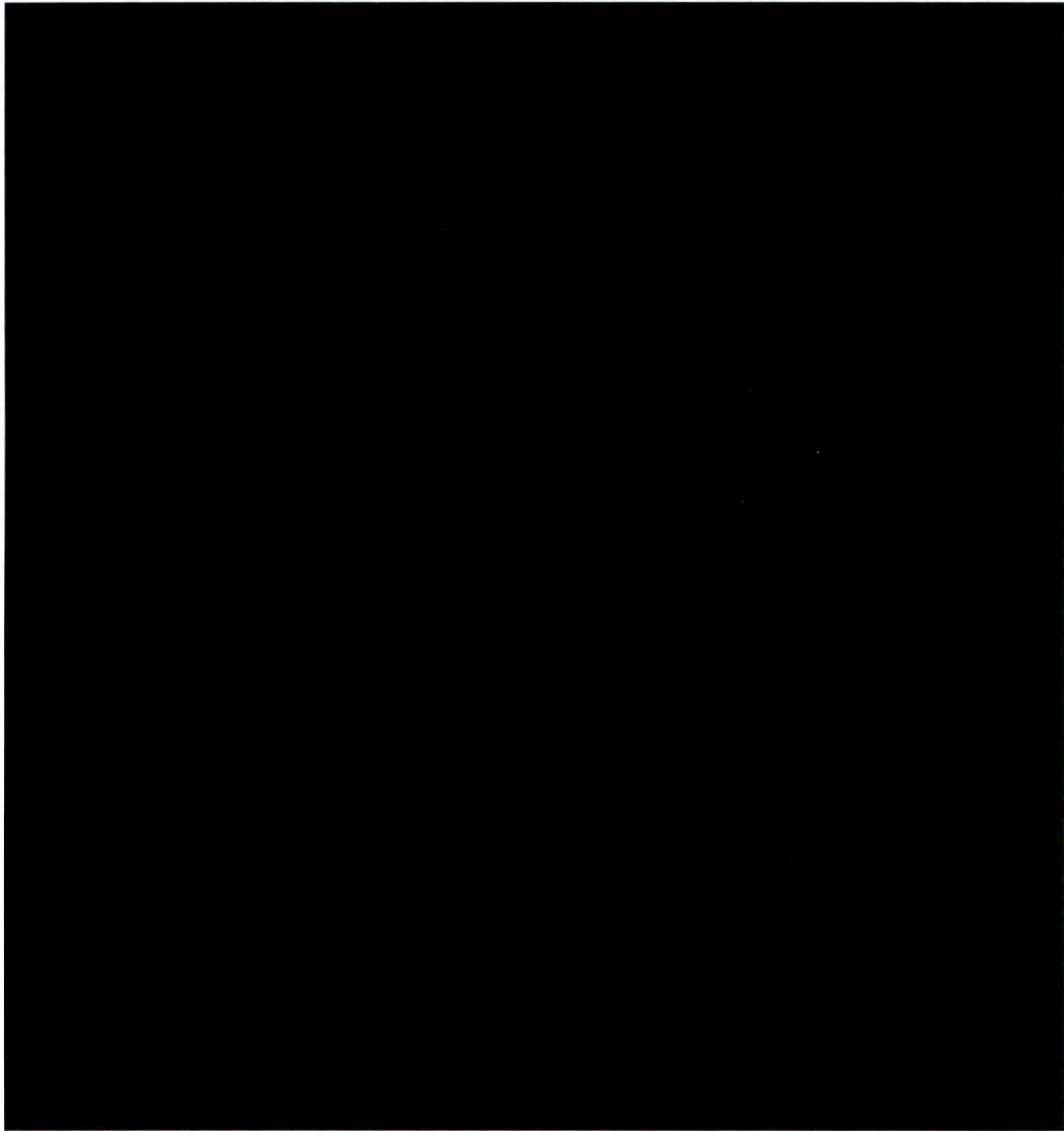
5a, d, e, f

5a, d, e, f

Test 3 did not achieve critical heat flux prior to reaching the maximum heat flux available of 9.6MW/m². This heat flux is 4.19% higher than the estimated CHF of [redacted] derived from the Groeneveld (2007) LUT. Conditions at the highest heat flux achieved for this run can be found in Table 1.

5a, d, e, f





5a, d, e, f

Figure 46: High Speed Video Images, Test#3



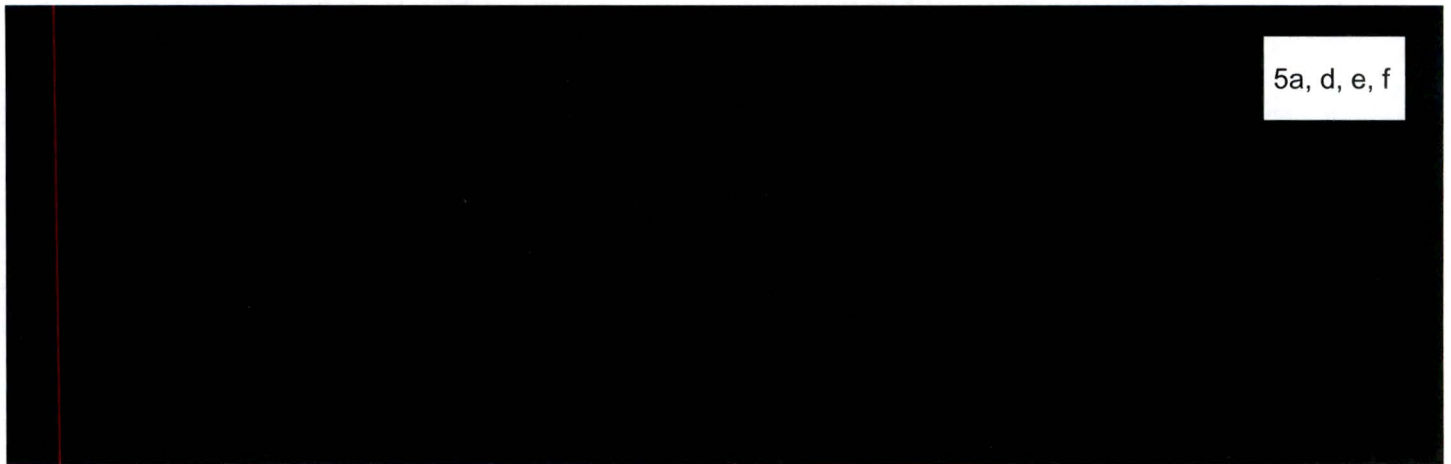


Figure 47: Experimental Matrix, Test #3

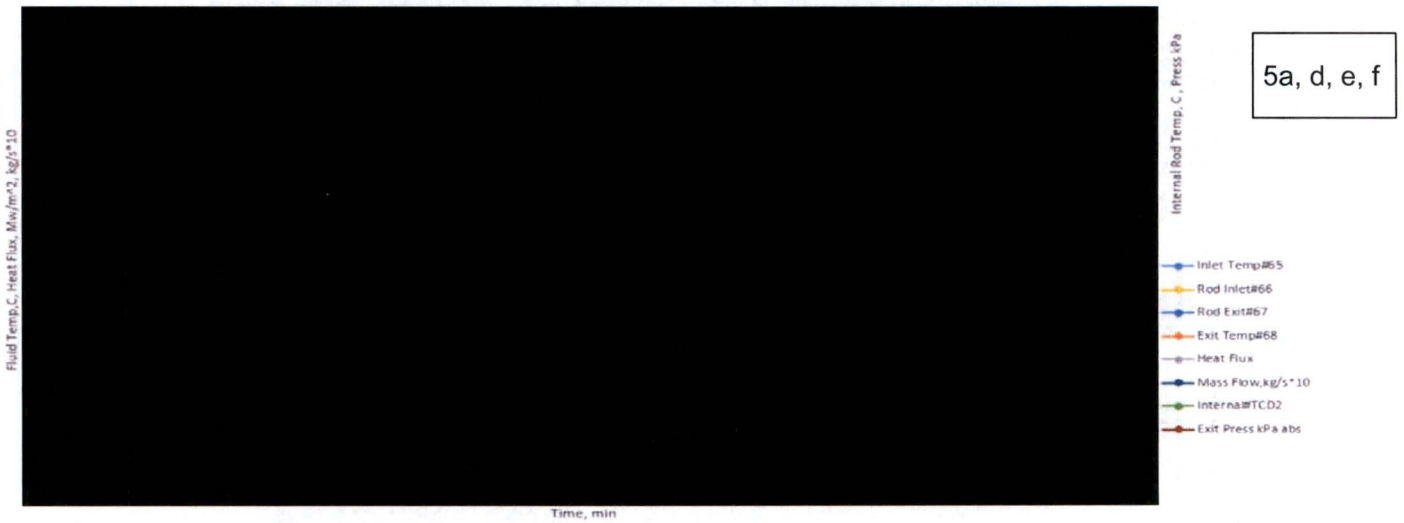


Figure 48: Data from Experiment #3, Constant Exit Temperature

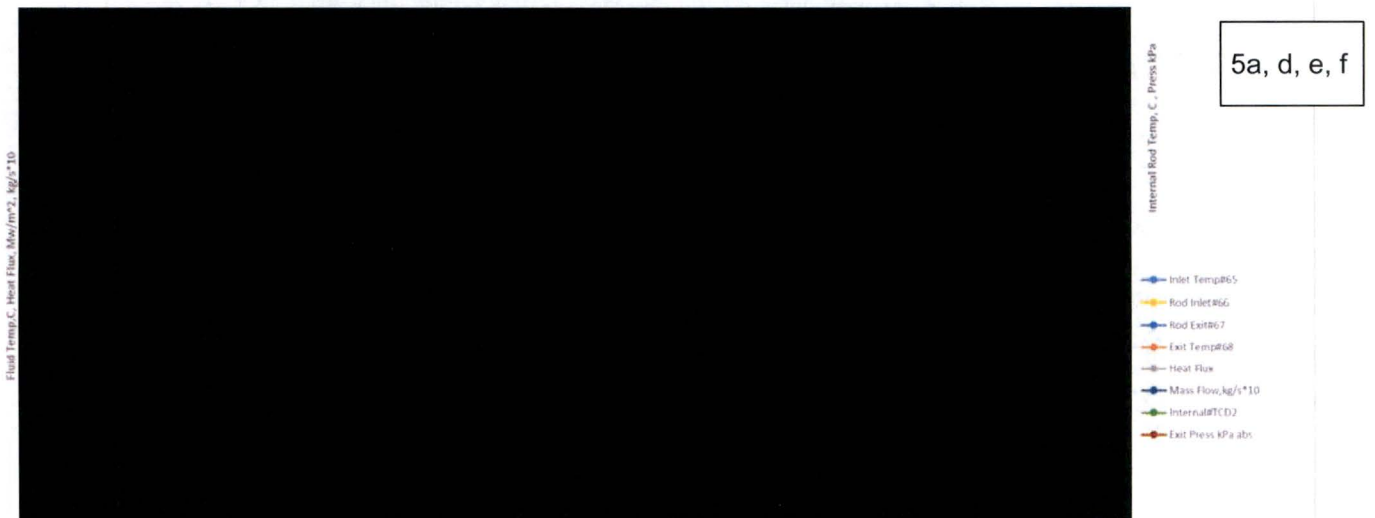


Figure 49: Data from Maximum Heat Flux Run

SAFER PRACTICES IN A NATION

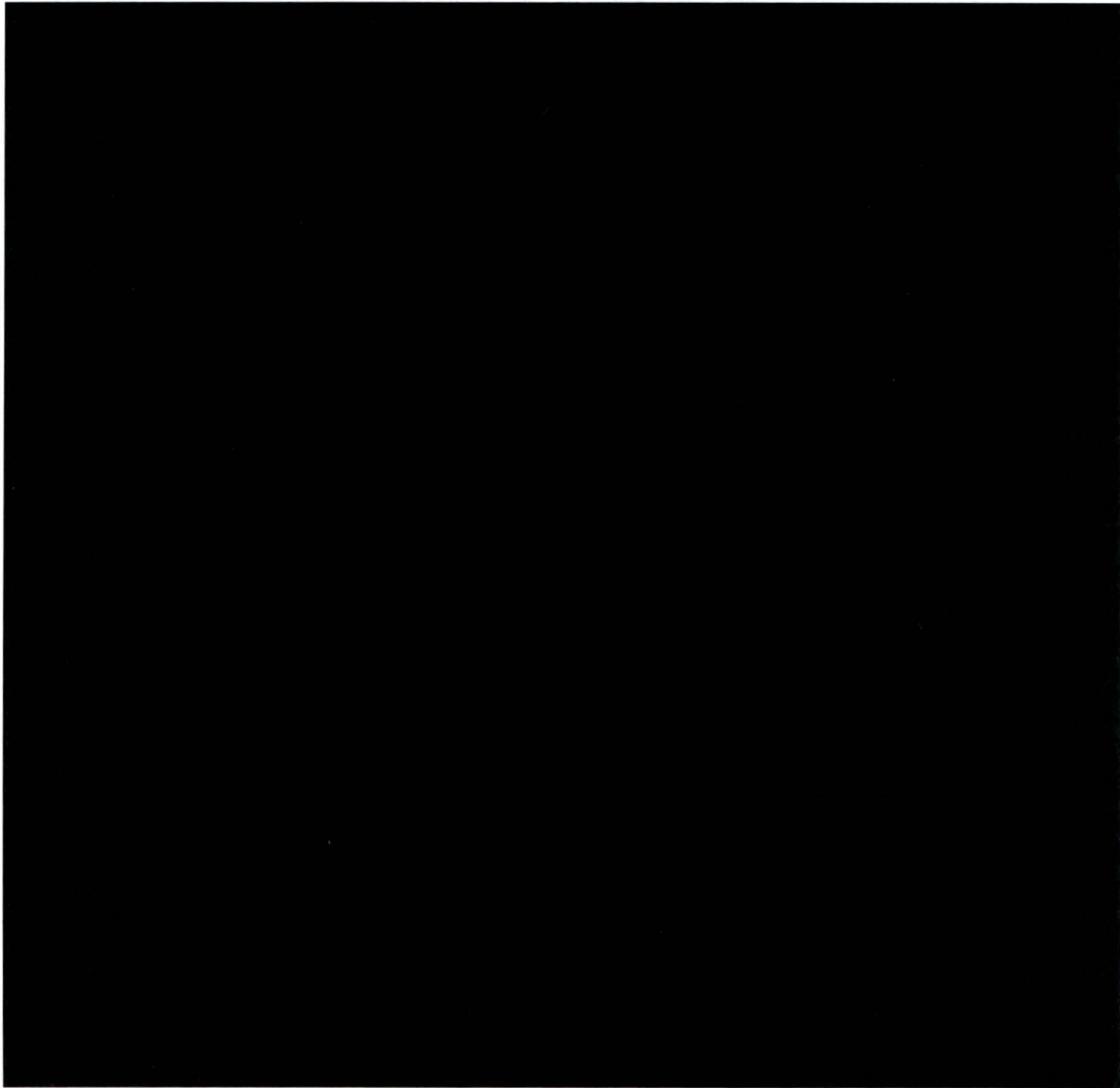
Test 4 – Heater Rod 3 – 01/30/17

Target Conditions: $T_{out} =$ [REDACTED], $P_{out} =$ [REDACTED], $G =$ [REDACTED]

5a, d, e, f

Test 4 was conducted employing the same method as test 3. The test section exit pressure was adjusted to [REDACTED], the mass flow was adjusted to [REDACTED], and the inlet temperatures were recalculated to achieve an outlet temperature of [REDACTED]. Test 4 did not achieve critical heat flux prior to reaching the maximum heat flux available of 9.6MW/m^2 . This heat flux is 11.3% higher than the estimated CHF of [REDACTED] derived from the Groeneveld (2007) LUT. Conditions at the highest heat flux achieved for this run can be found in Table 1.

5a, d, e, f



5a, d, e, f

Figure 50: High Speed Video Images, Test #4





Figure 51: Experimental Matrix, Test #4

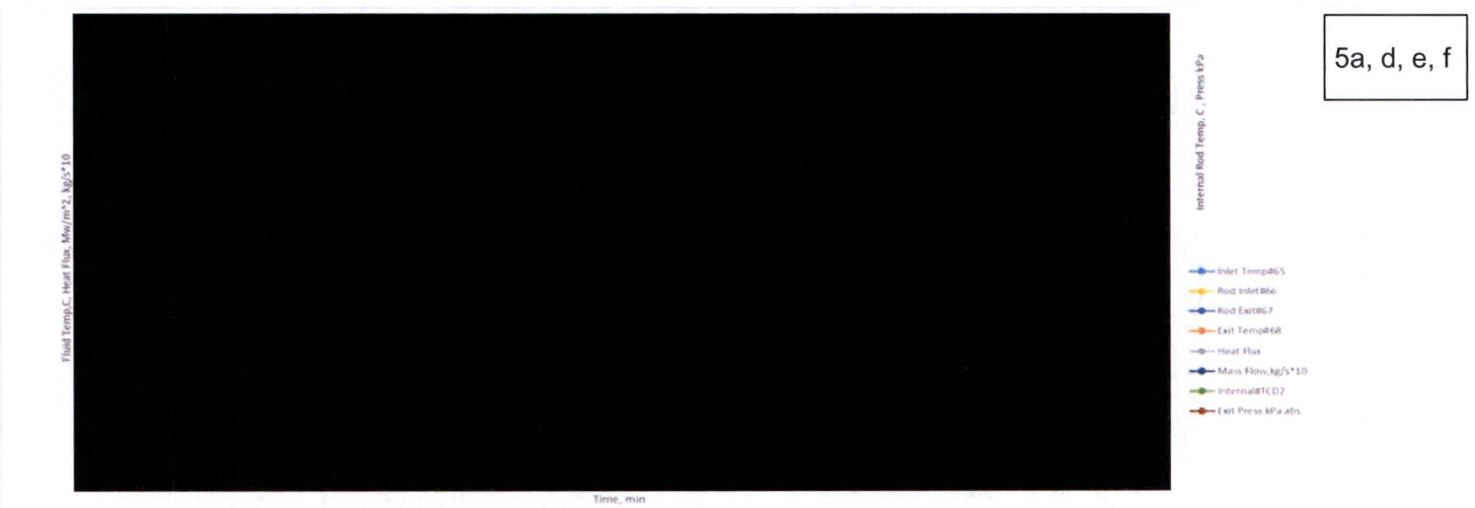


Figure 52: Data from Test #4, Constant Exit Temperature

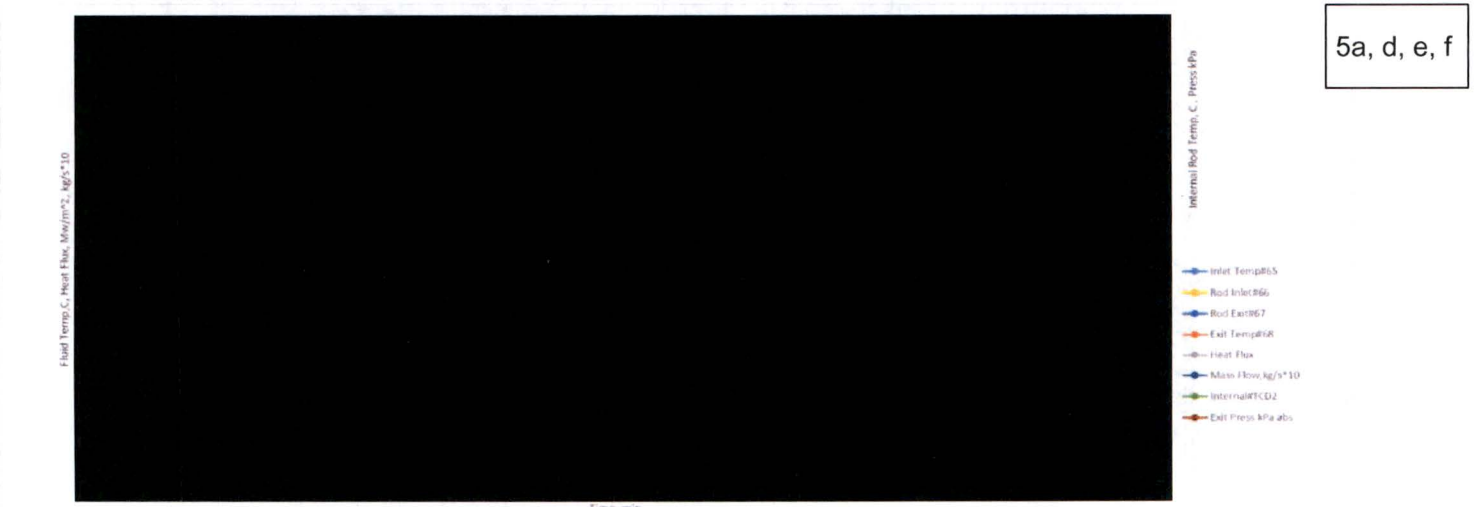


Figure 53: Data from Maximum Heat Flux Run, Test #4

UNIVERSITY OF WISCONSIN
Nuclear Engineering Center
3A PROGRESS / INNOVATION

Test 5 – Heater Rod 3 – 02/09/17

Target Conditions: $T_{out} =$ [REDACTED], $P_{out} =$ [REDACTED], $G =$ [REDACTED]

5a, d, e, f

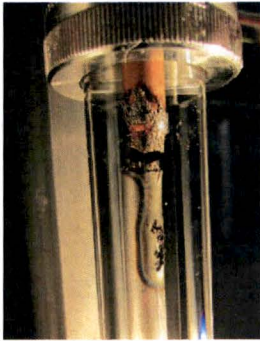
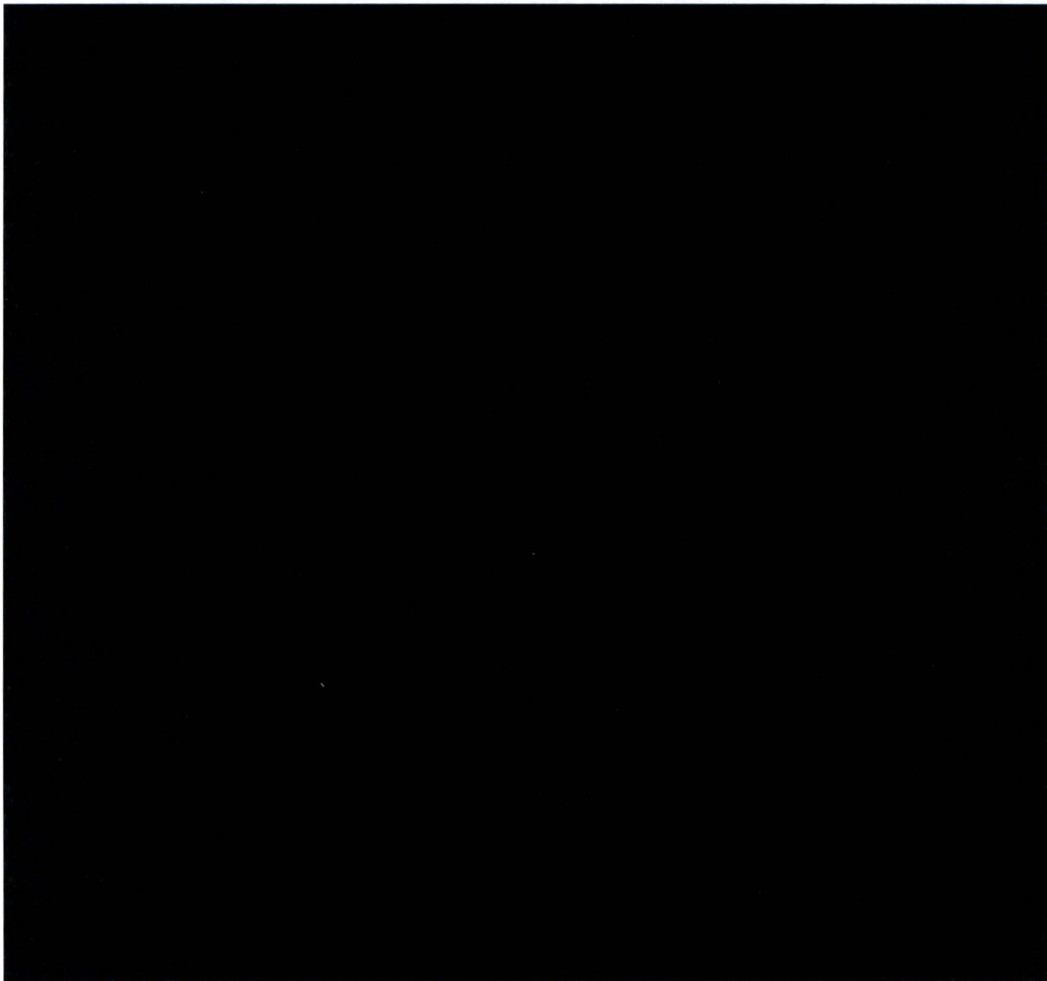


Figure 54: Failed Rod #3, After Test #5

Test 5 was conducted employing the same method as test 3 and 4. The exit pressure was adjusted to [REDACTED], the mass flow was adjusted to [REDACTED], and the inlet temperatures were recalculated to achieve an outlet temperature of [REDACTED]. Test 5 achieved critical heat flux at [REDACTED], 3.94% higher than the estimated CHF of [REDACTED] derived from the Groenveld LUT. The power supply was not able to be shut down prior to the rod failing during the CHF event. CHF appears to have initiated ~1cm down from the top of the rod burning a hole in the wall with the heater ultimately failing at the solder joint at the top of the rod. Conditions at the highest heat flux achieved prior to CHF as well as the conditions at which CHF occur can be found in Table 1.

5a, d, e, f



5a, d, e, f

Figure 55: High Speed Video Images, Test #5

[REDACTED]

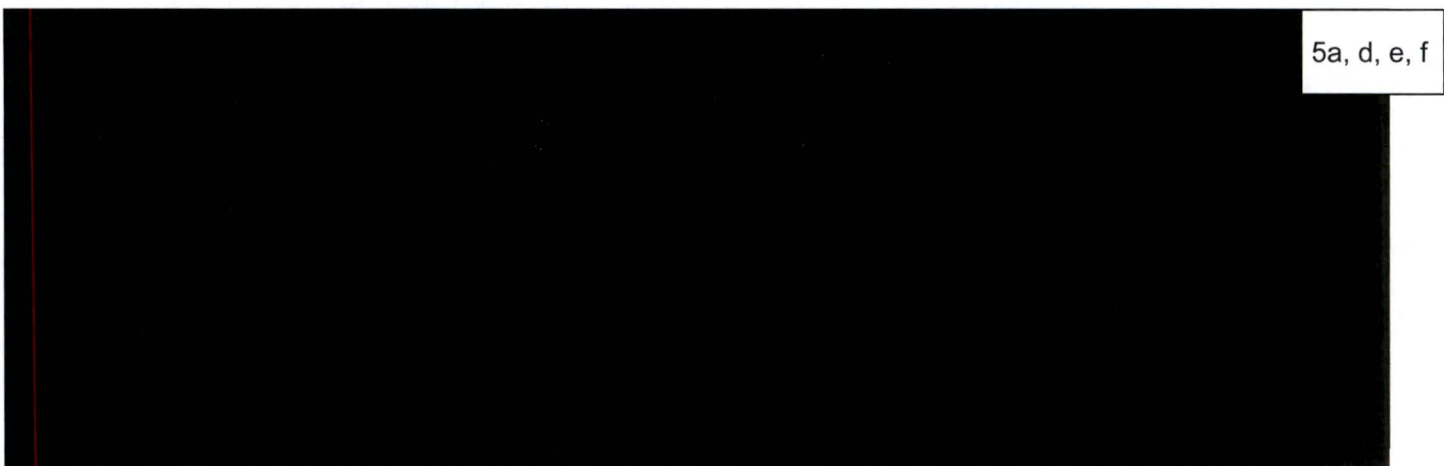


Figure 56: Experimental Matrix, Test #5

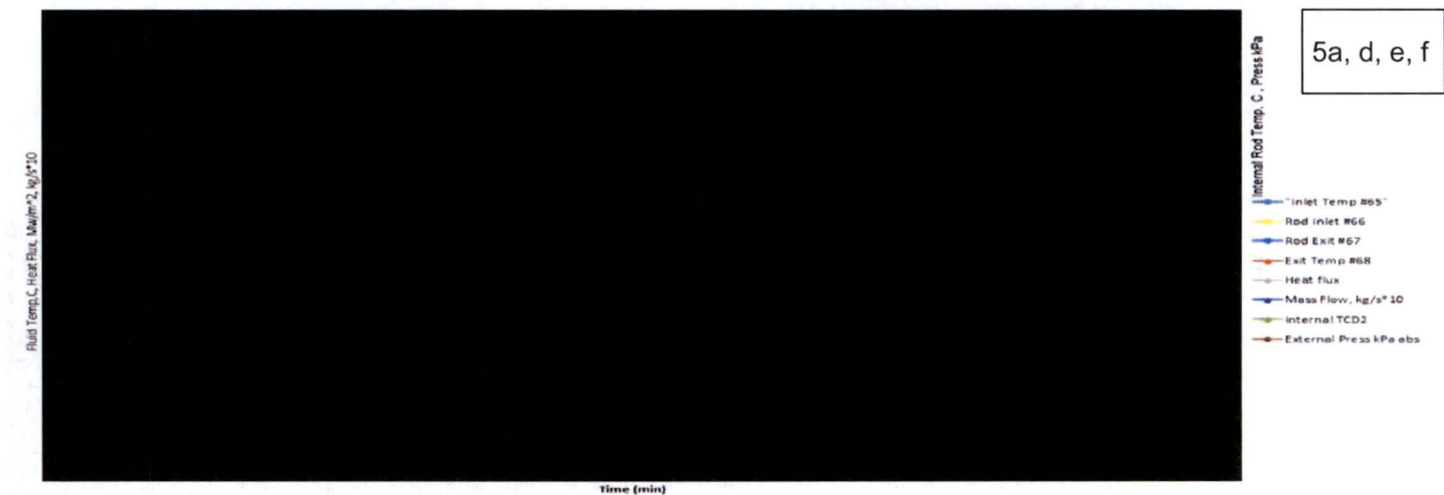


Figure 57: Data from Test #5, Constant Exit Temperature

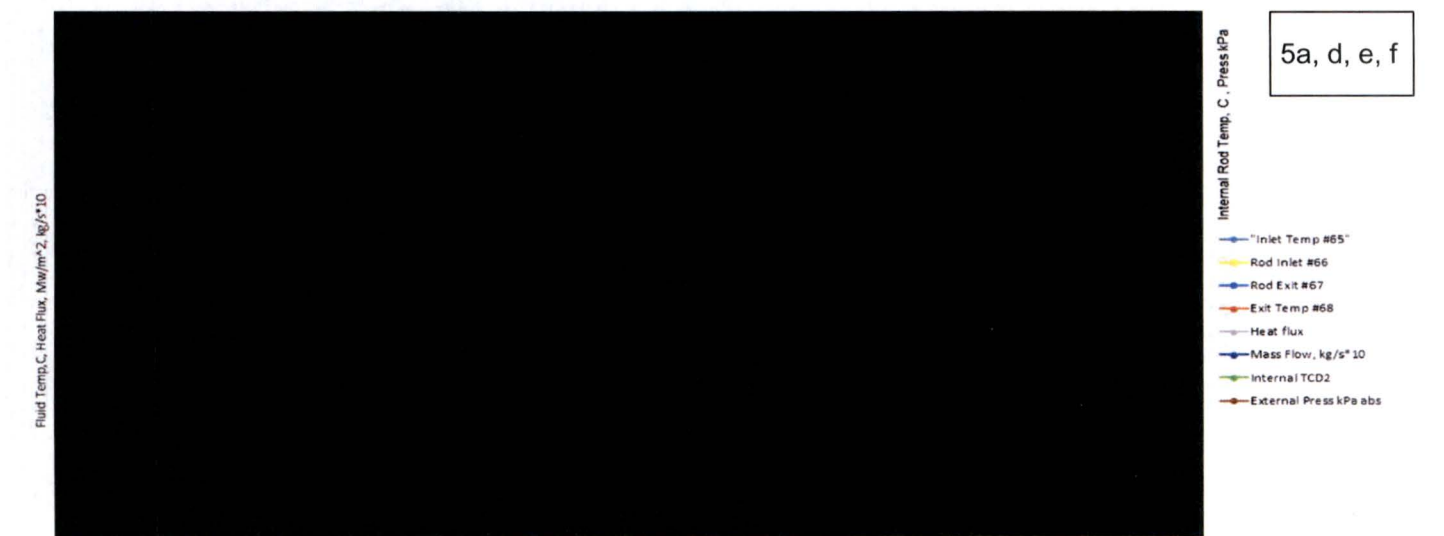


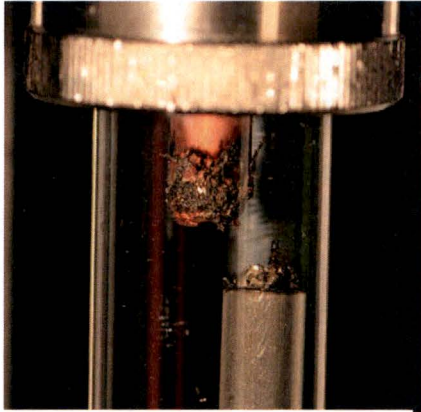
Figure 58: Data from CHF Event, Test #5

CONFIDENTIAL - NOT FOR DISTRIBUTION

Test 6 – Heater Rod 4 02/21/17

Target Conditions: $T_{out} =$ [REDACTED], $P_{out} =$ [REDACTED], $G =$ [REDACTED]

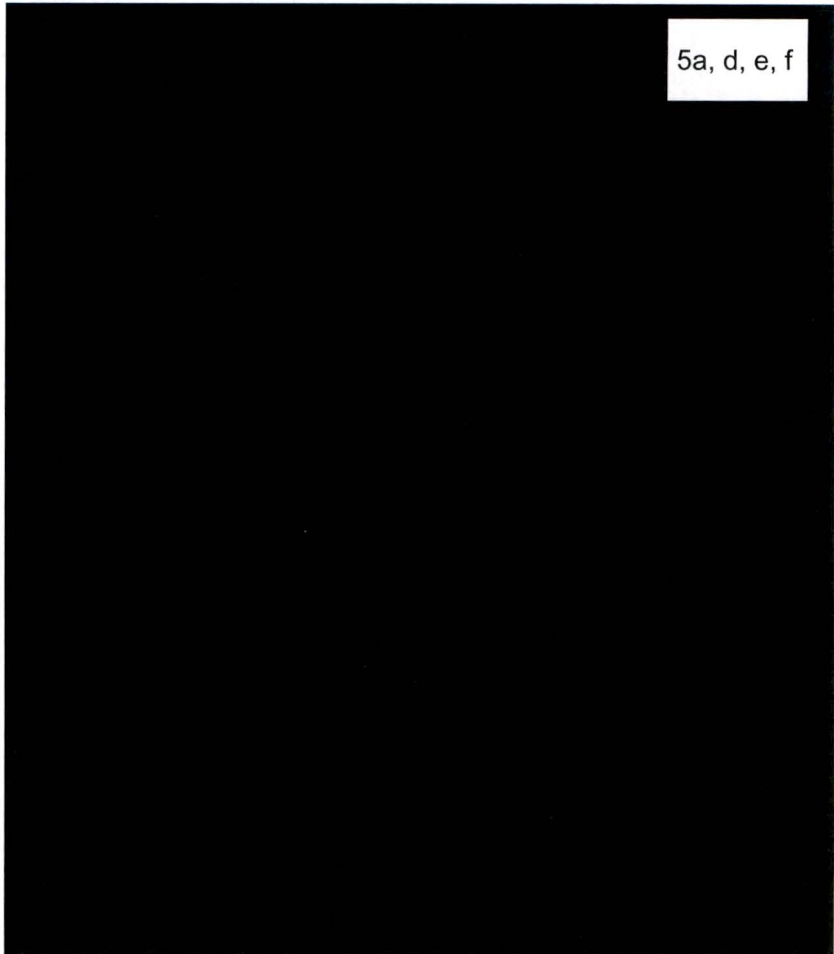
5a, d, e, f



For test 6 the exit pressure was adjusted to [REDACTED], the mass flow was adjusted to [REDACTED], and the inlet temperatures were recalculated to achieve an outlet temperature of [REDACTED]. Test 6 achieved critical heat flux at [REDACTED], 2.54% lower than the estimated CHF of [REDACTED] derived from the Groeneveld (2007) LUT. The power supply was not able to be shut down prior to the rod failing during the CHF event. Heater rod 4 appears to have failed at the solder joint at the top of the rod. Conditions at the highest heat flux achieved prior to CHF as well as the conditions at which CHF occur can be found in Table 1.

5a, d, e, f

Figure59: Failed Rod #4 After Test #6



5a, d, e, f

Figure60: High Speed Video Images, Test #6



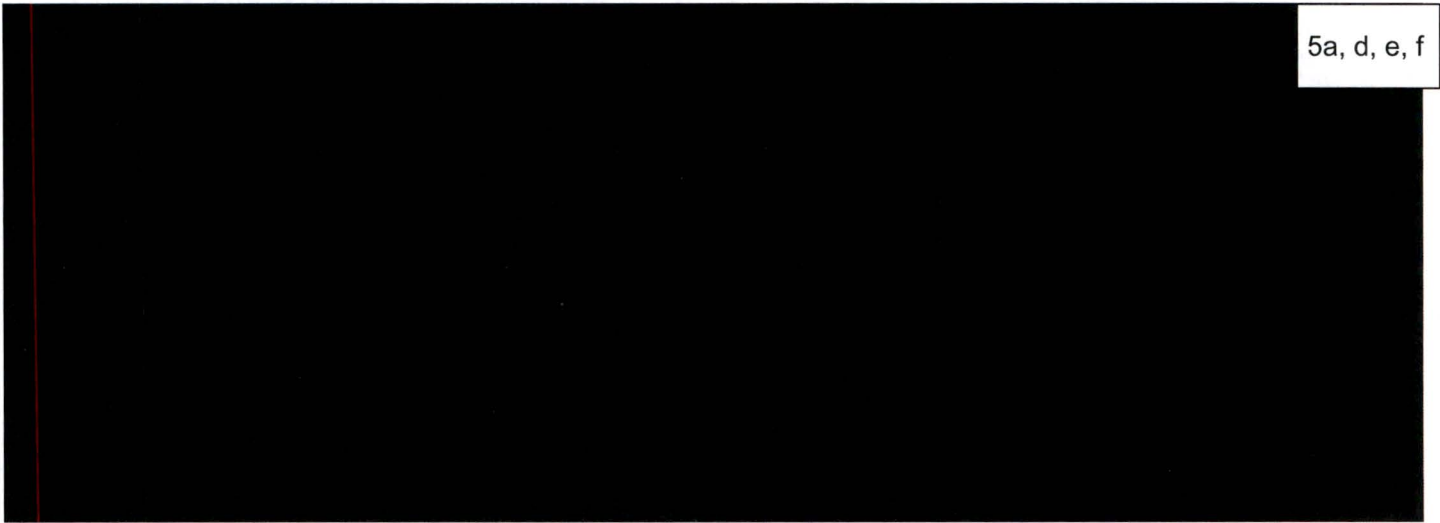


Figure61: Experimental Matrix, Test #6

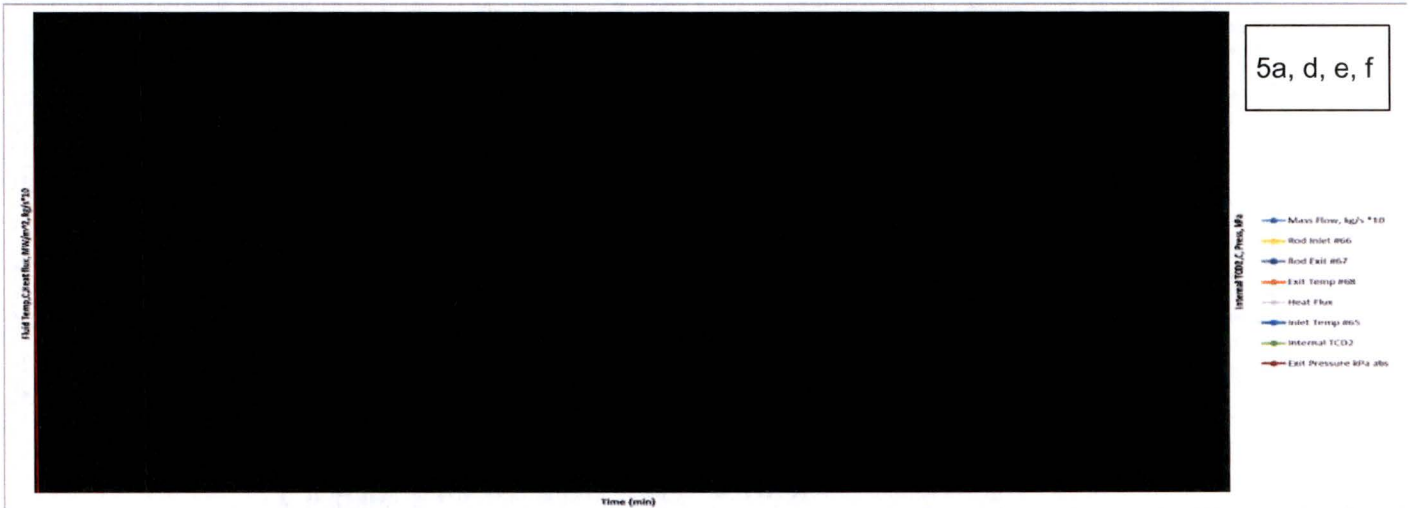


Figure62: Data from Test #6, Constant Exit Temperature

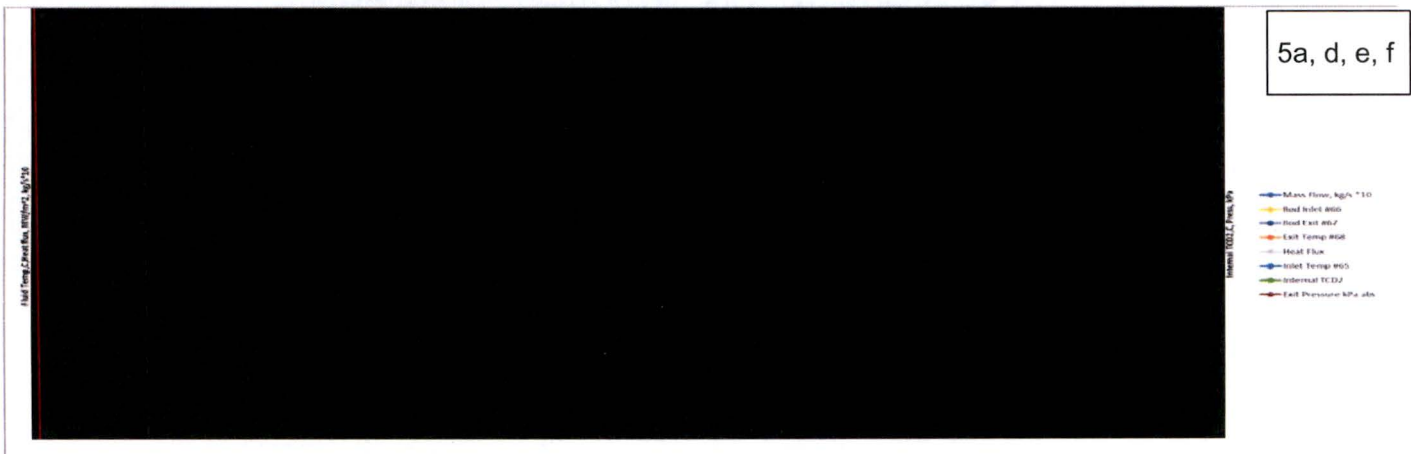


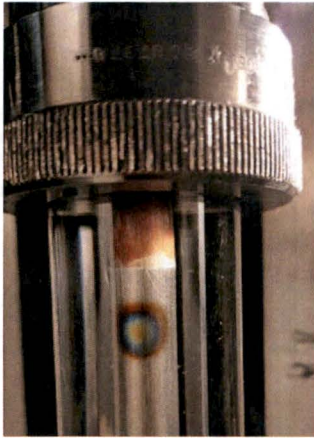
Figure63: Data from CHF Event, Test #6

CONFIDENTIAL - NO DISSEMINATION

Test 7 – Heater Rod 5 – 02/23/17

Target Conditions: $T_{out} =$ [REDACTED], $P_{out} =$ [REDACTED], $G =$ [REDACTED]

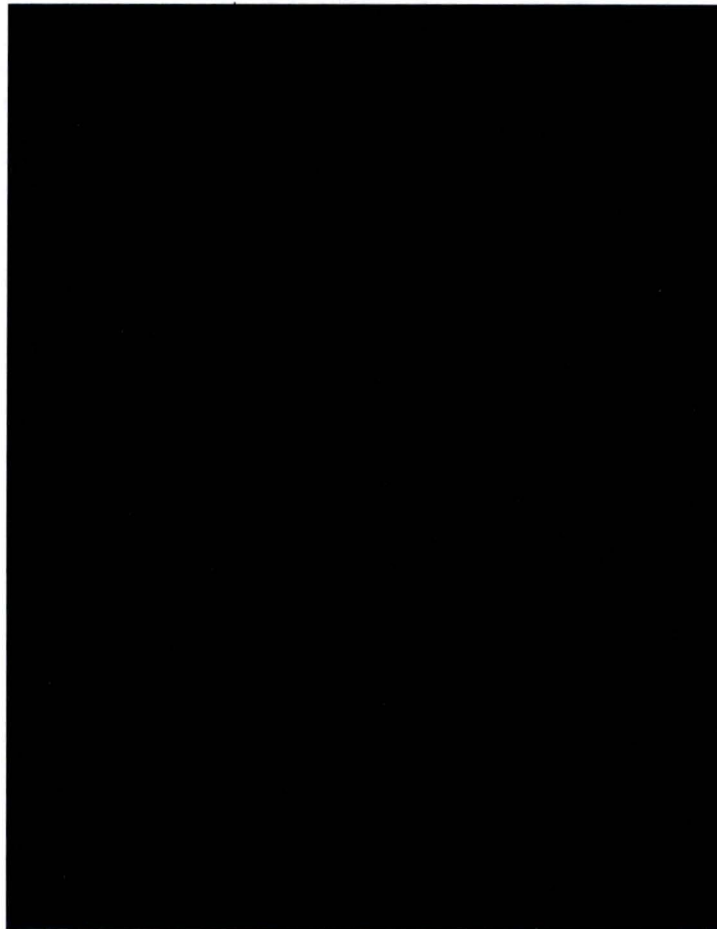
5a, d, e, f



For test 7 the exit pressure was adjusted to [REDACTED], the mass flow was adjusted to [REDACTED], and the inlet temperatures were recalculated to achieve an outlet temperature of [REDACTED]. Test 7 achieved critical heat flux at [REDACTED], 5.24% higher than the estimated CHF of [REDACTED] derived from the Groeneveld (2007) LUT. Heater rod 5 is the first heater to survive a CHF event. A circular heat mark is clearly visible ~0.6cm below the solder joint at the top of the rod. Rod 5 will be used to rerun test 6-4 in an attempt to show repeatability in the tests. Conditions at the highest heat flux achieved prior to CHF as well as the conditions at which CHF occur can be found in Table 1.

5a, d, e, f

Figure 64: Hot Spot on Rod #5 After Test #7



5a, d, e, f

Figure 65: High Speed Videos, Test #7





Figure66: Experimental Matrix, Test #7

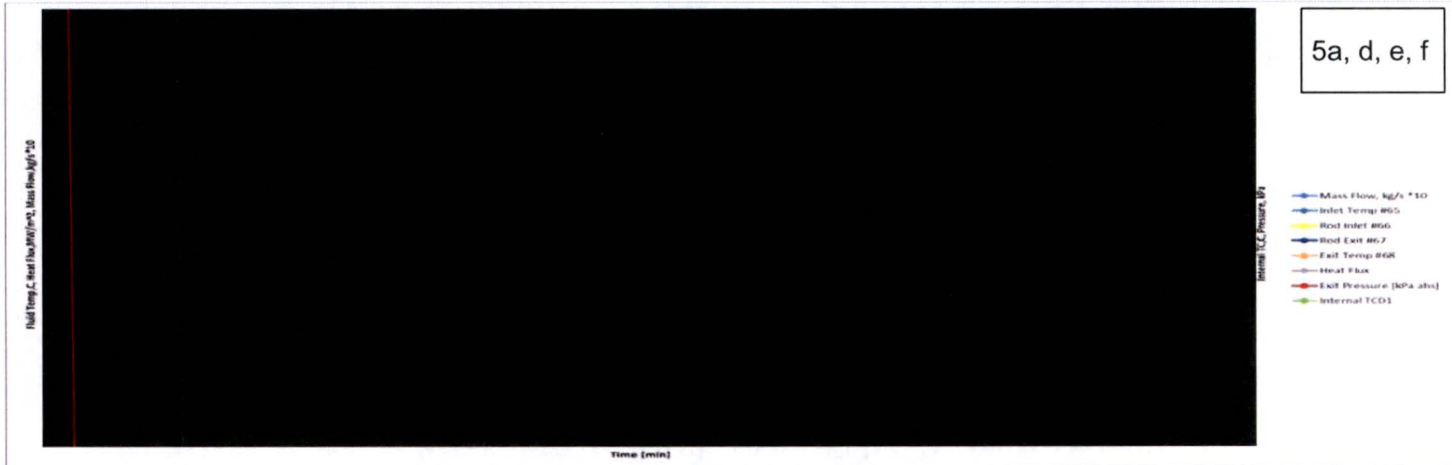


Figure67: Data from Test #7, Constant Exit Temperature

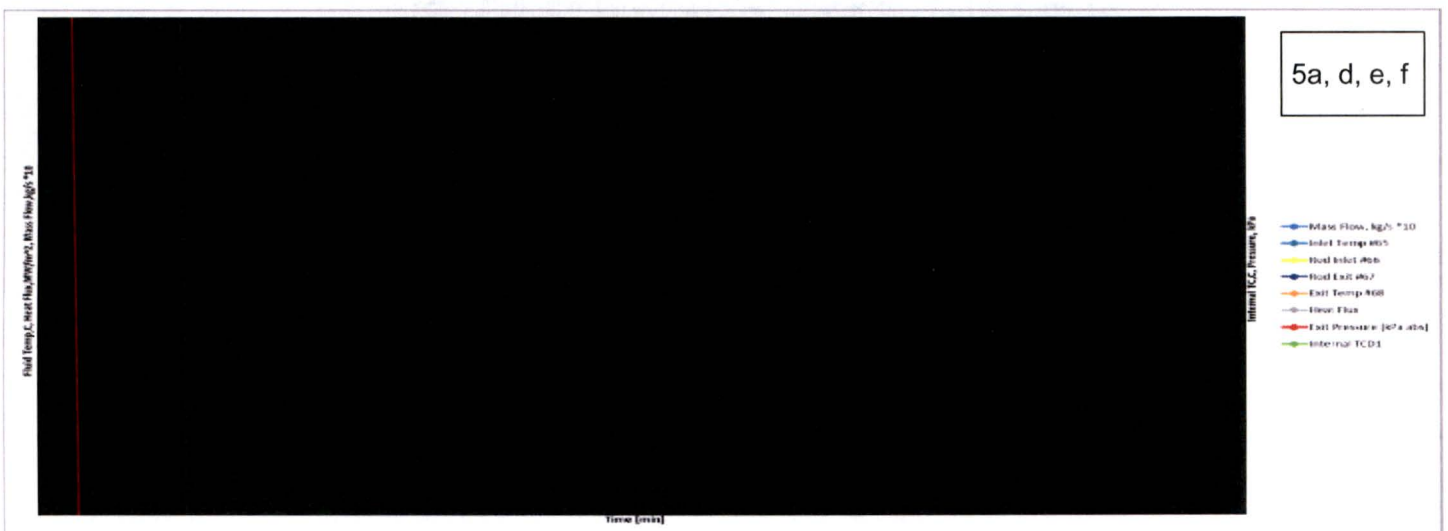


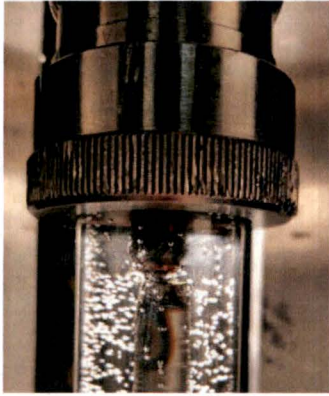
Figure68: Data from CHF Event, Test #7



Test 8 – Heater Rod 5 – 02/23/17

Target Conditions: [REDACTED], $P_{out} =$ [REDACTED], $G =$ [REDACTED] (Re-run of Test #6)

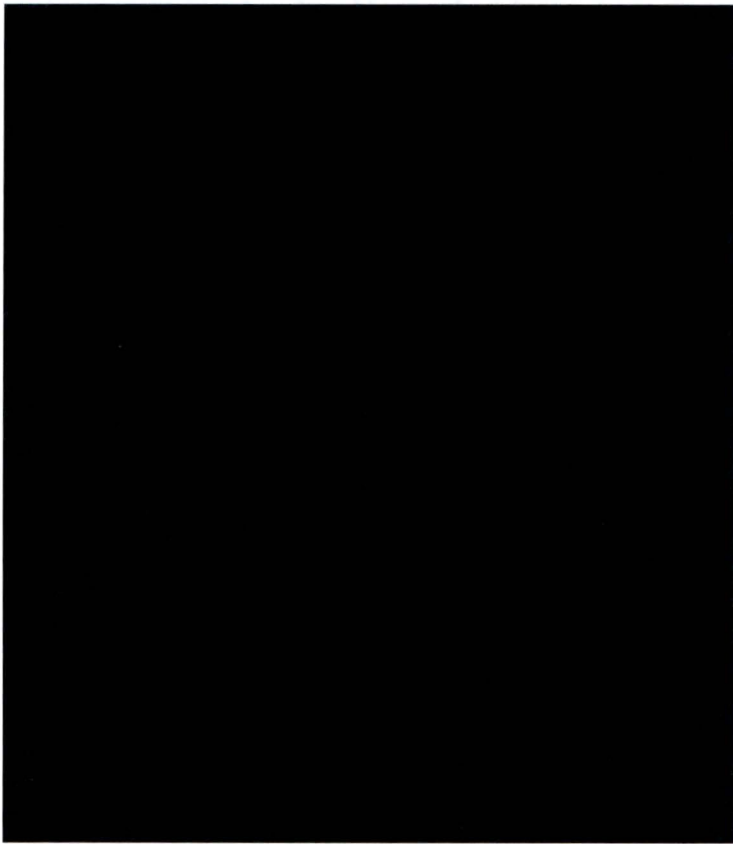
5a, d, e, f



For test 8 the exit pressure was adjusted to [REDACTED], the mass flow was adjusted to [REDACTED], and the inlet temperatures were recalculated to achieve an outlet temperature of [REDACTED]. Test 8 achieved critical heat flux at [REDACTED], 0.62% lower than the estimated CHF of [REDACTED] derived from the Groeneveld (2007) LUT. The power supply was not able to be shut down prior to the rod failing during the CHF event. The heater failed in almost the exact location as the previous run at the same conditions as well as having CHF events within 1.5% of each other. The heat mark from the previous CHF run can be seen in the post test photos below. Conditions at the highest heat flux achieved prior to CHF as well as the conditions at which CHF occur can be found in Table 1.

5a, d, e, f

Figure69: Failed Rod #5 After Test #8



5a, d, e, f

Figure70: High Speed Video, Test #8





Figure 71: Experimental Matrix, Test #8

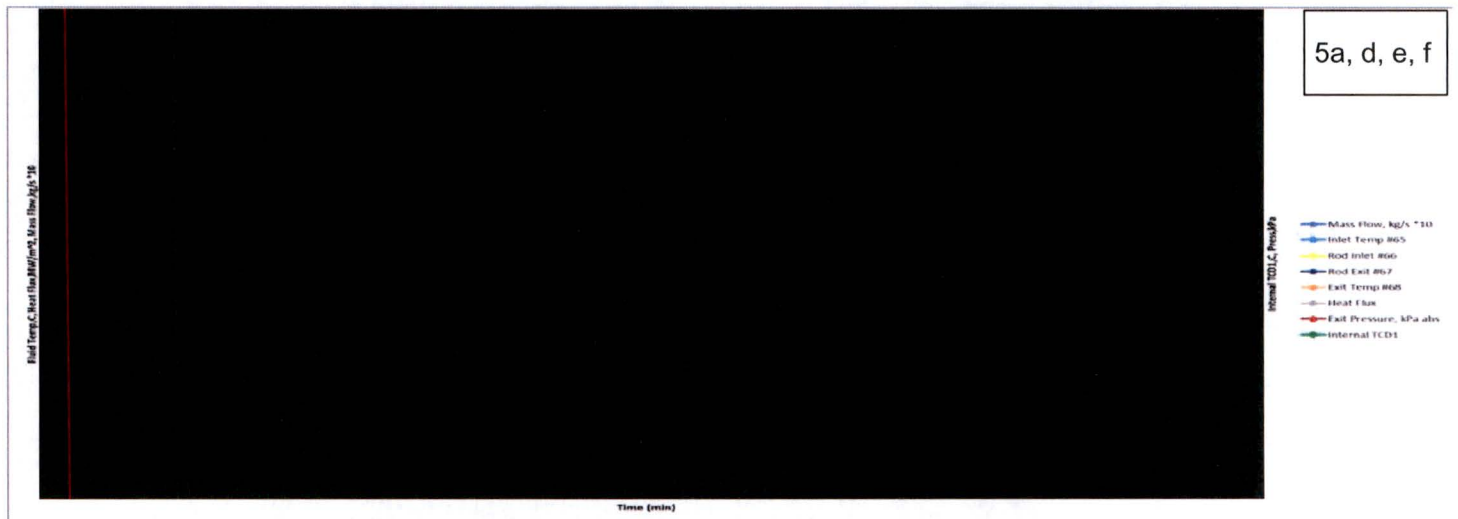


Figure 72: Data from Test #8, Constant Exit Temperature

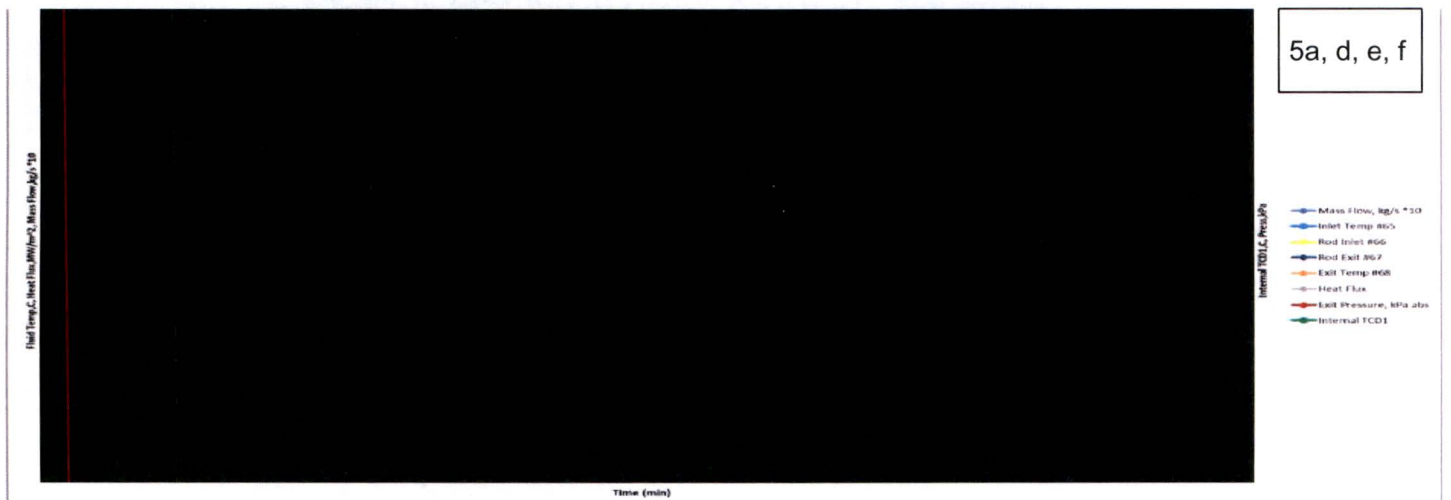


Figure 73: Data from CHF Event, Test #8

3A PROPRIETARY INFORMATION

Test 9 – Heater Rod 6 – 02/27/17

Target Conditions: $T_{out} =$ [REDACTED], $P_{out} =$ [REDACTED], $G =$ [REDACTED]

5a, d, e, f

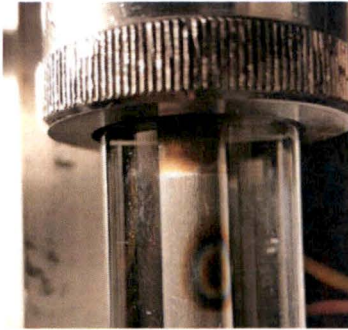
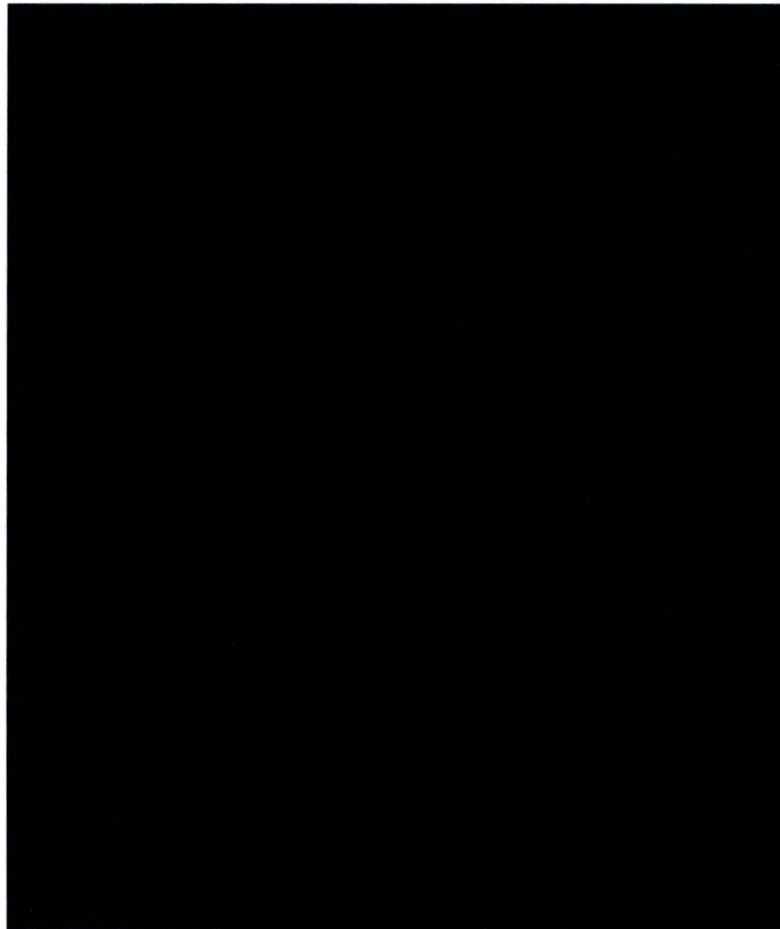


Figure 74: Hot Spot on Rod #6, After Test #9

For test 9 the pressure was adjusted to [REDACTED], the mass flow was adjusted to [REDACTED], and the inlet temperatures were recalculated to achieve an outlet temperature of [REDACTED]. Test 9 achieved critical heat flux at [REDACTED], 8.83% higher than the estimated CHF of [REDACTED] derived from the Groeneveld (2007) LUT. The power supply was not able to be shut down prior to the rod failing during the CHF event. Heater rod 6 is the second heater to survive a CHF event. A circular heat mark is clearly visible ~1.0cm below the solder joint at the top of the rod. Conditions at the highest heat flux achieved prior to CHF as well as the conditions at which CHF occur can be found in Table 1.

5a, d, e, f



5a, d, e, f

Figure75: High Speed Video, Test #9





Figure 76: Experimental Matrix, Test #9

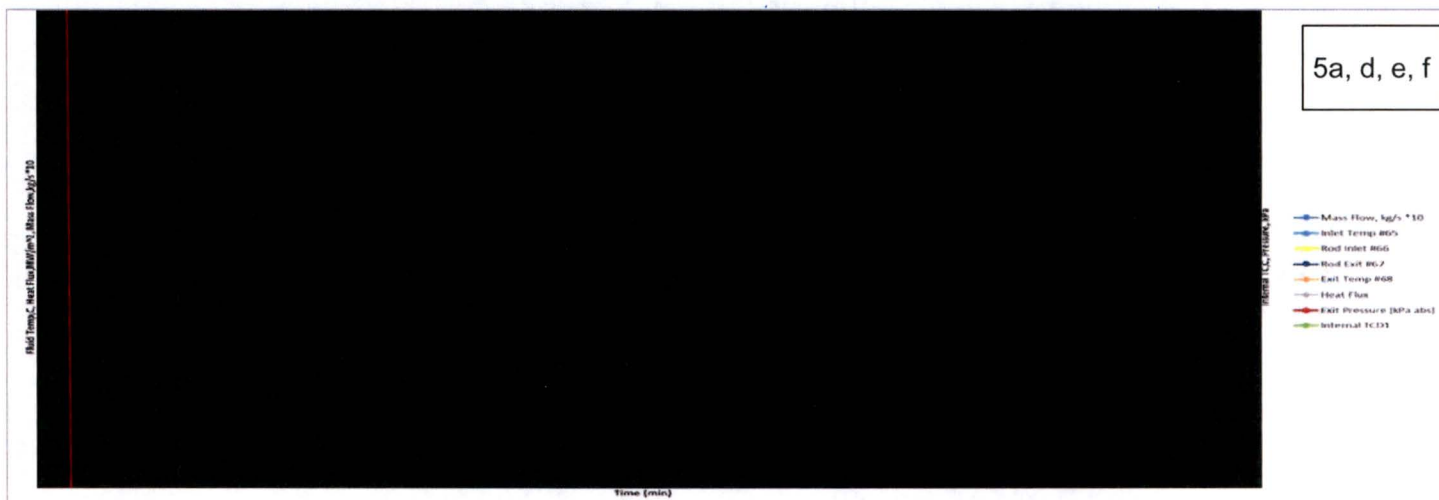


Figure 77: Data from Test #9, Constant Exit Temperature

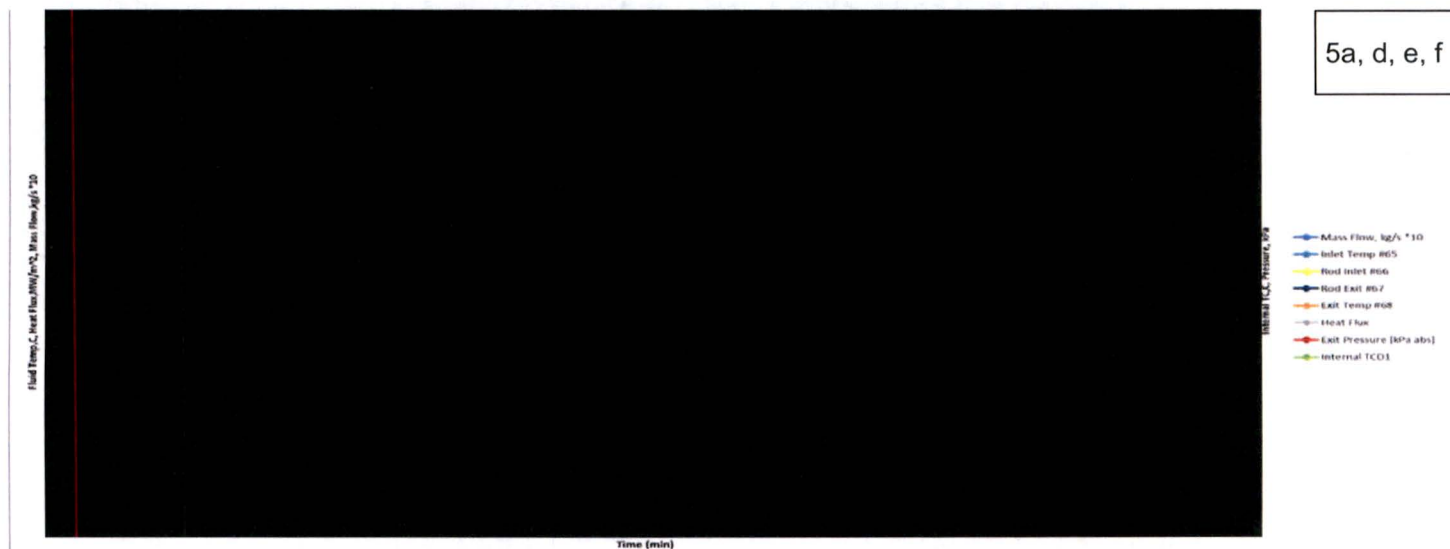


Figure 78: Data from CHF Event, Test #9

SA PROPRIETARY INFORMATION

Table 1: CHF Testing Results

Date	Test#- Rod#	T _{in} [°C]	Stdev	+/- Error [°C]	T _{out} [°C]	Stdev [C]	+/- Error [°C]	P _{out} [kPa abs]	Stdev [kPa]	+/- Error [kPa]	DP test section [kPa abs]	Stdev [kPa]	+/- Error [kPa]	Mass Flux [kg/(m ² *s)]	Stdev	% Error	Rod Pow [kw]	Stdev [kw]	% Error	Actual Heat Flux [kw/m ²]	Stdev	% Error	Estimated CHF [kw/m ²]	% Error	% Difference (Act-Est)/Act	
1/5/2017	*1-1																									
1/5/2017	*1-1																									
1/11/2017	*2-2																									
1/11/2017	*2-2																									
1/28/2017	**3-3																									
1/30/2017	**4-3																									
2/9/2017	5-3																									
2/9/2017	5-3																									
2/21/2017	6-4																									
2/21/2017	6-4																									
2/23/2017	7-5																									
2/23/2017	7-5																									
2/23/2017	***8-5																									
2/23/2017	***8-5																									
2/27/2017	9-6																									
2/27/2017	9-6																									

Test 1-1 and 2-2 were ran with pressure and temperature being controlled at the entrance of the test section. All subsequent tests were completed controlling exit pressure and exit temperature.

CHF not observed up to maximum heat flux of 9.6MW/m²

* Rerun of Test #6 - Rod #4

d Resistance = 0.0593Ω

d Surface Area = 0.008977m²

= 0.01032 m

ow Area = 1.863*10⁻⁴ m² (Area of inner flow tube - Area of heater rod)

Estimated CHF derived from Groeneveld LUT [Groeneveld, et al, 2006]

Green highlighted cells indicate conditions at highest heat flux prior to reaching CHF for each test - Data averaged over 30 seconds

Red highlighted cells indicate conditions at which CHF occurred for each test - Data averaged over 10 seconds if available

Results

Table 1: Testing Results

5a, d, e, f

The table above summarizes the results of the CHF testing requested by General Atomics. A heating rod was custom designed for this series of experiments and six were fabricated and used. Eight distinct conditions were tested and one condition was repeated (tests 6 & 8). Tests 3 and 4 reached the limit of the power supply (9.6Mw.m²) before CHF occurred. Due to the local nature of the temperature sensing and the high heat flux involved, the rods, were in general, not re-usable after a CHF event. The first two tests were conducted with constant inlet conditions. These two were operated with a continuously ramped heat flux until CHF, with inlet conditions being held constant. The remainder of the tests were conducted with constant exit conditions. This involved pre-calculating inlet conditions for a given heat flux, setting the temperatures and pressures accordingly, and operating at a uniform heat flux for approximately 5 minutes. If CHF did not occur, conditions were pre-set for the next higher heat flux (generally steps of 200kw/m²) and this power level was run. This process was continued until either CHF or the limit of the power supply (9.6Mw/m²) was reached.

Table #1 summarizes the results of this critical heat flux testing. The table is chronologically ordered to maintain clarity in data retrieval. The first column is the date of the run. The second column is the test number followed by the rod number used in the test. The third column, T_{in} (inlet water temperature), is the reading from the lower inlet thermocouple followed by the standard deviation for this measurement, followed by the error in this measurement. Agreement between the lower inlet thermocouple and the thermocouple located near the bottom of the rod was very good.

The sixth column, T_{out} (exit water temperature), is the reading from the upper exit thermocouple, followed by the standard deviation of this measurement, followed by the error in this measurement. There was some discrepancy between the upper exit thermocouple and lower exit thermocouple. It is surmised this was caused by the flow not being mixed upstream of the rod before interaction with the lower exit thermocouple. An energy balance was performed with the input power, mass flow, inlet temperature, and exit temperature based on the upper exit thermocouple. The table below reports the results.

Table 1: Energy balance from CHF (or Maximum) Runs

Energy Balance at CHF							
Date	delta T, C	Specific Heat, J/kg	Mass Flow, kg/s	delta H, W	Rod Power, W	% difference	# Data Points
1/5/2017							10
1/11/2017							12
1/28/2017							1040
1/30/2017							1394
2/9/2017							1496
2/21/2017							635
2/23/2017							35
2/23/2017							108
2/27/2017							72

5a, d, e, f

The ninth column, "P_{out}", is the corrected reading from the gauge pressure transmitter, followed by the standard deviation of this reading, followed by the accuracy of this reading. For the first two runs, this was connected to and located level with the entrance pressure tap. The vertical distance between the pressure taps was 24.97" (63.4cm). For the remaining runs this pressure transmitter was connected to and located level with the exit pressure tap.

The twelfth column, "DP test section", is the reading from the delta pressure transmitter, followed by the standard deviation of this reading, followed by the accuracy of this reading. The high side



of this gauge was connected to the lower pressure tap, while the low side of the gauge was connected to the upper pressure tap. This transmitter and the lines to it were bled of air before starting the experiment, to result in a zero reading at zero test section flow. This measurement was used to calculate the exit pressure for the first two tests (where gauge transmitter was located at lower pressure tap).

The fifteenth column, "mass flux", is the mass flow rate generated by the Coriolis flow meter divided by the flow area, followed by the standard deviation of this measurement, followed by the error in this measurement. The accuracies of the flow meter and flow area were considered to attain the proper error values.

The eighteenth column, "rod pow", is the power supplied to the rod, followed by the standard deviation of this measurement, followed by the error in this measurement. Voltage and amperage measurement accuracies were considered to attain the proper error values.

The twenty first column, "actual heat flux", is the heat flux applied to the rod, followed by the standard deviation of this measurement, followed by the error in this measurement. Rod power and heated surface area accuracies were considered to attain the proper error values. Note that the values of the "actual heat flux" highlighted in maroon, are the heat flux values at which CHF occurred.

The twenty fourth column, "Estimated CHF", is the value at which CHF is predicted by Groeneveld et al. (2007) LUT to occur at the testing conditions, followed by the error in this measurement. This error was calculated by offsetting flow rate, heat flux, and fluid qualities (due to temperature errors) in both directions, by the maximum error, to both maximize and minimize predicted CHF. All predictions were done in F-Chart Software, Engineering Equation Solver, via the integrated "CHF Local" look-up tables. These tables are based on Groeneveld et al. (2007) LUT and utilize the suggested diameter correction.

The last column, " % difference", is the difference between predicted and actual CHF values. Note the maroon shaded rows are where CHF actually occurred. This value was attained by the equation: $100 * (\text{Actual CHF} - \text{Estimated CHF}) / (\text{Actual CHF})$. It is felt this value represents the agreement between this testing and the Groeneveld et al. (2007) LUT.

Examples of the error calculations are included in appendix three. The base and processed data will be provided to General Atomics, via a hard drive, due to the size of the video files.

Discussion:

Eight distinct conditions were tested for CHF values. One condition was repeated. Exit temperatures at CHF varied between [REDACTED] to [REDACTED]. Mass flux at CHF was varied between [REDACTED] and [REDACTED]. Exit pressures at CHF varied from [REDACTED] to [REDACTED] abs. Optical imaging at various frequencies was acquired throughout the testing.

5a, d, e, f

At all of these test conditions, as noted in the last column of our table, there is reasonable agreement between the testing performed and the 2007 Groeneveld et al. LUT prediction. For all tested conditions, the CHF predictions were well within ten percent of the actual CHF. The repeated test (conducted with a different heater rod) resulted in a CHF value that was within two percent of the original test.

The optical imaging with the Ametek Phantom camera framing at 12,696 frames per second revealed some interesting phenomena. From these video files it is obvious the vapor generation is not uniform with time (there is some oscillation of the vapor generation at high heat flux at conditions below CHF). There are obvious times of maximum vapor present, and obvious times of minimum vapor present. The frequency of the oscillation between the two states was investigated and did not seem to be uniform. It also did not seem to be necessarily sinusoidal, as the peak generation time was often present for longer than adjacent periods.

Quality imaging of the actual CHF event was difficult. One camera was available with the capability to frame with enough speed to produce a quality image. This camera position dictated what side of the rod was imaged. The CHF event azimuthal initiation point seemed to be random, and if the camera was not in the correct position (the location where CHF initiated), it was difficult to see the event. Another issue was that the intensity of the light that was produced during CHF typically saturated the camera. . Even with this limitation, some very interesting high speed videos were acquired that show the existence of the vapor bubble at the initiation point and a hot spot on the rod beneath the vapor bubble.

Rod failure at CHF was a major issue. Two thermocouples were placed in the rod to measure wall temperature. If the CHF did not initiate at the azimuthal and axial location of one of these thermocouples, the wall of the rod would melt before CHF could be detected and the power shut down. Even if the CHF initiated near one of these thermocouples, the rod was discolored (at the least) in a somewhat circular area where the CHF had occurred. At these high heat flux levels, preserving a heater rod after a CHF event was difficult, or a matter of chance.

Several modeling procedures were attempted and the TRACE code was used to try to predict the CHF. It was however found that this code uses the 1997 LUT and resulted in significant under prediction of the CHF. This is discussed in detail in appendix 1. Predictions with the 2007 Groeneveld LUT however were found to be quite accurate and in all cases predicted the CHF within 10%. Under two sets of conditions we were unable to reach CHF even at a value that was larger than 10% higher than predicted.

Appendix 1: Trace Code



GENERAL ATOMIC
TRACE CRITICAL HEAT FLUX ANALYSIS

Juliana Pacheco Duarte

February 28, 2017

TRACE Overview

The TRAC/RELAP Advanced Computational Engine (TRACE - formerly called TRAC-M) is the latest in a series of advanced, best-estimate reactor systems codes developed by the U.S. Nuclear Regulatory Commission for analyzing transient and steady-state neutronic-thermal-hydraulic behavior in light water reactors. It is the product of a long-term effort to combine the capabilities of the NRC's four main systems codes (TRAC-P, TRAC-B, RELAP5 and RAMONA) into one modernized computational tool.

TRACE has been designed to perform best-estimate analyses of loss-of-coolant accidents (LOCAs), operational transients, and other accident scenarios in pressurized light-water reactors (PWRs) and boiling light-water reactors (BWRs). It can also model phenomena occurring in experimental facilities designed to simulate transients in reactor systems. Models used include multidimensional two-phase flow, non-equilibrium thermo-dynamics, generalized heat transfer, reflood, level tracking, and reactor kinetics.

TRACE takes a component-based approach to modeling a reactor system. Each physical piece of equipment in a flow loop can be represented as some type of component, and each component can be further nodalized into some number of physical volumes (also called cells) over which the fluid, conduction, and kinetics equations are averaged. The number of reactor components in the problem and the manner in which they are coupled is arbitrary. Reactor hydraulic components in TRACE include PIPEs, PLENUMs, PRIZERS (pressurizers), CHANs (BWR fuel channels), PUMPs, JETPs (jet pumps), SEPDs (separators), TEEs, TURBs (turbines), HEATRs (feed water heaters), CONTANs (containment), VALVEs, and VESSELs (with associated internals). HTSTR (heat structure) and REPEAT-HTSTR components modeling fuel elements or heated walls in the reactor system are available to compute two-dimensional conduction and surface-convection heat transfer in Cartesian or cylindrical geometries. POWER components are available as a means for delivering energy to the fluid via the HTSTR or hydraulic component walls. FLPOWER (fluid power) components are capable of delivering energy directly to the fluid (such as might happen in waste transmutation facilities). RADENC (radiation enclosures) components may be used to simulate radiation heat transfer between multiple arbitrary surfaces. FILL and BREAK components are used to apply the desired coolant-flow and pressure boundary conditions, respectively, in the reactor system to perform steady-state and transient calculations.

EXTERIOR components are available to facilitate the development of input models designed to exploit TRACE's parallel execution features.

TRACE CHF Correlations

The point where the maximum heat flux occurs in the idealized boiling curve shown is denoted as the CHF point, (q''_{CHF}, T_{CHF}) , and is characterized by both the critical heat flux and the wall temperature at which it occurs. This is the point where the heat transfer regime transitions from that where the liquid phase wets the wall (i.e., nucleate boiling), to the post-CHF regimes where liquid-wall contact is either transient (transition boiling) or non-existent (film boiling).

In TRACE, the role of the CHF model is two-fold:

- 1) Determine the transition point for the heat transfer regime, and
- 2) Serve as an anchor point for the transition boiling wall heat flux.

To serve both these roles, the CHF model in TRACE must provide a continuous estimate of the CHF over a wide range of conditions with reasonable but conservative accuracy. This range of conditions must extend from the high pressure, high-flow conditions typical of operating PWRs and BWRs, to the low pressure, low-flow conditions.

For the analysis of anticipated transients, such as a perturbation in the core flow or inlet sub cooling, the metric is the departure from nucleate boiling (DNB) margin. DNB is one of the types of CHF and for each fuel type there are specific DNB correlations with high accuracy. Most of these correlations employ the boiling length concept, in which the core inlet quality or enthalpy explicitly appears in the correlation. During many transients and postulated accidents, however, the use of boiling length correlations is not appropriate. For example, during a cold-leg-break LOCA, the core experiences a flow reversal thereby rendering the definition of the core inlet ambiguous. In addition, these correlations are unsuited for general use in TRACE because they are highly empirical with a limited range of validity, and are unreliable when extrapolated outside their original database.

Therefore, for the default CHF model in TRACE the 1995 AECL-IPPE CHF look-up table [2] was selected. It is based on an extensive database of CHF values obtained in tubes with a vertical up flow of a steam-water mixture and provides the value of the critical heat flux as a function of the local conditions. As described below, a correction factor is included to improve the accuracy of this table when applied to rod bundles. This look-up table allows for a reasonable predictions of CHF based on the local flow conditions for a wider range of conditions than would be possible with either empirical correlations or phenomena based models.

The method of determining the value of the critical heat flux was selected for TRACE because of its reasonable accuracy and wide range of applicability. The AECL-LUT CHF table is based upon an extensive database of CHF values obtained in tubes for a vertical upward flow of a steam-water mixture. While the database covers a wide range of flow conditions, the look-up

table was designed to provide CHF values for 8 mm tubes at discrete values of pressure, mass flux, and quality.

TRACE Analysis of GA Subcooled CHF Experiments

The TRACE model for the annular test section was developed based on the test facility specifications, input conditions, and the simulation method as discussed in Appendix A. The current simulations use the hydraulic diameter for the characteristic length in the heated transfer calculations. The hydraulic diameter for the annular flow channel is found to be equal to the outer channel diameter minus the inner channel diameter; i.e., 10.31 mm. This is used in the simulation as well as in the K_1 diameter correction term instead of the recommended heated diameter. The reason for this choice is based on our analysis of the TRACE user guidelines and the determination that the recommended use of the heated diameter for the correction factor in the CHF look-up table [2, 3] is inappropriate. The use of the conventional heated diameter (defined as four times the flow area divided by the heated perimeter) underestimates the critical heat flux and, as suggested by Ref. [3], the hydraulic diameter should be used (see Appendix B for details)

$$CHF = CHF_{TABLE} \times K_1 \quad \text{where } K_1 = \sqrt{\frac{0.008}{D_{hy}}} \quad (1)$$

The TRACE results using the 1995 Look-up Table [2] are shown below. More recent CHF data for highly subcooled conditions are only incorporated into later data sets not used in TRACE [3]. This seems to be the only reason that TRACE underestimates the experimental observed CHF point.

Inlet Temp. °C	Mass flux kg/m ² -s	Local quality -	CHF MW/m ²
30	█	█	█
30	█	█	█
40	█	█	█
40	█	█	█

5a, d, e, f

References

1. USNRC, TRACE V5.840 THEORY MANUAL, Field Equations, Solution Methods, and Physical Models, Dec. 2014.
2. Groeneveld, D. C., et al, "The 1995 look-up table for critical heat flux in tubes", Nuclear Engineering and Design, 163, 1-23, 1996.
3. Groeneveld, D. C., et al., "The 2006 CHF look-up table", Nuclear Engineering and Design, 237, pp190-1922, 2007.



Appendix A – Test Facility Specs, TRACE Input Parameters and Simulation Method

Table A.1 - Test section parameters

Parameter	Value	Units
Channel outer diameter	16.66	mm
Cladding tube OD/Channel ID	6.35	mm
Cladding wall thickness	0.51	mm
Cladding material	IN-625	-
Nominal heat flux	█	MW/m ²
Heated length	█	m
Inlet temperature	█	°C
Inlet pressure	█	kPa
Minimum mass flux	█	kg/m ² -s
Nominal mass flux	█	kg/m ² -s

5a, d, e, f

Table A.2 – TRACE input parameters

Parameter	Value	Units
Hydraulic diameter	10.31	mm
Heat diameter (assumed)	10.31	mm
Flow area	186.32	mm ²
Minimum mass flow	█	kg/s
Maximum mass flow	█	kg/s
Outlet pressure	█	kPa
Maximum time step	0.01	sec
Minimum time step	10 ⁻¹²	sec

5a, d, e, f

The TRACE input model and associated boundary conditions are shown in Figure A.1. Flow channel length is equal to 558.3 mm divided in sixty uniform mesh size and the heated length started at 56.6 mm. The heated length has a structured mesh that is uniformly divided in 45 nodes. A power component for the heated structure, not shown in the figure, is used to uniformly



heat the clad with thickness 0.51 mm and inner of the heated cylinder is filled with Boron Nitride. The IN-625 properties were included as a user-defined material from GA information.

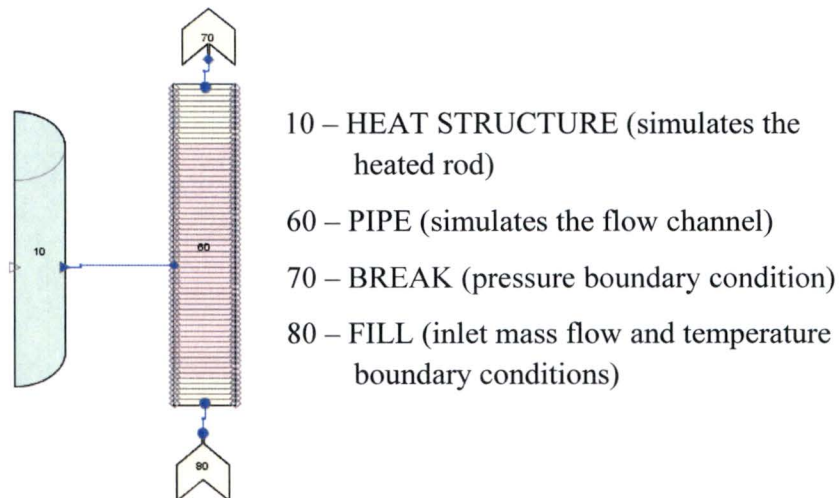


Figure A.1 – TRACE model and boundary conditions.

The onset of CHF was determined by increasing the total power by 1kW at each 50 seconds as it was assumed to occur during the experiment operation. The temperatures of the wall at the end of the heated length (*tsurf-10A44*), the liquid (*tlm-60A50*) and the local heat flux (*qppo-10A44*) are shown in Fig. A.2 for the nominal mass flux and at the higher inlet temperature condition.

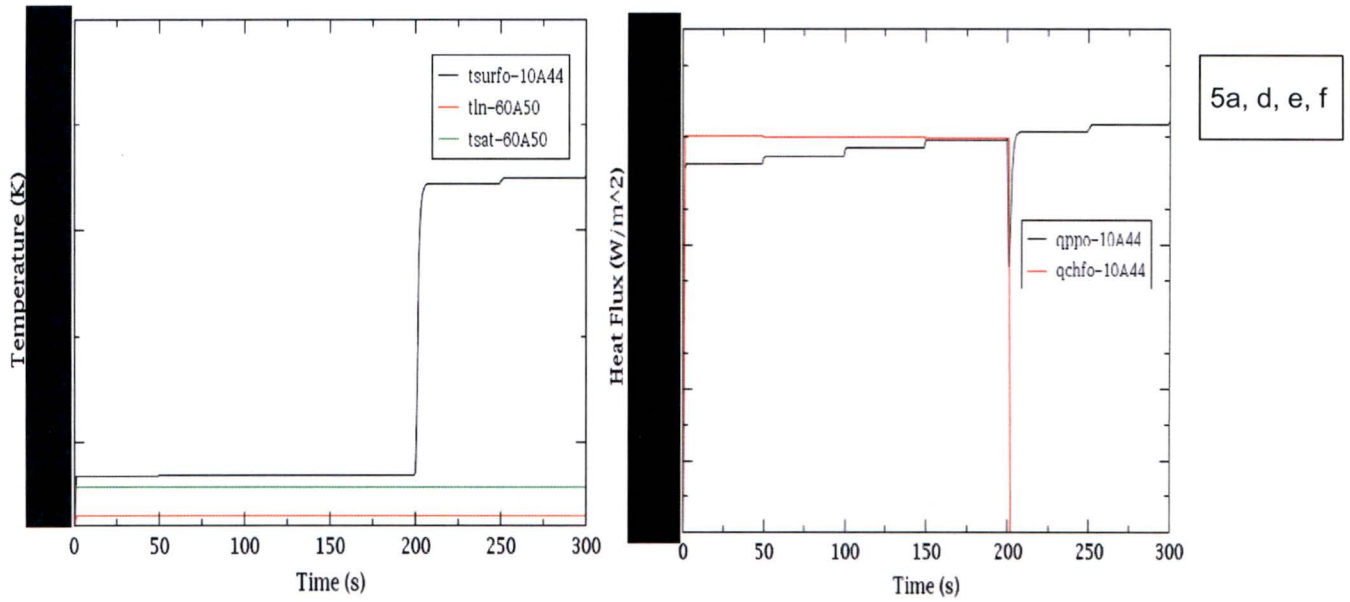


Figure A.2 – CHF for the nominal mass flux and 40 °C inlet temperature.

Appendix B

Hydraulic and heated equivalent diameters in heat transfer correlations

Summary

Hydraulic and heated equivalent diameter are approximations to take into account different geometries in thermal-hydraulic analysis. These concepts can be misinterpreted and they are discussed here based on well-known heat transfer correlations.

Nomenclature

A – Flow area
 P_w – wetted perimeter
 P_{he} – heated perimeter
 D_{hy} – hydraulic equivalent diameter
 D_{he} – heated equivalent diameter
 D_o – outer diameter in an annular geometry
 D_i – inner diameter in an annular geometry
 D_e – equivalent diameter
 D – rod diameter
 P – pitch
 c_p – specific heat
 G – mass flux
 m – viscosity
 k – thermal conductivity
 h – heat transfer coefficient
 Nu – Nusselt number
 Re – Reynolds number
 L – square channel width
 N – number of rods in a bundle

Introduction

The hydraulic and heated equivalent diameters are widely used in friction and heat transfer coefficients in nuclear thermal-hydraulic calculations. Most of the correlations used in nuclear reactor systems codes (e.g. TRACE, RELAP, MELCOR, etc.) and sub channel codes (e.g. COBRA, VIPRE, etc.) are empirical correlations or phenomenological models based on data collected in heated tubes. To apply these correlations to different geometries, such as annular channels and rod bundles, the concept of equivalent diameters is used. Although it is simple in concept, it is very common to mistake them and a more careful attention is required in this context.

Discussion

The hydraulic diameter is well defined and explained in many engineering textbooks (e.g., Kazimi and Todreas, 2012 & El-Wakil 1978) as a value equivalent to the round tube diameter, i.e., four times the flow area divided by the wetted perimeter, Eq. (1), where the wetted perimeter is defined as the sum of all perimeters in contact with the fluid.

$$D_{hy} = 4 \frac{A}{P_w} \quad (1)$$

Eq. (1) is, in general, accepted and used in most friction factor correlations for internal flow. Note that, for a pipe geometry, the hydraulic diameter is the diameter of the pipe. For a square rod bundle with width L and N rods of radius R , the hydraulic diameter is

$$D_{hy} = 4 \frac{L^2 - N(\pi R^2)}{4L + N(2\pi R)} \quad (2)$$

The misunderstanding arises when heat transfer correlations are used. Kazimi and Todreas (2012), and El-Wakil (1978) suggest to use the hydraulic diameter as the characteristic length for heat transfer correlations for geometries other than circular, which is in agreement with Weisman (1959) correlation. Weisman (1959) correlation is a well-known correlation based on square and triangular lattice rod bundles where the Nusselt and Reynolds numbers are evaluated using an equivalent diameter equal to the hydraulic diameter, Eq. (3). The fluid properties are evaluated at the film temperature except c_p .

$$\frac{hD_{hy}}{k} = C \left(\frac{D_{hy} G}{\mu} \right)^{0.8} \left(\frac{c_p \mu}{k} \right)^{1/3} \quad (3)$$

where

$$C = 0.026(P/D) - 0.006 \quad \text{for } 1.1 \leq P/D \leq 1.5 \text{ (triangular pitch lattices)}$$

$$C = 0.042(P/D) - 0.024 \quad \text{for } 1.1 \leq P/D \leq 1.3 \text{ (square pitch lattices)}$$

A more recent correlation for square lattices (El-Genk et al, 1993) uses the heated equivalent diameter to evaluate the dimensionless coefficients and the mean bulk temperature for water properties. Dingee et al (1955) also use the heated equivalent diameter to evaluate the dimensionless numbers for the heat transfer calculation in rod bundles of different geometries. The authors call the heated diameter as an infinite array diameter reasoning that for heat transfer calculation the effect of the non-heated wall can be disregarded. The heated diameter is defined as four times the heated area divided by the heated perimeter, Eq. (4).

$$D_{he} = 4 \frac{A}{P_{he}} \quad (4)$$

Again, for a heated tube, the heated diameter is equal to diameter of the tube. For a square rod bundle with N heated rods, the heated diameter is given by

$$D_{he} = 4 \frac{L^2 - N(\pi R^2)}{N(2\pi R)} \tag{5}$$

which it is greater than the hydraulic diameter.

Kim and Li (1988) shows a semi-analytical solution for infinity square arrays and the Nusselt number in laminar flow evaluated using both the hydraulic and the heated perimeter. The results are plotted in Figure 1, where constant properties were assumed.

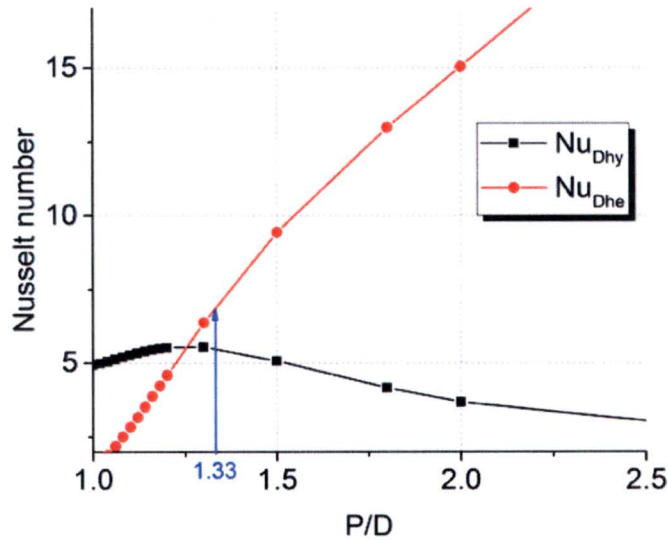


Figure 1 – Semi-analytical solution for laminar flow along circular rods (Kim and Li, 1988).

It is worth noting that Weisman (1959) and El-Genk et al (1993) correlations predicts closer results when they are evaluated using the same characteristic length as shown in Figure 2 (for $G = 1000 \text{ kg/m}^2\text{s}$, water properties at 15.5 MPa and 310 °C, and $L = N \times P$).



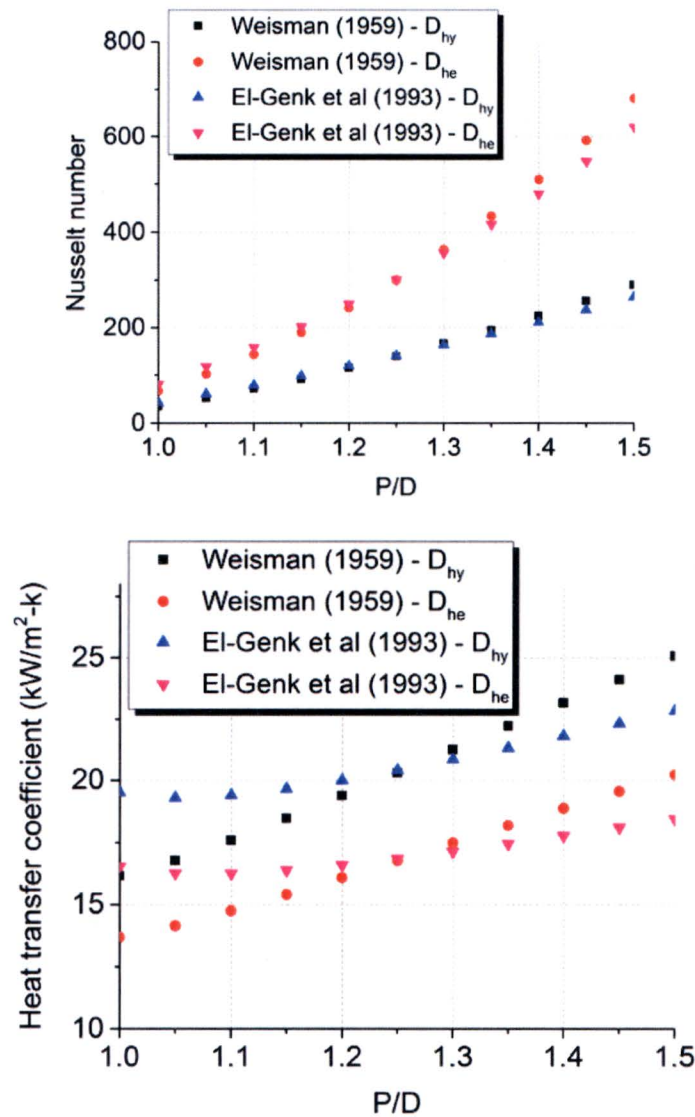


Figure 2 – Comparison of turbulent single-phase heat transfer coefficient evaluated using the hydraulic and the heated diameters in a square bundle.

For annular flow geometry internal heated, it seems like the hydraulic diameter is more commonly accepted as the characteristic length for heat transfer calculations. McAdams et al (1949) studied the heat transfer from an electrically heated element to water flowing in annular channel. The equivalent diameter in this case, simplifies to

$$D_{he} = 4 \frac{A}{P_w} = D_o - D_i \quad (6)$$

For critical heat flux (CHF) prediction, a widely used method is the look-up tables developed by Groeneveld et al (1986, 1989, 1999, 2007). The CHF experiments were performed in heated tubes for a

broadly range of pressure, mass flow and local qualities, and normalized to an 8 mm tube. The effect of the tube diameter is taken into account by a correction factor

$$K_1 = \max\left(0.57, \sqrt{\frac{8 \text{ mm}}{D_{hy}}}\right) \quad (7)$$

The first papers (Groeneveld 1986; 1989) suggest the heated diameter as correction factor while a more recent one (Groeneveld, 1999) suggest the hydraulic equivalent diameter is more appropriate.

For annular geometry the hydraulic and heated diameter can be significantly different. For example, the experiment #95 from Barnett (1966), the rod diameter is equal to 0.375 in (9.53 mm) and the surround unheated tube 0.875 in (22.2 mm) giving $D_{he} = 42.3$ mm and $D_{hy} = 12.3$. Using Eq. (7) and the more recent CHF look-up table (Groeneveld, 2007), the predicted CHF is equal to 3348 kW/m² (12% higher than the experimental data presented by Barnett, 1966). However, when the heated diameter is used, the K_1 factor is equal to its minimum value of 0.57, which reduces the predicted CHF to 2405 kW/m². For a rod bundle geometry, the difference between hydraulic and heated diameters may not be as large as for annuli. In both cases, however, the hydraulic diameter should be used, in the lack of experimental data, as indicated by Groeneveld (1999).

Conclusion

The hydraulic and heated equivalent diameters are approximations used to translate more complex flow geometries into equivalent circular tube geometries. The diameters should not be used interchangeable but accordingly with the suggestion by whomever developed the correlation in the case where no experimental data is available. Although the definitions are not always clear, it is a general assumption to assume the heated diameter for rod bundle geometries and the hydraulic diameter for annular geometries as the appropriate characteristic length in heat transfer calculation. In the case of the Look-up table for critical heat flux developed by Groeneveld et al (2007), the author (Groeneveld et al, 1999) explicitly suggest a correction factor based on the hydraulic diameter and, therefore, the use of the heated diameter underestimates the critical heat flux.

References

- Barnett, P. D., "A correlation of burnout data for uniformly heated annuli and its use for predicting burnout in uniformly heated rod bundles", AEEW-R 463, 1966.
- Dingee, D. A., Bell, W. B., Chastain, J. W., and Fawcett, S. L., "Heat transfer from parallel rods in axial flow", Battelle Memorial Institute, Report BMI-1026, 1955.
- El-Genk, M. S., Su, b., and Guo, z., "Experimental Studies of Forced, Combined and Natural Convection of Water in Vertical Nine-Rod Bundles with a Square Lattice," *Int. J. Heat Mass Transfer*, 36, 2359-2374, 1993.
- Groeneveld, D. C., Cheng, S. C., and Doan, T., "1986 AECL-UO Critical Heat Flux Lookup Table," *Heat Trans. Eng.*, 7, 46-62, 1986.
- Groeneveld, D. C., et al, "Computation of single- and two-phase heat transfer rates suitable for water-cooled tubes and sub channels", *Nuclear Engineering and Design*, 144, 61-77, 1989
- Groeneveld, D. C., et al, "The 2006 CHF look-up table", *Nuclear Engineering and Design*, 237, 1909-1922, 2007.

Attachment 10

Critical Heat Flux Testing at the University of Wisconsin Final Report

30441R00041/A

Groeneveld, D. C., et al., "A General Method of Predicting Critical Heat Flux in Advanced Water-Cooled Reactors," Proceedings of the 9th International Topical Meeting on Nuclear Reactor Thermal Hydraulics (NURETH-9), San Francisco, California, October 1999

Kim, J.H., and Li, W.-H., "Heat Transfer in Laminar Flow Along Circular Rods in Infinite Square Arrays," J. Heat Transfer, 110, 252-257, 1988.

McAdams, W. H., et al., "Heat Transfer at High Rates to Water with Surface Boiling," Ind. Eng. Chem., 41, 1945-1955, 1949.

Weisman, J., "Heat Transfer to Water Flowing Parallel to Tube Bundles," Nuclear Science and Engineering, 6, 78-79, 1959.

Appendix 2: Operational Procedure

OPERATIONAL PROCEDURE

1. Turn on computer and open labview program controlling experiment
2. Turn on VFD's controlling primary and heat exchanger pumps
3. Visual check that all instrumentation is working properly
 - a. TC's, Pressure, Flow meters, etc.
4. Fill reservoir with deionized water to level slightly above test section return port
 - a. Open ball valve at water storage tank
 - b. Open ball valve at test rig inlet
 - c. Open ball valve at primary pump outlet (water can now flow to test loop)
 - d. Turn on primary pump to fill reservoir to desired level – pump flow $>0.5\text{kg/s}$
 - e. Close ball valve at test rig inlet and water storage tank
5. Energize glycol chiller for heat exchanger cooling
 - a. Ensure that chiller pump starts and VFD is outputting 40Hz
6. Turn on heat exchange pump to flow reservoir water through heat exchanger, adjust pump speed to achieve a flow rate of $\sim 50\text{GPM}$
7. Open return side cooling valve (valve is for water returning from the reservoir), leave supply side closed
8. Open pneumatic ball valves at the entrance and exit of the test section
9. Energize and adjust primary pump to achieve a flow rate of $\sim 1\text{kg/s}$ through test section and let run for a minimum of 5 minutes in order to remove any air entrained within the system
10. Adjust regulator to pressurize system to desired pressure level
11. Bleed air from the high pressure and low pressure sides of the differential pressure transducer
12. Zero coriolis flow meter
 - a. Shut off primary pump, allow system flow to stabilize
 - b. Close pneumatic ball valves
 - c. Utilize flow meter transmitter to zero flow meter
 - i. Enter Setup mode
 - ii. Enter Calibration mode
 - iii. Enter Flow Zero mode
 - iv. Push "0" to calibrate flow meter
 - v. Accept calibration – write down zero value
 - vi. Return to Measure mode
 - d. Open pneumatic ball valves
13. Energize and adjust primary pump to achieve flow rate for desired testing conditions
14. Prepare to turn on main power supply
 - a. Turn on power supply disconnect switch
 - b. Check labview to verify that the power level is set to 0
 - c. Check controller to verify that no signal is present
 - d. If 0 voltage present, turn on power supply at power supply main controller panel
 - e. Power supply can now be operated from labview control screen
15. Increase power level in labview to reach desired rod power, ($\sim 20\text{-}30\text{kW}$), for preheating water in reservoir to desired testing conditions
16. While waiting for reservoir to reach temperature
 - a. Setup lights to illuminate test section

- b. Setup high speed cameras and SLR camera
 - c. Verify that thermal trigger and optical trigger are functioning
- 17. Once the desired reservoir temperature is reached verify that the mass flow and pressure are also within specifications, adjust if needed
- 18. Adjust glycol flow through heat exchanger to maintain desired inlet water temperature by partially opening (1 full turn to start) the supply side cooling valve
- 19. Once inlet temperature stabilizes slowly lower heater rod power level to zero
- 20. Allow inlet temperature to drop 0.5°C below
- 21. Increase power level to reach desired heat flux according to test matrix
 - a. Increase data collection to 0.1 seconds while heating
- 22. Adjust glycol flow through heat exchanger to limit the temperature increase to less than 1°C/5minutes
- 23. Allow inlet temperature to rise 0.5°C above desired inlet temperature
- 24. Slowly lower heater rod power level to zero
 - a. Decrease data collection to 1 second while cooling
- 25. Allow inlet temperature to drop 0.5°C below desired inlet temperature according to the test matrix
- 26. Repeat steps 21-25 until all runs within the test matrix are completed or a CHF event has occurred

Appendix 3: Sample Error Calculations



: Example Error Calculations

 T_{in} Error Calculation Example

$$\text{Error } +/- = T_{in} +/- 1.1^*$$

* Special Limits of Error for K-Type Thermocouples

 T_{out} Error Calculation Example

$$\text{Error } +/- = T_{out} +/- 1.1^*$$

* Special Limits of Error for K-Type Thermocouples

 P_{out} Error Calculation Example

$$\text{Error } +/- = (P_{out} +/- 0.414^{**})$$

** Calculated from Reference Accuracy Equations from manufacturer

$$+/- (0.0075 * ([URL/Span]) \% \text{ of Span})$$

$$URL = 800 \text{ psi}$$

$$Span = 50 \text{ psi}$$

$$0.06 \text{ psi} = 0.414 \text{ kPa}$$

DP Error Calculation Example

$$\text{Error } +/- = (DP +/- 0.076^{**})$$

** Calculated from Reference Accuracy Equations from manufacturer

$$+/- (0.005 + 0.0035 * ([URL/Span]) \% \text{ of Span})$$

$$URL = 300 \text{ psi}$$

$$Span = 10 \text{ psi}$$

$$0.011 \text{ psi} = 0.076 \text{ kPa}$$

Mass Flux Error Calculation Example

$$\text{Error } +/- = \text{Mass Flux } +/- \text{ Accuracy}^{***}$$

*** Calculated from Accuracy Equation from Manufacturer

$$+/- 0.10\% + ((\text{Zero Instability} / \text{Mass Flow Rate}) * 100) \% \text{ of mass flow}$$

$$\text{Zero Instability} = 7.56666 * 10^{-5} \text{ kg/s}$$

Example error calculations for Heat Flux, Mass Flux, and Rod Power calculated using EES software

File: C:\Users\THL\Desktop\GA error calculations EES 3/6/2017 1:36:55 PM Page 1
 EES Ver. 10.203: #100: For use only by Students and Faculty, College of Engineering University of Wisconsin - Madison

```
L= 17.85*convert(in,m)
L_error=
d_i=0.25029*convert(in,m)
d_i_error=
d_o=.656*convert(in,m)
d_o_error=
flow_a=pi#/4*(d_o^2-d_i^2)
m_dot=
m_dot_error=0.0011
Volt=67.30607
volt_error=0.01
Amp=1115.009
Amp_error=0.01
power=volt*amp
H_a=L*d_i*pi#
h_flux=power/h_a
mass_flux=m_dot/flow_a
```

5a, d, e, f

Unit Settings: SI C kPa kJ mass deg

Variable ± Uncertainty	Partial derivative	% of uncertainty
h_{flux} = [W/m²]		
Amp = 1115 ± 11.15 [A]	∂h _{flux} /∂Amp = 7433	37.56 %
d _i = 0.006357 [m]	∂h _{flux} /∂d _i = -1.304E+09	6.00 %
d _o = 0.01666 [m]	∂h _{flux} /∂d _o = 0	0.00 %
L = 0.4534 [m]	∂h _{flux} /∂L = -1.828E+07	18.89 %
ṁ = [kg/s]	∂h _{flux} /∂ṁ = 4.478E-10	0.00 %
Volt = 67.31 ± 0.6731 [V]	∂h _{flux} /∂Volt = 123134	37.56 %
mass_{flux} = [kg/(m²·s)]		
Amp = 1115 ± 11.15 [A]	∂mass _{flux} /∂Amp = 0	0.00 %
d _i = 0.006357 [m]	∂mass _{flux} /∂d _i = 265603	3.43 %
d _o = 0.01666 [m]	∂mass _{flux} /∂d _o = -696140	94.33 %
L = 0.4534 [m]	∂mass _{flux} /∂L = 0	0.00 %
ṁ = [kg/s]	∂mass _{flux} /∂ṁ = 5367	2.24 %
Volt = 67.31 ± 0.6731 [V]	∂mass _{flux} /∂Volt = 0	0.00 %
power = 75047 ± 1061 [W]		
Amp = 1115 ± 11.15 [A]	∂power/∂Amp = 67.31	50.00 %
d _i = 0.006357 [m]	∂power/∂d _i = 0	0.00 %
d _o = 0.01666 [m]	∂power/∂d _o = 0	0.00 %
L = 0.4534 [m]	∂power/∂L = 0	0.00 %
ṁ = [kg/s]	∂power/∂ṁ = 0	0.00 %
Volt = 67.31 ± 0.6731 [V]	∂power/∂Volt = 1115	50.00 %

5a, d, e, f

5a, d, e, f

5a, d, e, f

No unit problems were detected.

Appendix 4: Calibrations

1/8" Thermocouples



Form:053-0005-3 Rev.C

Certificate Of Calibration

for

University of Wisconsin-Madison

Cust. P.O. #: GA101016

Report #: OM- 121123315

Test Item: KMQ316SS-125U-12-CAL-3

WO : SC00215380

Recal Date: Per System Application

Ref. I.D.: WK140410-02

CAL-3

Omega Engineering, Inc. certifies that the above instrumentation has been calibrated and tested to **meet or exceed** the published specifications. This calibration and testing was performed using instrumentation and standards that are traceable to the **National Institute of Standards and Technology**. Calibration has been performed in compliance with ISO 10012-1, ISO 9001 and ANSI/NCSL Z540-1-1994 as well as ASTM E 230 and ANSI MC96.1. This Certificate/Report shall not be reproduced, except in full, without written consent of Omega Engineering Inc.

Test Conditions: Temperature 73°F Relative Humidity 29%

Procedure used: QAP-2100

The maximum calibration uncertainty is calculated to be 0.3C from -25C to 500 C and 0.55C from 500C to 1100C.

INSTRUMENTS USED:

MODEL	SERIAL#	CAL DUE DATE	N.I.S.T. NUMBERS
RTD (Burns)	745098	06/29/17	NNPR-100-01
RTD (Burns)	765565	06/29/17	NNPR-100-05
RTD (Burns)	765566	06/29/17	NNPR-100-06
Agilent 34401A	US36027293	04/02/17	NNDM-100-31
TRCIII	I-0012	06/10/17	NNCL-098-31
DP251	2193-022-2473	06/29/17	NNDP-100-10

Probe No.	Nominal Temperature	Actual Test Temperature	Indicated Temperature
1	212 °F	212.0 °F	211.7 °F
1	392 °F	392.0 °F	393.3 °F
1	752 °F	752.0 °F	753.0 °F

Brian Arnone
Metrology Technician
 Calibration Date: 10-28-16

Carl J. Munkin Jr.
Quality Assurance Inspector
 Page 1 of 2

OMEGA Engineering, Inc., One Omega Circle, P.O. Box 336, Bridgeport, NJ 08014-0336 Telephone: (856) 467-4200 · FAX: (856) 467-1212

www.omega.com e-mail: info@omega.com

WCS - 0638A

1/16" Thermocouples:



Form: 053-0001-3 Rev. E

Certificate Of Calibration

for

University Of Wisconsin - Madison

Cust. P.O. #: GA Report #: OM- 121123377
 Test Item: KMQ316SS-062U-18-CAL-4-3P WO : SC00224992

Recal Date: Per System Application

Ref. I.D.: VK141013-07

CAL-4

Omega Engineering, Inc. certifies that the above instrumentation has been calibrated and tested to **meet or exceed** the published specifications. This calibration and testing was performed using instrumentation and standards that are traceable to the **National Institute of Standards and Technology**. Calibration has been performed in compliance with ISO 10012-1, ISO 9001 and ANSI/NCSS Z540-1-1994 as well as ASTM E 230 and ANSI MC96.1. This Certificate/Report shall not be reproduced, except in full, without written consent of Omega Engineering Inc.

Test Conditions: Temperature 72°F Relative Humidity 21%

Procedure used: QAP-2100

The maximum calibration uncertainty is calculated to be 0.3C from -25C to 500 C and 0.55C from 500C to 1100C.

INSTRUMENTS USED:

MODEL	SERIAL	CAL DUE DATE	N.I.S.T. NUMBERS
Agilent 34401A	US36127770	04/02/17	NNDM-100-32
DP251	3010-018-1409	12/07/16	NNDP-098-02
DP251	1360-007-924	06/01/17	NNDP-100-12
TRCIII	5	06/10/17	NNCL-098-19
RTD (Burns)	912379	06/16/17	NNPR-100-13
RTD (Rosemount)	5061	06/01/17	NNPR-100-18
RTD (ASL)	B448507	06/29/17	NNPRB-100-02

Probe No.	Nominal Temperature	Actual Test Temperature	Indicated Temperature
1	0°C	0.00°C	0.60°C
1	100°C	100.00°C	99.83°C
1	300°C	300.00°C	299.74°C
-----	-----	-----	-----

[Signature]
Metrology Technician

Calibration Date: 11/28/16

[Signature]
Quality Assurance Inspector


Page 1 of 2

OMEGA Engineering, Inc., One Omega Circle, P.O. Box 336, Bridgeport, NJ 08014-0336 Telephone: (856) 467-4200 · FAX: (856) 467-1212

www.omega.com e-mail: info@omega.com

WCS - 0638A

Shunt:



RAM METER INC.®
Instrument Sales & Service Center
Electronic Development & Manufacturing
FOUNDED 1936

CERTIFICATE OF CALIBRATION
UNIVERSITY OF WISCONSIN
1500 ENGINEERING DR
MADISON, WI 53706

Manufacturer RAM METER	Model Number 22M	Serial Number N/A	Description 1200AMP 50MV	
Calibration Date 10/18/16	Calibration Due Date 10/18/17	Lab Supervisor TODD RUTILA	<i>Todd Rutilla</i>	
Purchase Order No. PAUL BROOKS 10/12/16	Ram Meter Number SR-0005420	Ambient Temperature 73°F	Relative Humidity 64%	Accurate Within ±0.6%

Certification
Ram Meter Inc. certifies that the instrument listed above has been calibrated to the Manufacturer's specifications (tolerances). The calibration of our laboratory standards used in calibrating your instrument is traceable to the National Institute of Standards and Technology or other national physical measures recognized as equivalent to NIST. The NIST numbers of traceability are listed below.

NIST Number(s)
2358200002 T
2358200001 T
012011-2
ELR001:1340626375

FINAL READING: 0.00004165Ω

Additional Information
THE CALIBRATION SYSTEM TO CONTROL THE ACCURACY OF OUR MEASURING AND TEST EQUIPMENT COMPLIES WITH MIL-STD-45662A.

1903 Barrett Dr. • Troy, Michigan 48064-5396 • (248)362-0990 • FAX (248)362-1818

Gauge Pressure Transmitter:



22 November, 2016

Emerson Process Management
Rosemount Inc.
6021 Innovation Blvd
Shakopee, MN 55379

Calibration Data Sheet Consistent with ISO 10474 3.1 or EN 10204 3.1

Customer Information Name: WISCONSIN UNIVERSITY OF PO: CC-Anderson-09-Nov-16	Manufacturer Information Sales Order: 4748656 Line: 2
Device Information Device Type: Pressure Transmitter PTag: Serial No: 2875322 Model No: 3051TG3A2B21AQ4M5 Module Serial No: 16114932 Output: Linear Device ID: 16114932	Calibration Information Factory: SHAKOPEE, MN, USA Station Name: SHAK_INLINE_CALIBRATION_04 Operator ID: 60525 Calibration Date: 11/21/2016 1:53:26PM Internal Ref # 20041114

Equipment Used

EqNumber:	EqName:	CalDueDate:
E3-59379	Multimeter	5/20/2017 8:40:00AM
E3-59386	Load Box	7/20/2017 9:35:00AM
P3-55130	Pressure Controller	2/21/2017 11:38:00AM

Calibration Data

Range: 0.000 TO 800.000 PSI

% of Range	Applied Pressure	Requested Applied Pressure	Analog Output (mA)	% Span Error	Pass/Fail
100.000	800.000 PSI	800.0000 PSI	20.00010	0.00063	PASS
80.000	640.000 PSI	640.0000 PSI	16.79992	-0.00050	PASS
60.000	480.000 PSI	480.0000 PSI	13.59988	-0.00075	PASS
40.000	320.000 PSI	320.0000 PSI	10.39998	-0.00012	PASS
20.000	160.000 PSI	160.0000 PSI	7.20018	0.00113	PASS
0.000	0.000 PSI	0.0000 PSI	4.00014	0.00088	PASS

This is to certify that the listed product meets the applicable Rosemount Specifications. Measuring and test equipment used in the manufacture and inspection of the listed product are traceable to the National Institute of Standards and Technology. The calibration system was designed to meet the intent of ANSI Z540-1-1994.

Kelly Klein
Vice President of Global Quality, Approvals & EHS


DP Pressure Transmitter:



22 November, 2016

Emerson Process Management
Rosemount Inc.
6021 Innovation Blvd
Shakopee, MN 55379

Calibration Data Sheet Consistent with ISO 10474 3.1 or EN 10204 3.1

Customer Information Name: WISCONSIN UNIVERSITY OF PO: CC-Anderson-09-Nov-16	Manufacturer Information Sales Order: 4748656 Line: 1
Device Information Device Type: Pressure Transmitter Tag No: Serial No: 0887364 Model No: 3051S1CD4A2E12A1AM5Q4 Module Serial No: 14409685 Output: Linear	Calibration Information Factory: SHAKOPEE, MN, USA Station Name: SHAK_CPLR_CALIBRATION_03 Operator ID: 46369 Calibration Date: 11/21/2016 8:22:44AM Internal Ref # 20041113 

Equipment Used

EqNumber:	EqName:	CalDueDate:
E3-59122	Load Box	2/20/2017 10:53:00AM
E3-59128	Multimeter	9/20/2017 9:30:00AM
P3-55024	Pressure Controller	12/26/2016 7:23:00AM

Calibration Data

Range: 0.000 TO 300.000 PSI

% of Range	Applied Pressure	Requested Applied Pressure	Analog Output (mA)	% Span Error	Pass/Fail
100.000	300.000 PSI	300.0000 PSI	20.00010	0.00063	PASS
80.000	240.000 PSI	240.0000 PSI	16.80056	0.00350	PASS
60.000	180.000 PSI	180.0000 PSI	13.60072	0.00450	PASS
40.000	120.000 PSI	120.0000 PSI	10.40092	0.00575	PASS
20.000	60.000 PSI	60.0000 PSI	7.19932	-0.00425	PASS
0.000	0.000 PSI	0.0000 PSI	4.00052	0.00325	PASS

This is to certify that the listed product meets the applicable Rosemount Specifications. Measuring and test equipment used in the manufacture and inspection of the listed product are traceable to the National Institute of Standards and Technology. The calibration system was designed to meet the intent of ANSI Z540-1-1994.

Kelly Klein
Vice President of Global Quality, Approvals & EHS

Reference Multimeter:

CERTIFICATE OF CALIBRATION		Page: 01 of 01
PRECISION METROLOGY		
7350 North Teutonia Avenue Milwaukee, WI 53209 (414) 351-7420 * FAX: (414) 351-7429		
1001960527		
Certification Number		
Gage ID	MY41026086	Manufacturer AGILENT
Type	MULTIMETER AGILENT 34401A	Model Number 34401A
Company	UNIVERSITY OF WI - MADISON/PHYSICS	Serial Number MY41026086
		Size N/A
		Department N/A
		Cal Date 01/21/2017
Calibrated By: MJG	Gage Calibrated at Precision Metrology	Next Cal Due 01/2018
		Temp 73.0°F Humidity 29.0%RH
		Standard Used ED1414
		Proc: MSP.00754 (P)

This is to certify that the above instrument was calibrated by Precision Metrology using standards traceable to the National Institute of Standards & Technology (NIST). The results indicated on this certificate relate only to the item(s) calibrated. Precision Metrology is accredited to ISO/IEC 17025:2005 which satisfies all requirements of ISO 9001:2008 & ANSI/NCCL Z.540-1:1994. Unless otherwise stated, all of the parameters calibrated on this certificate are within Precision Metrology's scope of accreditation. The expanded measurement uncertainty is reported at k=2, 95% confidence level. This certificate and attachments may not be reproduced, except in full, without the written approval of Precision Metrology.

CALIBRATION STD(s)	DESCRIPTION	Cal Due Date	Test Report#
ED0344	CALIBRATOR FLUKE 5520A WITH 600MHZ OPT	01/31/2017	1001787551

TOLERANCE
 PER MANUFACTURER'S SPECIFICATIONS
 SEE ATTACHED SPREADSHEET FOR READINGS

CONDITION
 RECEIVED WITHIN MANUFACTURER'S SPECIFICATIONS
 RETURNED WITHIN MANUFACTURER'S SPECIFICATIONS

Unless otherwise stated, measurements have been compared to the unmodified tolerances and dimensional values are referenced to 68°F.
 Precision Metrology's responsibility shall in no event, nor for any cause whatsoever exceed the purchase price of this certification. Last Page unless stated.
 -----Last Page-----



Reference Handheld Thermocouple Reader:

 Ω OMEGA	
CERTIFICATE OF CALIBRATION	
Model: <u>HH506A</u>	Serial Number: <u>1600566</u>
<p>Omega Engineering, Inc., certifies that the above listed instrument has been calibrated using standards whose accuracy is traceable to the U.S. National Institute of standards and Technology, and meets or exceeds its published specifications. Calibration traceability of the above listed instrument is in full compliance with ANSI/Z540-1-1994 standards and requirements.</p>	
	<u>SEP 20 2016</u>
<u>DATE</u>	<u>L.M. Pereng</u>
<u>TESTED</u>	<u>Y.I. Tsung</u>
<u>AUTHORIZED SIGNATURE</u>	
<small>MO-4 ©Copyright 1999 Omega Engineering, Inc.</small>	

Coriolis Flow Meter:



I/A Series
Mass Flowmeter

CUSTOMER NAME.....UNIVERSITY OF WISCONSIN
CUSTOMER DATA.....03-FE-2002A.
FoxboroSAP, Number...60166749/10
MODEL CODE.....CFS10-08SCFNN-F
Style.....B
Serial Number.....01063106
Calibration transmitter: CFT10-....s/n 6360040.

Actual Flowrate (lb/min)	Ind. Flowrate (lb/min)	Error
193.6595	193.5712	-.046 %
193.1751	193.1162	-.030 %
101.4301	101.4576	.027 %
51.5955	51.5869	-.017 %
20.1748	20.1881	.066 %

DENSITY and FLOW CONSTANTS

Density Coefficient (DC1) -4.299400E+01
Density Coefficient (DC2) +8.962600E+04
Density Coefficient (DC3) +1.215900E-01
Density Coefficient (DC4) -2.555900E+03

Flow Coefficient (FC1) -2.842200E-04
Flow Coefficient (FC2) +6.721100E-01
Flow Coefficient (FC3) -6.959700E-07
Flow Coefficient (FC4) +6.721100E-01

Nominal Capacity 1.51

ALL MEASUREMENT STANDARDS ARE CALIBRATED AT SCHEDULED INTERVALS BY THE NATIONAL INSTITUTE OF STANDARDS AND TECHNOLOGY (NIST), OR AGAINST CERTIFIED STANDARDS WHICH ARE TRACEABLE TO THE NATIONAL INSTITUTE OF STANDARDS AND TECHNOLOGY, FORMELY NATIONAL BUREAU OF STANDARDS (NBS).

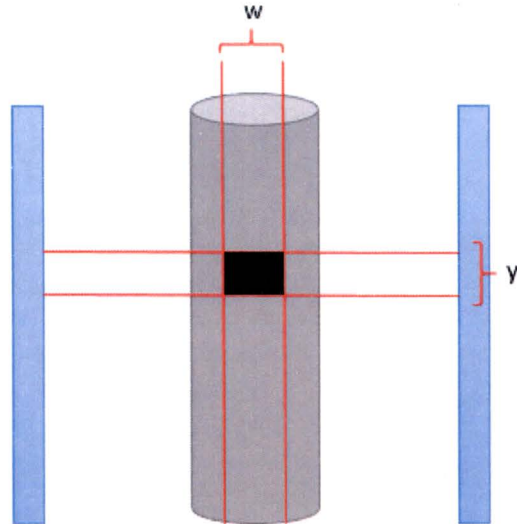
Test Date 7/11/2016
Calibrated by ... LVN
Approved by..... CW 7/11/16

Neponset Field Devices,
38 Neponset Ave.,
Foxboro, Ma. 02035 USA T +1 866 746 6477
www.fielddevices.foxboro.com

Appendix 5: Void Generation Sample Calculation

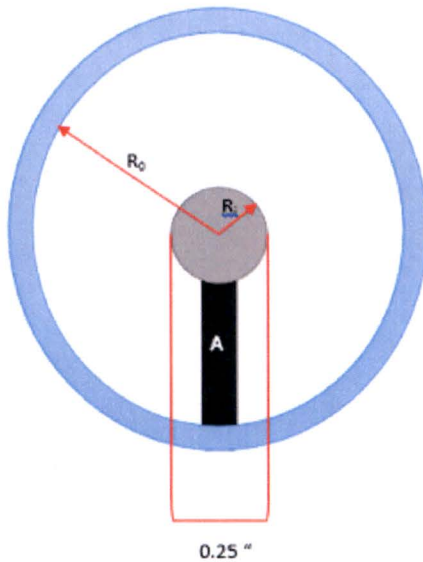


1. Measure 0.25" Inconel Rod, set scale to (6.35 mm)
2. Chop off (1.590 mm) from each side of 0.25" rod, leaving center region (w = 3.17 mm)
3. Looking at the cross section, shaded area is bubble measurement was taken. "y" changed slightly for each picture so splicing bubbles could be avoided – would be close to 3.5 mm.



R_i = Heater Rod = 3.175 mm

R_o = Glass Rod (Inner diameter) = 8.017 mm



$$A = \int_{-R_i/2}^{R_i/2} \sqrt{R_o^2 - x^2} - \sqrt{R_i^2 - x^2} dx$$

$$A = \int_{-1.59}^{1.59} \sqrt{69.41 - x^2} - \sqrt{10.08 - x^2} dx$$

$$A = 16.6745 \text{ mm}^2$$

$$\text{Volume}(\text{total}) = A * y = 16.6745 \text{ mm}^2 * (\sim 3.5) \approx 58.4 \text{ mm}^3$$

Appendix 6: Rod Surface Roughness

A Zygo New View 6K White Light Interferometer (*Figure 32: Zygo New View 6K White Light Interferometer*) was used to measure the surface roughness of the rods. The Zygo functions by directing white light at a surface and measuring the resulting interference caused by the reflected light to create a scan of the surface.



Figure 32: Zygo New View 6K White Light Interferometer

Most rods were scanned in three places before and after testing to determine surface roughness. These scans were done on the heated surface of the rod, namely the 0.25" diameter X 0.02" wall Inconel 625 tube. The first scan was near the bottom of the rod. The second was in the middle of the rod. The final scan was 1-2cm from the point of failure. The software generates an image of the surface (*Figure 33: Typical zygo scan of a rod surface*) and calculates a root mean square (RMS) and roughness average (RA) which can be used to compare the rod before and after the test (Table 2 and Figure 34). The software is able to correct for the cylindrical shape of the rod so no extra calculations need to be done to the values.

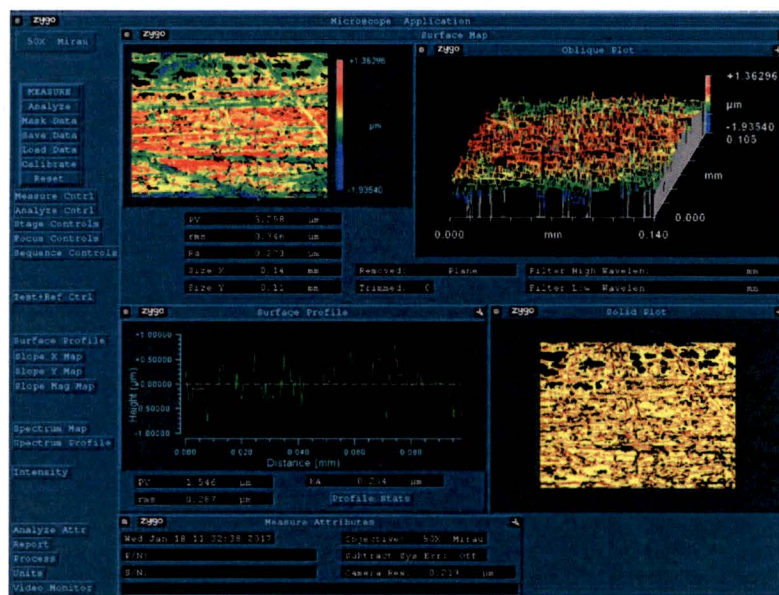


Figure 33: Typical zygo scan of a rod surface

Table 2: Surface Roughness Measurements

	RMS Before (μm)	RA Before (μm)	RMS After (μm)	RA After (μm)
Rod 1 (bottom)			0.726	0.575
Rod 1 (middle)			0.487	0.35
Rod 1 (top)			0.528	0.384
Rod 2 (bottom)			0.947	0.765
Rod 2 (middle)			0.461	0.331
Rod 2 (top)			0.583	0.437
Rod 3 (bottom)	0.287	0.234	0.527	0.416
Rod 3 (middle)	0.441	0.355	0.452	0.348
Rod 3 (top)	0.499	0.371	0.427	0.32
Rod 4 (bottom)	0.574	0.445	0.308	0.233
Rod 4 (middle)	0.373	0.274	0.314	0.245
Rod 4 (top)	0.458	0.37	0.318	0.24
Rod 5 (bottom)	0.357	0.279	0.442	0.343
Rod 5 (middle)	0.349	0.279	0.387	0.29
Rod 5 (top)	0.39	0.279	0.629	0.489
Rod 6 (bottom)	0.345	0.272		
Rod 6 (middle)	0.284	0.224		
Rod 6 (top)	0.303	0.225		

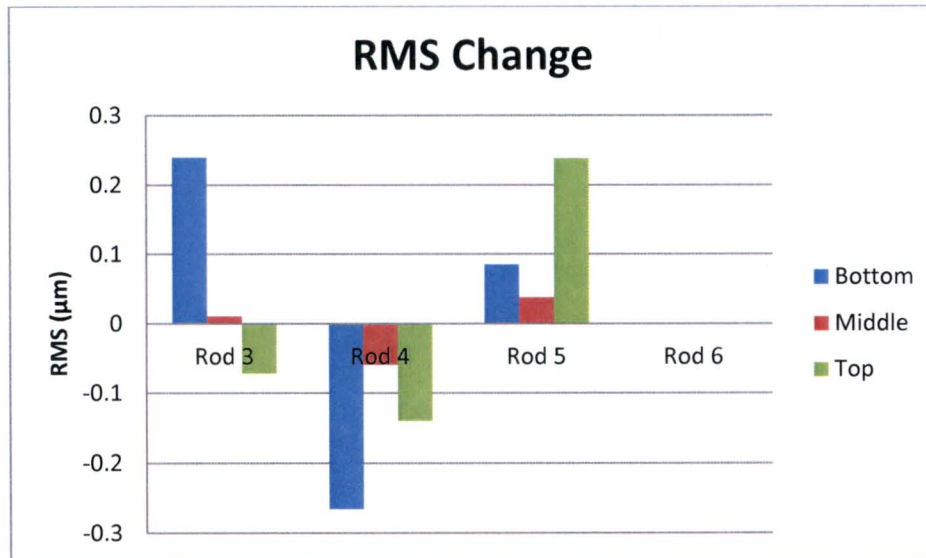


Figure 34: RMS Change of Rods 3-6

The change at the top of the rod is of particular interest because this is where the CHF occurs. It can be seen that the surface roughness typically decreases near the area where the CHF occurs, with rod 5 being an exception where the surface roughness appears to have increased. The middle of the rod is largely unchanged due to testing. The bottom of the rods indicate large variances.



Appendix 7: List of Experimental Runs

CHF Run Conditions Index

By date

- 01.05.2017
 - Conditions:
 - Flow: [REDACTED]
 - $T_{in}(\text{fixed})$: [REDACTED]
 - Pressure: [REDACTED] inlet
 - Notes on test results

- 01.10.2017
 - Conditions:
 - Flow: [REDACTED]
 - $T_{in}(\text{fixed})$: [REDACTED]
 - Pressure: [REDACTED] inlet

- 01.11.2017
 - Conditions:
 - Flow: [REDACTED]
 - $T_{in}(\text{fixed})$: [REDACTED]
 - Pressure: [REDACTED] inlet

- 01.26.2017
 - Conditions:
 - Flow: [REDACTED]
 - $T_{out}(\text{fixed})$: [REDACTED]
 - Pressure: [REDACTED] outlet

- 01.27.2017
 - Conditions: Data was not writing from NI (i.e. no NI data)
 - Flow: [REDACTED]
 - $T_{out}(\text{fixed})$: [REDACTED]
 - Pressure: [REDACTED] outlet

- 01.28.2017
 - Conditions:
 - Flow: [REDACTED]
 - $T_{out}(\text{fixed})$: [REDACTED]
 - Pressure: [REDACTED] outlet

- 01.30.2017
 - Conditions:



- Flow: [REDACTED]
- $T_{out}(\text{fixed})$: [REDACTED]
- Pressure: [REDACTED] outlet

5a, d, e, f

• 02.09.2017

○ Conditions:

- Flow: [REDACTED]
- $T_{out}(\text{fixed})$: [REDACTED]
- Pressure: [REDACTED] outlet
- CHF at [REDACTED], failed rod #3
- High speed videos at [REDACTED]

5a, d, e, f

• 02.21.2017

○ Conditions

- Flow: [REDACTED]
- $T_{in}(\text{fixed})$: [REDACTED]
- Pressure: [REDACTED] (actual pressure [REDACTED] due to neglected head pressure)
- Heat Flux: [REDACTED]
- High speed videos at 3 locations; top, middle, and bottom of heater rod

5a, d, e, f

• 02.21.2017

○ Conditions

- Flow: [REDACTED]
- $T_{in}(\text{fixed})$: [REDACTED]
- Pressure: [REDACTED] inlet (actual pressure [REDACTED] due to neglected head pressure)
- Heat Flux: [REDACTED]
- High speed videos at 3 locations; top, middle, and bottom of heater rod

5a, d, e, f

• 02.21.2017

○ Conditions

- Flow: [REDACTED]
- $T_{out}(\text{fixed})$: [REDACTED]
- Pressure: [REDACTED] outlet
- CHF at [REDACTED], failed rod #4
- High speed videos at [REDACTED]

5a, d, e, f

• 02/23/2017 – Run 1

○ Conditions:

- Flow: [REDACTED]
- $T_{out}(\text{fixed})$: [REDACTED]
- Pressure: [REDACTED] outlet
- CHF at [REDACTED]
- High speed videos at [REDACTED]

5a, d, e, f



- 02/23/2017 – Run 2
 - Conditions:
 - Flow: [REDACTED]
 - $T_{out}(\text{fixed})$: [REDACTED]
 - Pressure: [REDACTED] outlet
 - CHF at [REDACTED], failed rod #5
 - High speed videos at [REDACTED]

- 02/24/2017 – 02/27/2017
 - Conditions:
 - Flow: [REDACTED]
 - $T_{out}(\text{fixed})$: [REDACTED]
 - Pressure: [REDACTED] outlet
 - CHF at [REDACTED]
 - High speed videos at [REDACTED]

5a, d, e, f

5a, d, e, f

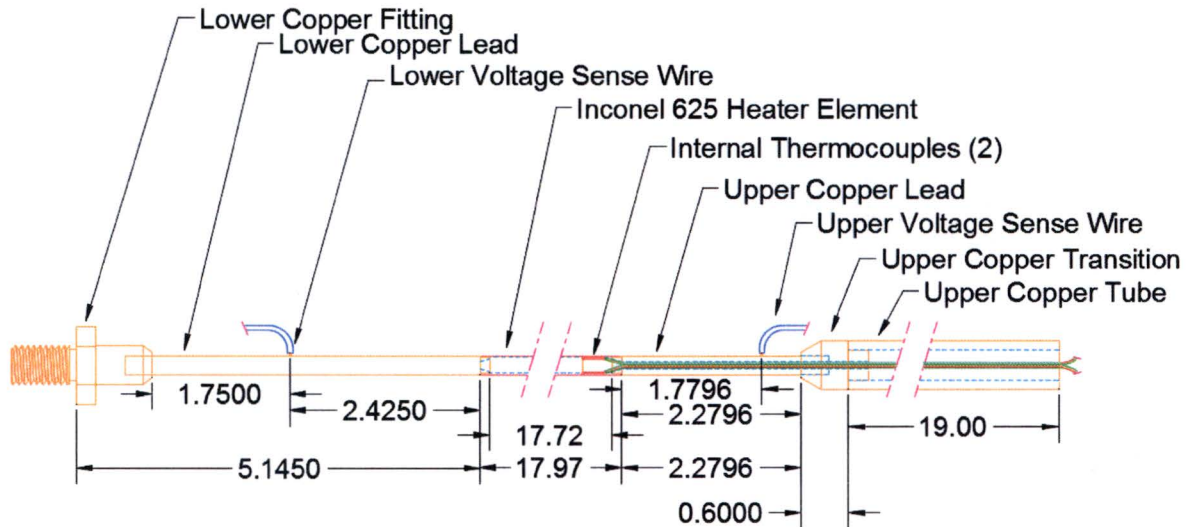


Appendix 8: Mechanical Drawings

(All Dimensions in Inches)

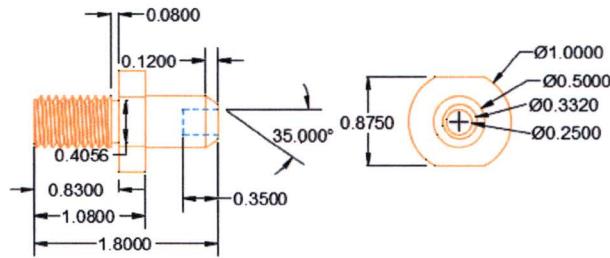


Heater Rod Assembly: inches

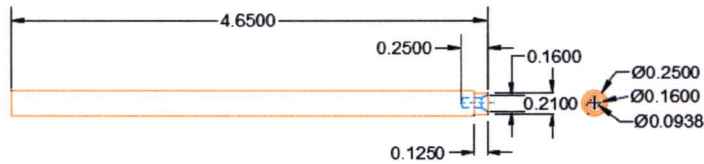


Heater Rod Components, inches

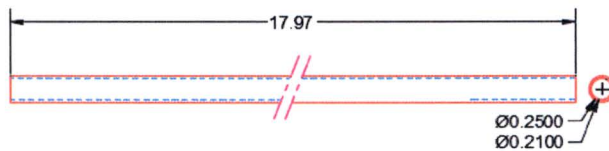
Lower Copper Fitting



Lower Copper Lead

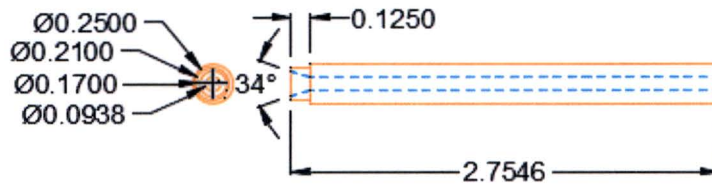


Inconel 625 Heater Element

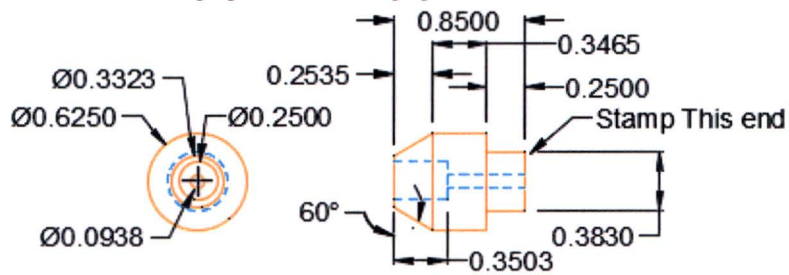


Heater Rod Components, inches

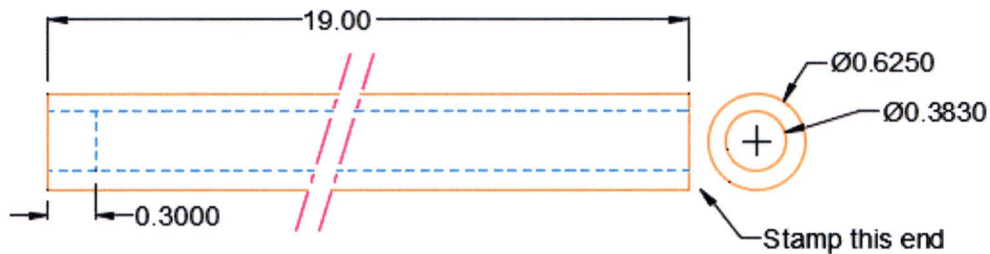
Upper Copper Lead



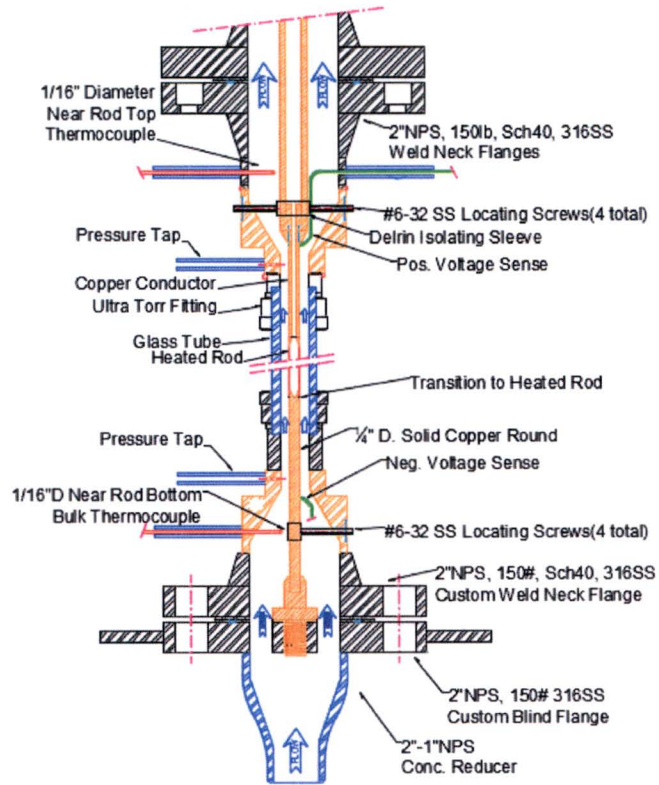
Upper Copper Transition



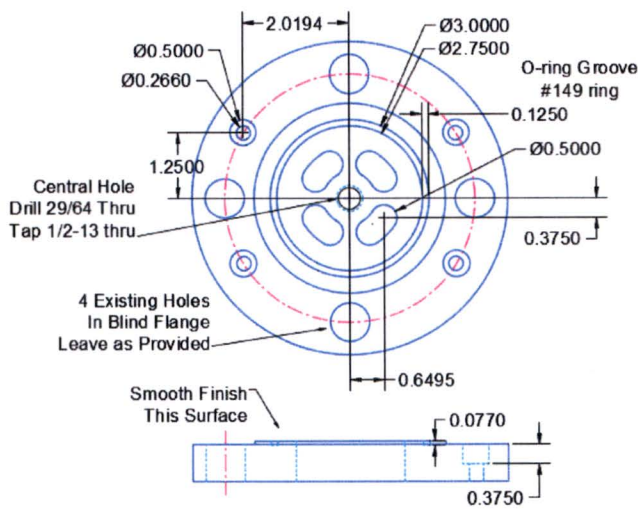
Upper Copper Tube



Test Section Components: inches

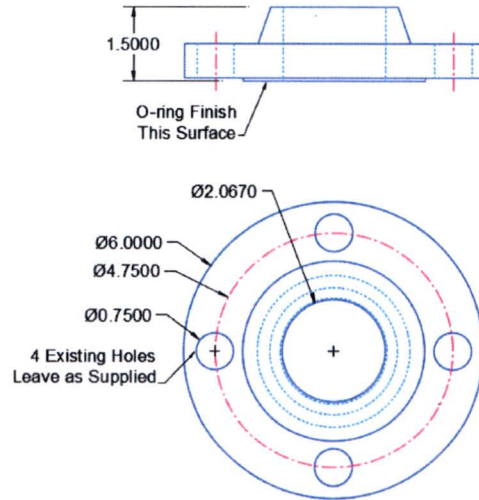


316SS Custom Blind Flange:
2"NPS,150lb, Blind Flange, 1 Required

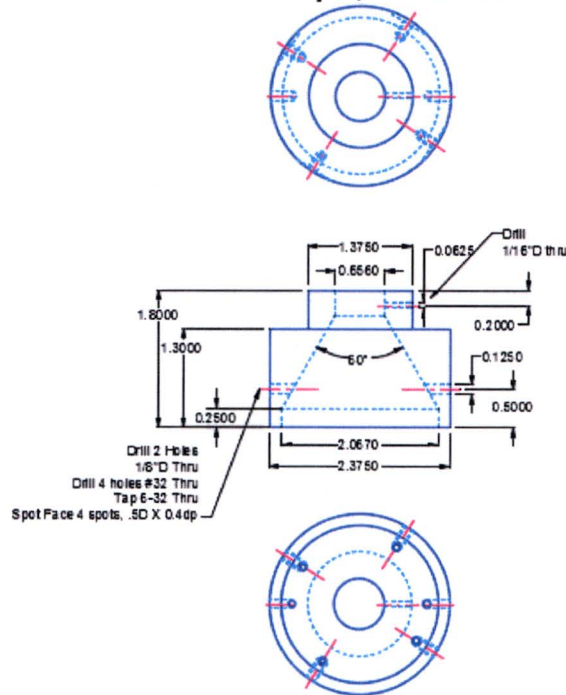


Test Section Components: inches

316SS Flange Beneath Test Section:
2"NPS,150lb, Sch40 bore, Weld Neck Flange, 1 Required

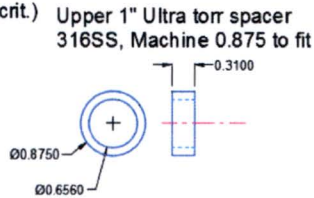
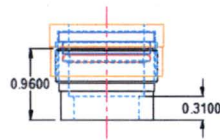


Lower Transition
1 Req'd, 316 SS

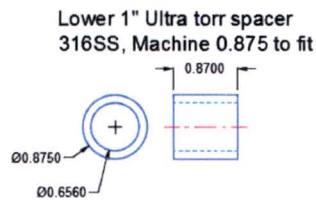
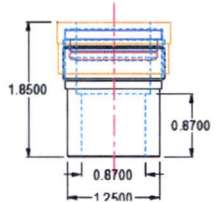


Test Section Components: inches

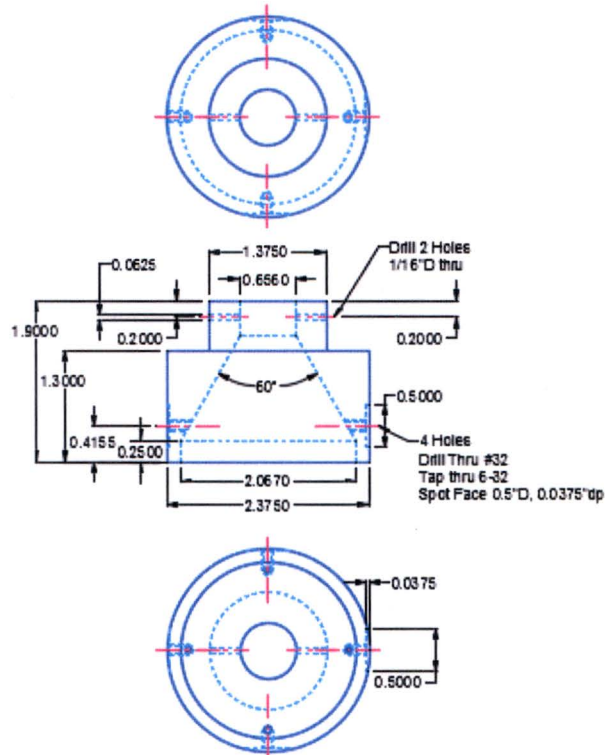
Upper Test Section
 1" Ultra Torr Fitting
 Machine Length to Dim(0.31 crit.)
 Tack in Spacer



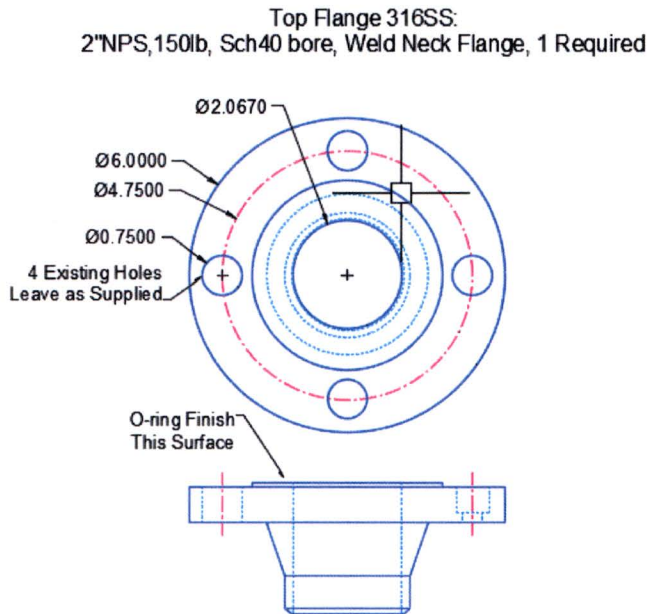
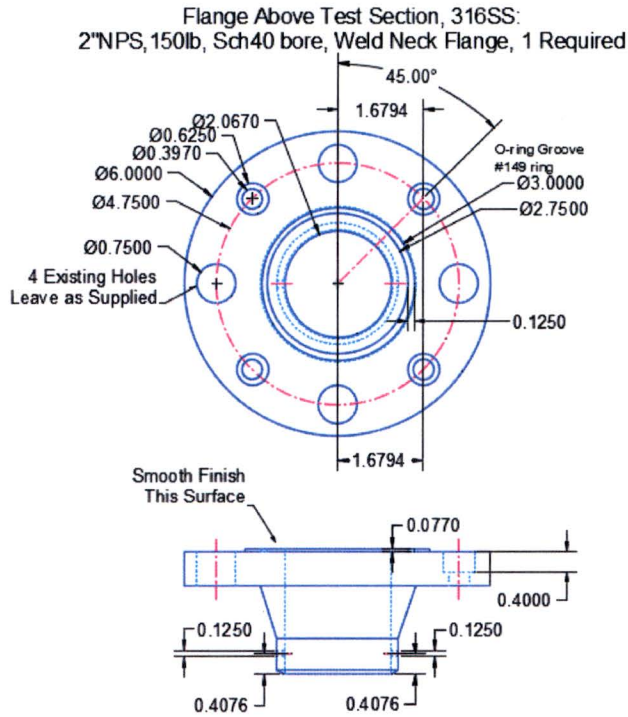
Lower 1" Ultra Torr Fitting
 Leave at original Length
 Tack in Spacer



Upper Transition
 1 Req'd, 316 SS

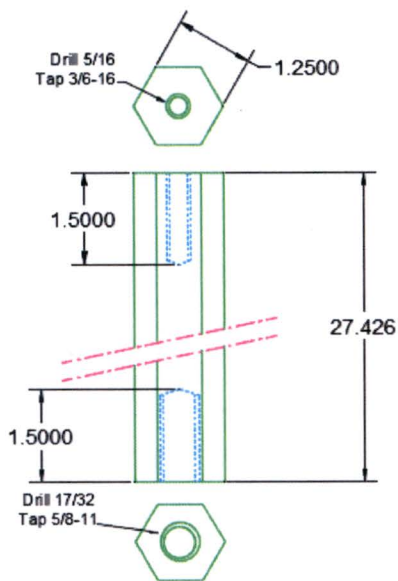


Test Section Components: inches

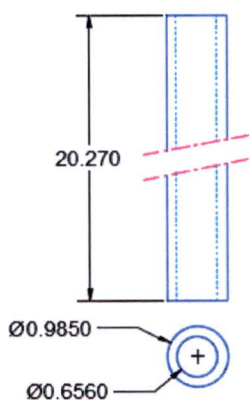


Test Section Components: inches

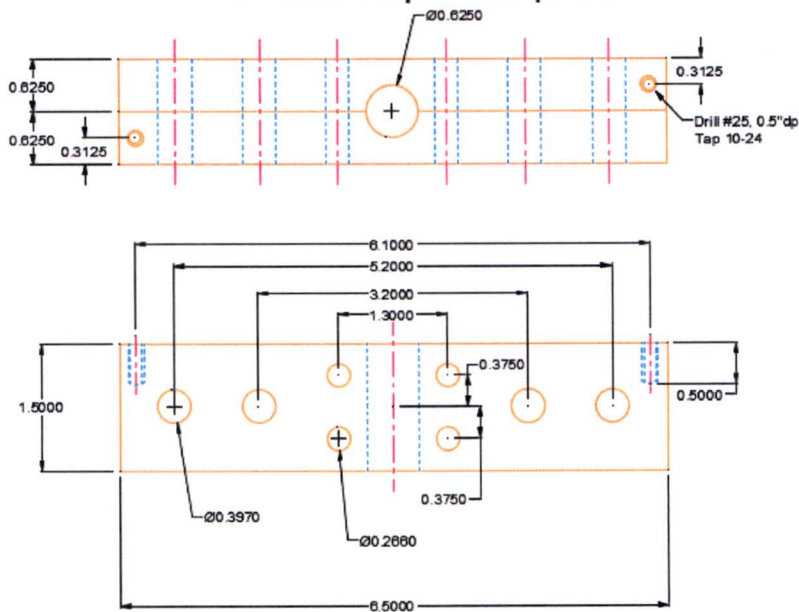
Hex Spacers
4 Req'd, 6061Al



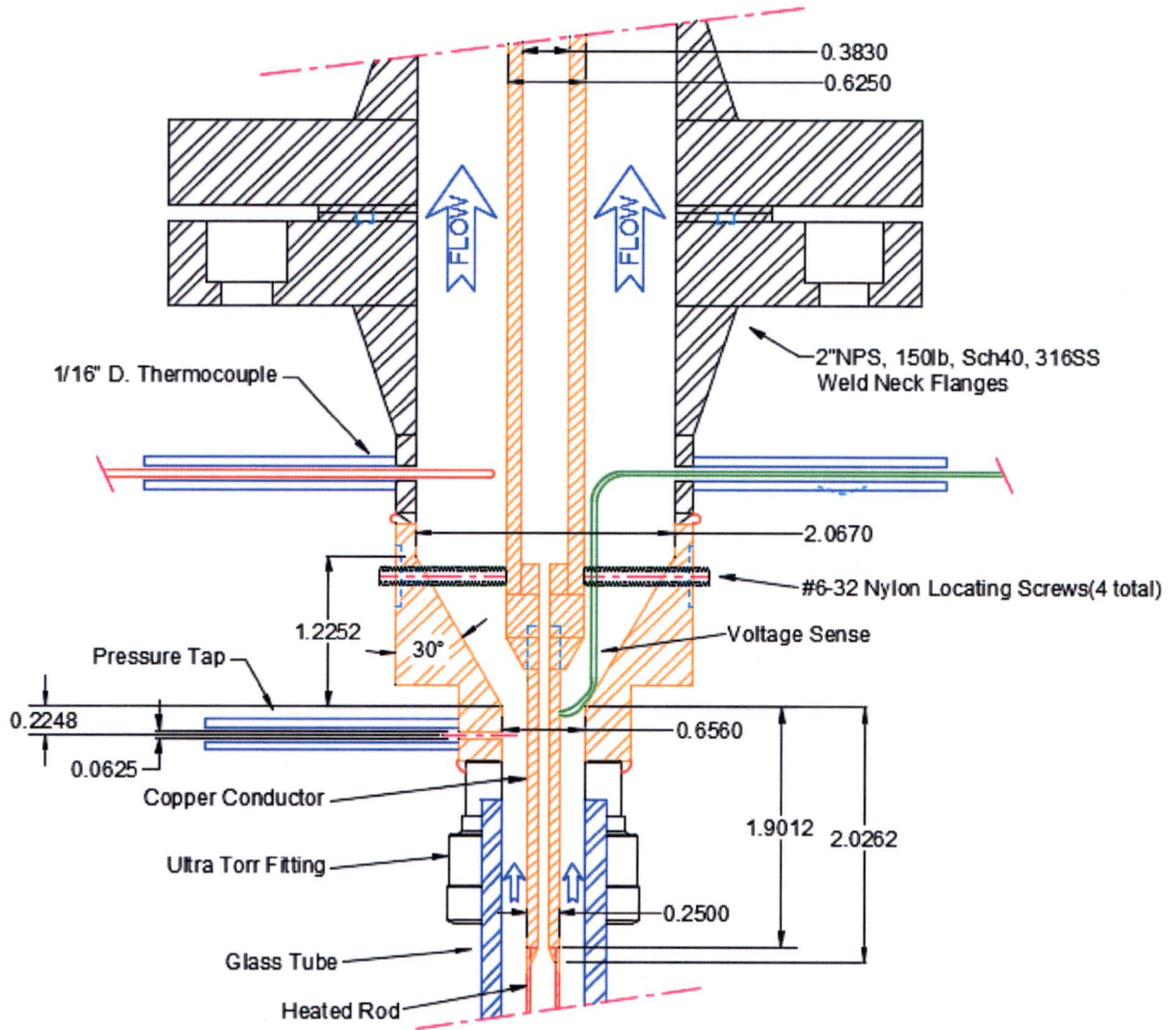
Borosilicate Glass
Tube, 6 Req'd



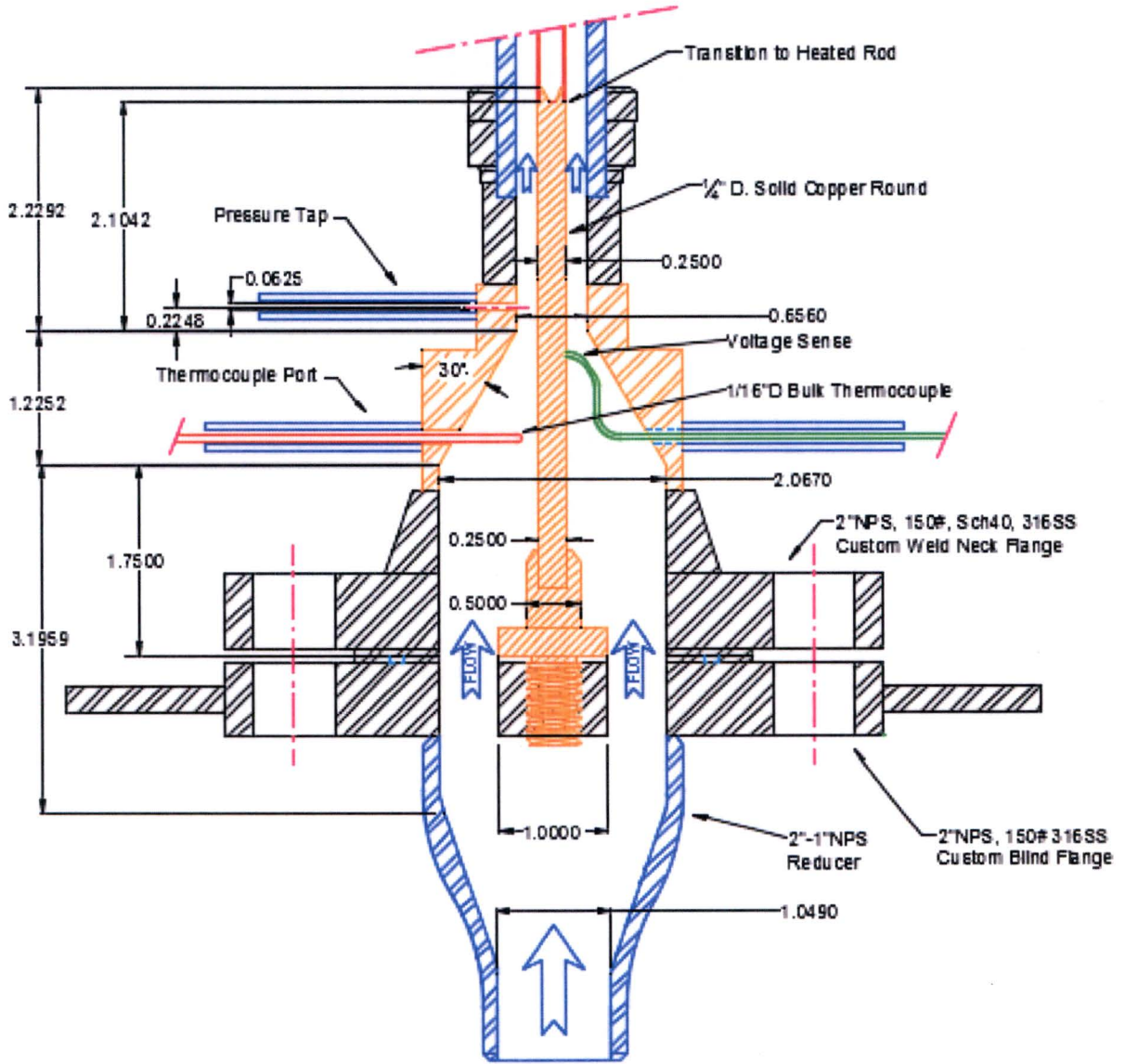
Upper Electrical Connector Blocks, Copper
2 matched pairs required



Exit Plenum



Entrance Plenum



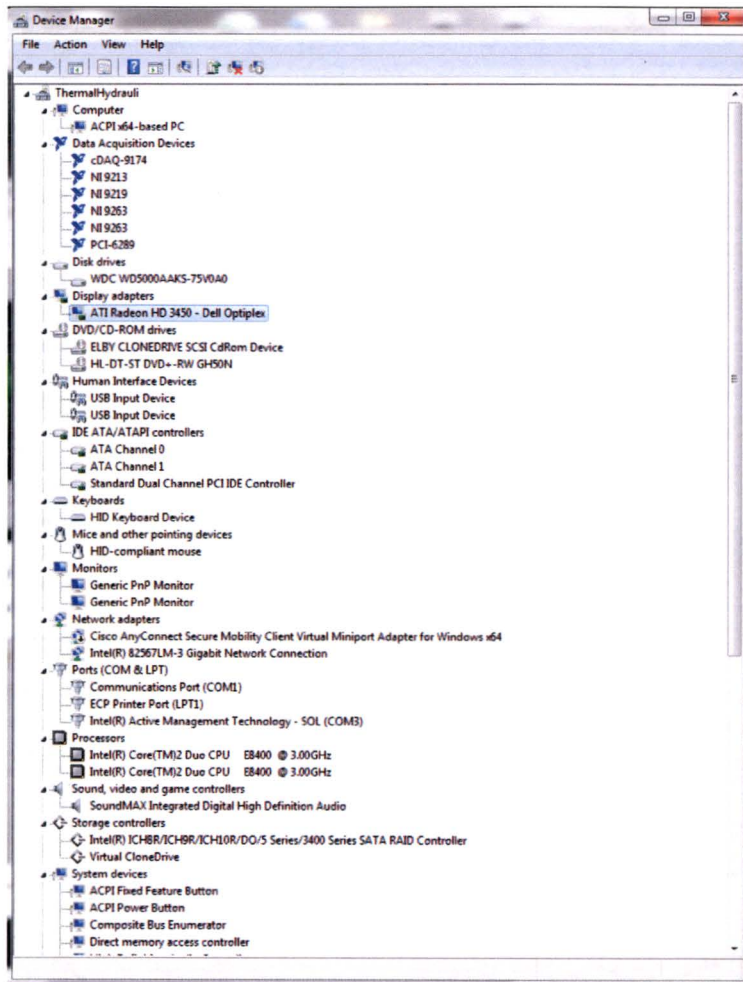
Appendix 9: Computer Platform and Software

Attachment 10

Critical Heat Flux Testing at the University of Wisconsin Final Report



30441R00041/A

Program Name	Labview 2013
Version	13.0f2 (32-bit)
Developer	National Instruments
Special Conditions	None
Type	PC
Manufacturer	Dell
Model	Optiplex 780
Processor	Intel®Core™2 Duo CPU E8400 @3.00Ghz 3.00Ghz
Installed Memory (RAM)	4.00 GB (3.87 GB usable), DDR3 1066Mhz/1333Mhz
Memory	
Video Card	ATI Radeon HD3450
CD/DVD drive	HL-DT-ST DVD+ -RW GH50N
Monitors (2)	Dell ASUS VH222 VerH-P, DELL 1704FPZT




Windows edition

Windows 7 Professional
Copyright © 2009 Microsoft Corporation. All rights reserved.
Service Pack 1
[Get more features with a new edition of Windows 7](#)



System

Manufacturer: Dell
Model: Optiplex 780
Rating:  Windows Experience Index
Processor: Intel(R) Core(TM)2 Duo CPU E8400 @ 3.00GHz 3.00 GHz
Installed memory (RAM): 4.00 GB (3.87 GB usable)
System type: 64-bit Operating System
Pen and Touch: No Pen or Touch Input is available for this Display

Dell support

Website: [Online support](#)


Computer name, domain, and workgroup settings

Computer name: Thermal-Hydrauli
Full computer name: Thermal-Hydrauli
Computer description:
Workgroup: WORKGROUP

[Change settings](#)

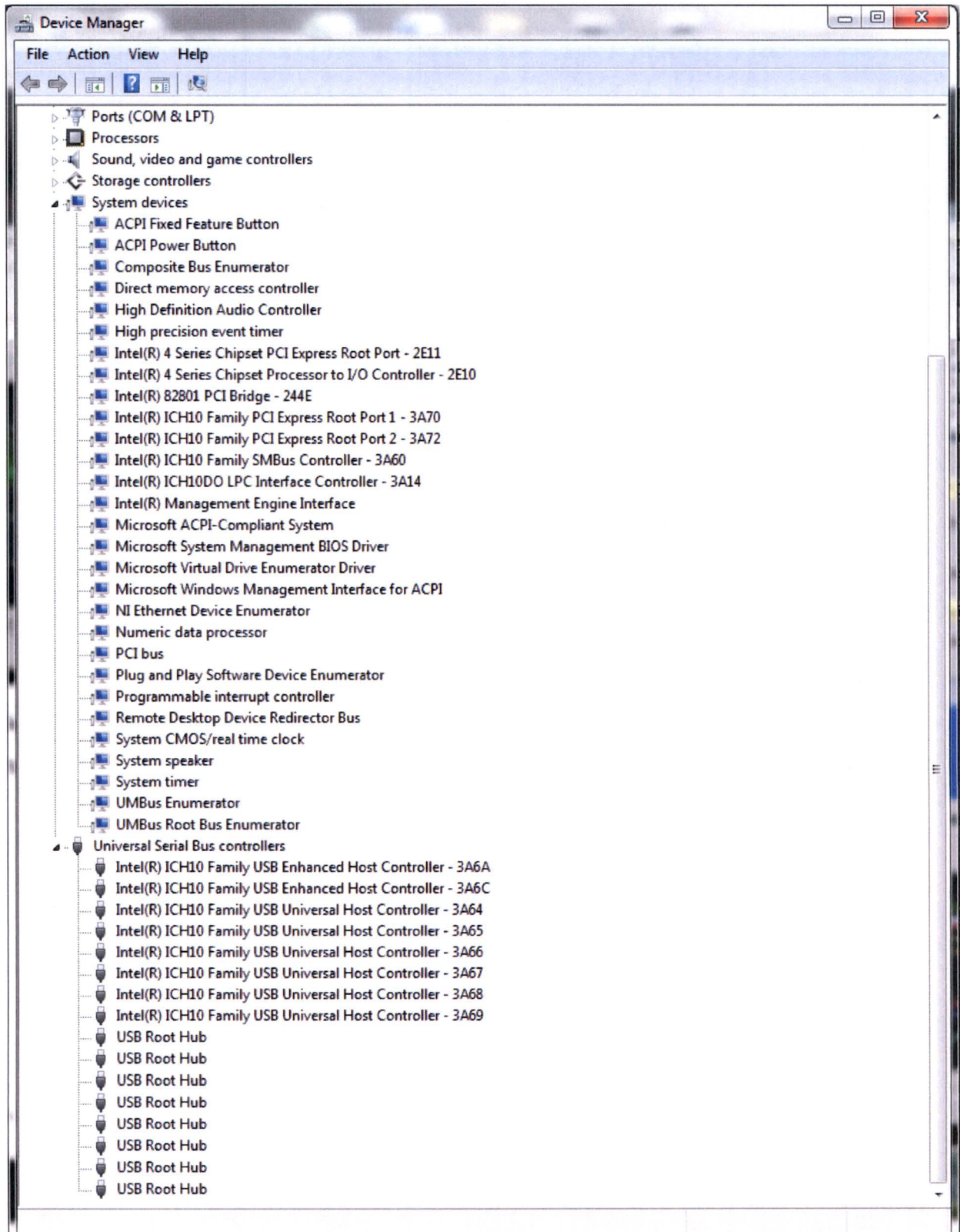
Windows activation

Windows is activated
Product ID: [REDACTED]



Learn more online...





Attachment 10



GENERAL ATOMICS

P.O. BOX 85608 SAN DIEGO, CA 92186-5608 (858) 455-3000